AN INVESTIGATION OF THE FAILURE MECHANISMS OF THERMOPLASTIC COMPOSITES AT VARIOUS RATES OF STRAIN AND TEMPERATURES

By

Phumudzo T. Netangaheni

A dissertation submitted to the Faculty of Engineering and the Built Environment in fulfillment of the requirements for the degree of Master of Science in Applied Science in Materials Engineering

Center for Materials Engineering

Department of Mechanical Engineering

University of Cape Town

2003

ACKNOWLEDGEMENTS

I would like to express my sincere appreciation and thanks to all those who helped and supported me throughout this research project, in particular:

- Dr K. Marcus, my supervisor, for his invaluable guidance, advice and encouragement throughout this research project.
- Professor G.N. Nurick, my co-supervisor, for his guidance and in helping me stay focused throughout this research project.
- Mr D. Tucker for his patience and invaluable assistance during the injection moulding of the test specimens.
- Mr C. Shea and Mr C. Goldman for their advice and encouragement.
- Mrs M. Waldron, of the Electron Microscope Unit (EMU), for her assistance in using the scanning electron microscope.
- Mr M. Batho for his invaluable patience and invaluable assistance during the machining of the moulds.
- Mr G. Newins and Mr P. Jacobs for their help in machining the test specimens.

- Mr M. Dlamini and Miss S. George for their help in using CAD.

- Staff and students in the Centre for Materials Engineering (CME) for their encouragement throughout this research project.

- The National Research Foundation (NRF) and KENTRON for their financial support.

- Special thanks to PLASTAMID (Pty) Ltd for the supply of materials (polymer pellets) and allowing me to use their injection-moulding machine.

- My close friends for their encouragement and support.

- I have no words to thank my parents (Thivhulawi and Elelwani Netangaheni) for their support and understanding during the entire period of my studies.

- Mr G. Ramuhapi, Mr N.L. Luruli and Dr T.I. Mukwevho for their words of encouragements and support.

- Very special thanks to the One above everyone (the Most High, the Creator) for a wonderful and successful life that he gave me, great appreciations.

ABSTRACT

The focus of this project is on the deformation behaviour of thermoplastic composites. The materials used were polypropylene and polyamide resins with glass fibres and talc as fillers. These materials were provided by PLASTAMID (Pty) Ltd. The injection moulded specimens of polypropylene, polyamide 6-6, 30% talc filled polypropylene, 30% short glass fibre reinforced polypropylene and 30% short glass fibre reinforced polyamide 6-6 were tested in tension, flexure and impact (Izod, Charpy and drop-weight). Two different injection-moulding machines were used for specimen manufacture. These were an automated injection moulding machine simulating good control of processing conditions and a simple hand operated injection moulding machine simulating different processing and cooling (crystallisation) conditions. The mechanical tests were performed at different rates of strain and temperatures.

The mechanical results show higher ductility of the unfilled polypropylene material. The strength and the elastic modulus of the materials are different for different materials. Addition of short glass fibres enhances the mechanical properties of polypropylene and polyamide 6-6. Talc fillers reduce the tensile, Izod and Charpy impact properties of polypropylene while the flexural and drop-weight impact strength is increased. Optical and scanning electron microscopy were used to observe the microstructural features and deformation behaviour such as matrix plastic deformation, matrix crazing and tearing, fibre-matrix debonding, fibre fracture, fibre orientation and crack propagation. These deformation behaviours are influenced by the test conditions such as strain rate, temperature and the type of the test conducted. The deformation behaviour is also dependent on the constituents of the material. The mechanical test response together with the macro- and microscopic features observed on the

fracture surfaces of tested specimens are evidence of the various mechanisms of failure that take place in different thermoplastic composites. The understanding of the mechanical response and the failure mechanisms of thermoplastic matrix composites is important in the design and processing stages.

TABLE OF CONTENTS

NOMENCLATURE

PP1100M	Unfilled polypropylene
EFE1147	Unfilled polyamide 6-6
w/w	Weight by weight
30SGFRPP	30% w/w short glass fibre reinforced polypropylene
30Talc/PP	30% w/w talc filled polypropylene
30SGFRPA 6-6	30% w/w short glass fibre reinforced polyamide 6-6
ISO	International Standard Organisation
ASTM	American Standard of Testing Methods
LM	Light microscope
SEM	Scanning electron microscopy
Tg	Glass transition temperature

CHAPTER 1

GENERAL INTRODUCTION

1.1 INTRODUCTION

Over the past two decades there has been a dramatic increase in the use of polymer matrix composites materials worldwide. This can be attributed to their ease of manufacture, low density, good mechanical and chemical resistance and low maintenance cost. Polymer composites were first developed during the Second World War. These were thermosetting matrix composites with fibrous reinforcements [1]. Thermoplastic composites were introduced in the early 1980's in an attempt to develop more easily processed polymer matrix composites. Thermosetting matrix composites account for more than two-thirds of the market. However, thermoplastic matrix composites have a higher yearly growth rate of 9 % as compared to the 3 % of the thermosetting matrix composites.

The automobile industry uses thermoplastic matrix composites extensively, followed by the aeronautic and aerospace industries. This explains why Germany is the largest thermoplastic matrix composite consumer, as it accounts for 28 % of the European market (see Figure 1.1). Belgium accounts for 6 % followed by a group of other European countries that, collectively, account for 10 % of the market. In the automobile industry, thermoplastic matrix composites are used in applications such as covering panels, spoilers, body parts, bumper beams and tailgates.

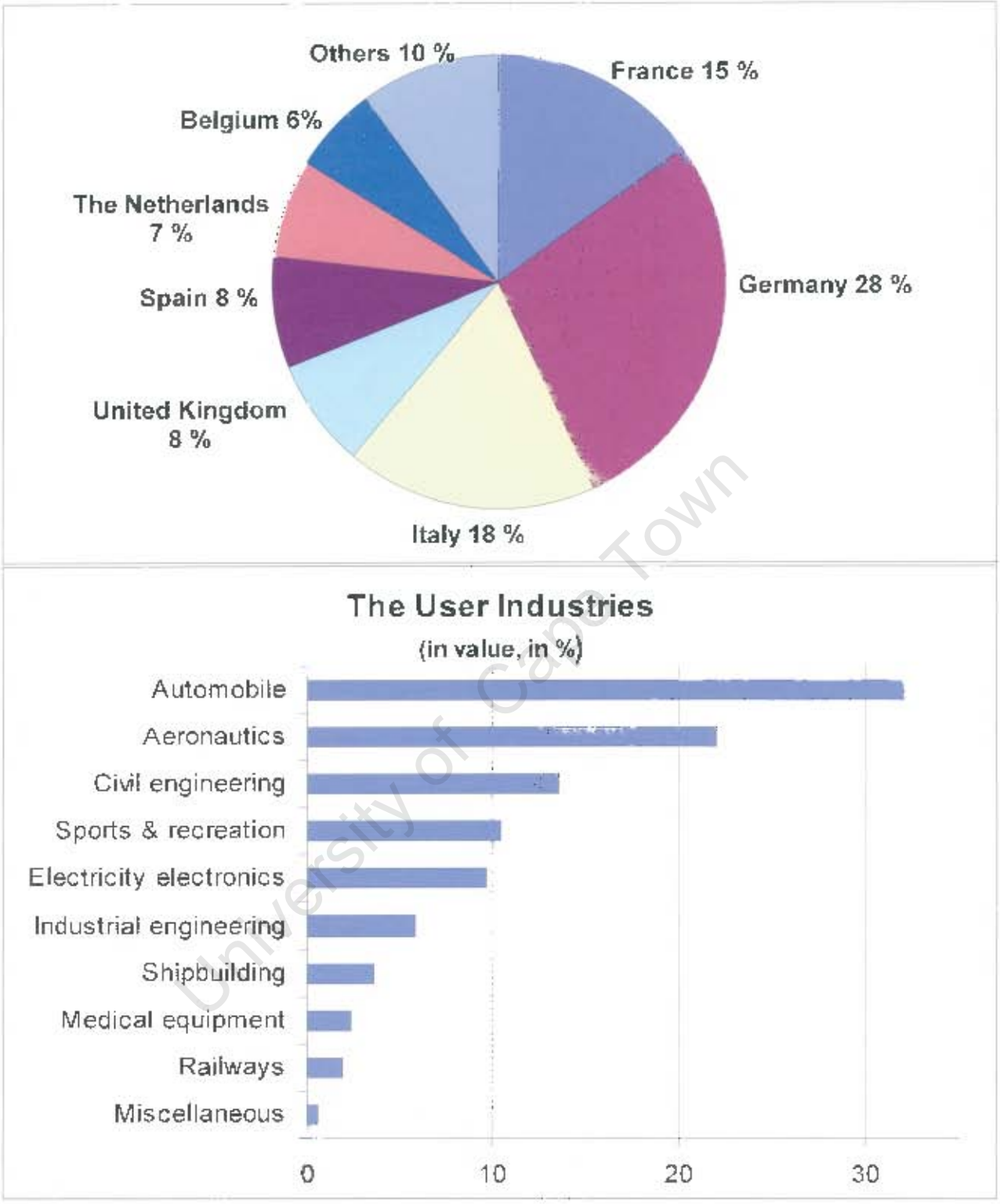

(Source: Study on composite materials – Nodal Consultants estimates – 2000)

Figure 1.1: *European market share breakdown and the user industry of thermoplastic composites in the year 2000*[1].

The increasing demand of the polymer composites calls for the need for researchers to study and understand the behaviour of these materials. This thesis was aimed at understanding the mechanical behaviour and the failure mechanisms of thermoplastic matrix composites at various rates of strain, temperatures and processing conditions. The behaviour of short fibre reinforced- and mineral filled thermoplastic composites is governed by complex interactions of internal and microstructure related parameters such as the matrix type, filler orientation and the fibre-matrix interface bond strength. A wide range of properties can be attained through careful selection of the polymer resin and filler type[2].

Experiments have shown that the mechanical properties and the mechanisms of failure are strongly affected by factors such as temperature, impact angle and strain rate. The strength of materials can be determined in tension, flexure as well as under impact loading. The mechanisms of failure and the fractographic features can be investigated using light microscopy (LM) and scanning electron microscopy (SEM). A significant amount of continuous and thermoset-based composites are used for structural applications in the construction, aerospace and satellite industries. Polymer matrix composites are also used extensively to manufacture parts for protection in the defence industries. In the defence and automobile industry where energy absorption-strain rate relationships and safety considerations are critical, a good understanding of failure behaviour can lead to the optimisation of certain parts. One of the fast cycle processes used for short fibre composites manufacture is injection moulding. Figure 1.2 below shows various interior fittings that are the products of injection moulded talc filled polypropylene.

This thesis covers the work done on short glass fibre reinforced polypropylene and polyamide 6-6 composites as well as talc filled polypropylene. The mechanical properties, fractographic features and the mechanisms of failure

were investigated. This work includes investigations on the influence of strain rate, temperature and processing conditions. It is hoped that the behaviour of short fibre reinforced thermoplastic composites at various environmental and testing conditions will be understood. Polypropylene and polyamide 6-6 thermoplastics are chosen for this thesis because they are extensively used in compounding formulations.

Figure 1.2: *Injection moulded car interior fittings from compounded talc filled polypropylene pellets* [3].

1.2 THESIS MOTIVATION

There has been an increase in the development and application of thermoplastic matrix composites. This has resulted in the need to enhance the understanding of the failure mechanisms and quantify the microstructural features that amount to the failure of thermoplastic matrix composites. Many researchers have studied the tensile and impact response of thermoplastic matrix composites at room temperature and at low or quasi-static strain rates. A better understanding of the mechanical response of thermoplastic matrix composites at various strain rates

and temperatures is required. The need to investigate the influence of processing conditions was also considered to be important.

1.3 RESEARCH OBJECTIVES

The objectives of this research work were:

- To study and understand the mechanisms of failure in polypropylene and polyamide based thermoplastic composites.
- To study the response of the composite materials under different loading and temperature conditions.
- To study the behaviour of the composite materials at different impacting modes.
- To study the effect of processing conditions using a commercial automated injection moulding machine and a simple hand operated injection moulder.

1.4 OUTLINE OF THE THESIS

Chapter two of this thesis gives a review of the available literature surveyed followed by the experimental techniques applied when conducting the macro-structural and micro-structural investigations in ***Chapter three***. ***Chapter four*** gives an outline of the results of the investigations. These results are discussed in ***Chapter five*** and the conclusions of the results are outlined in ***Chapter six.*** ***Chapter seven*** gives the recommendations for future work. The references used for the purpose this research work are sited in ***Chapter eight.*** This thesis concludes with appendices, which contains all the mechanical results and SEM micrographs that were not specifically included in the results chapter.

CHAPTER TWO

LITERATURE REVIEW

2.1 POLYMERS

Polymeric materials have mechanical strengths and moduli of between one to two orders of magnitude lower than that of metallic materials. Nowadays there are various methods to improve or alter the mechanical properties of polymeric materials. The desired properties for design can be achieved by a suitable combination of polymeric materials with reinforcing agents or fillers. Different polymer types can also be blended together for specific property requirements.

Polymers are long chain molecules made up of monomers joined together by chemical bonds. Different polymers are made from various monomers and the chemical bonds between the monomers are sometimes different. This is the reason for the different mechanical properties of polymers. Polymers are categorised into homopolymers and copolymers. Homopolymers are polymers constituted of the same monomers whereas copolymers are constituted of two or more different monomers[4]. Polymers can be delineated further into thermoplastics, thermosets and elastomers. Thermoplastic materials are fusible, i.e. when heated they melt and solidify again on cooling [5]. Thermosets cannot be melted when cured; once they solidify they are set and therefore are infusible. Thermoplastics have the ability to revert to their original shape after deformation. The polymer types of interest in this research are thermoplastics.

Thermoplastics are considered economical because they are easily fabricated and recyclable. Industries aim to produce a large number of quality products in the shortest possible time. Injection moulding and extrusion processing of thermoplastics are suitable techniques to achieve industry requirements. There are many different types of thermoplastic materials, however this discussion will focus on two types, namely polypropylene and polyamide 6-6 and their composites.

2.1.1 Molecular Weight and Molecular Weight Distribution

Molecular weight is an important factor in polymers. During polymerisation, not all the polymer chains grow to the same length. The number of repeat units (monomers) specifies the length of the polymer chain; this is called the degree of polymerisation. The molecular weight of a polymer is specified as the average molecular weight. The molecular weight can be divided into the number average and weight average molecular weight. The number average molecular weight ($\overline{M_n}$) is measured by counting the number of molecules in a known mass of material. This is achieved by methods based on colligative properties such as ebulliometry, cryoscopy and osmometry[6]. The weight average molecular weight ($\overline{M_w}$) is based on the size of the molecules rather than their number. It is usually measured by light-scattering or sedimentation methods[7]. $\overline{M_w}$ is always greater than $\overline{M_n}$ for a polydisperse system. The number average and weight average molecular weights are expressed as:

$$\overline{M_n} = \sum n_i M_i / \sum n_i$$

and

$$\overline{M_w} = \sum n_i M_i^2 / \sum n_i M_i$$

The relationship between $\overline{M_n}$ and $\overline{M_w}$ can be observed in Figure 2.1 and the ratio $\overline{M_w} / \overline{M_n}$ is a measure of the polydispersity (molecular weight distribution) of the system.

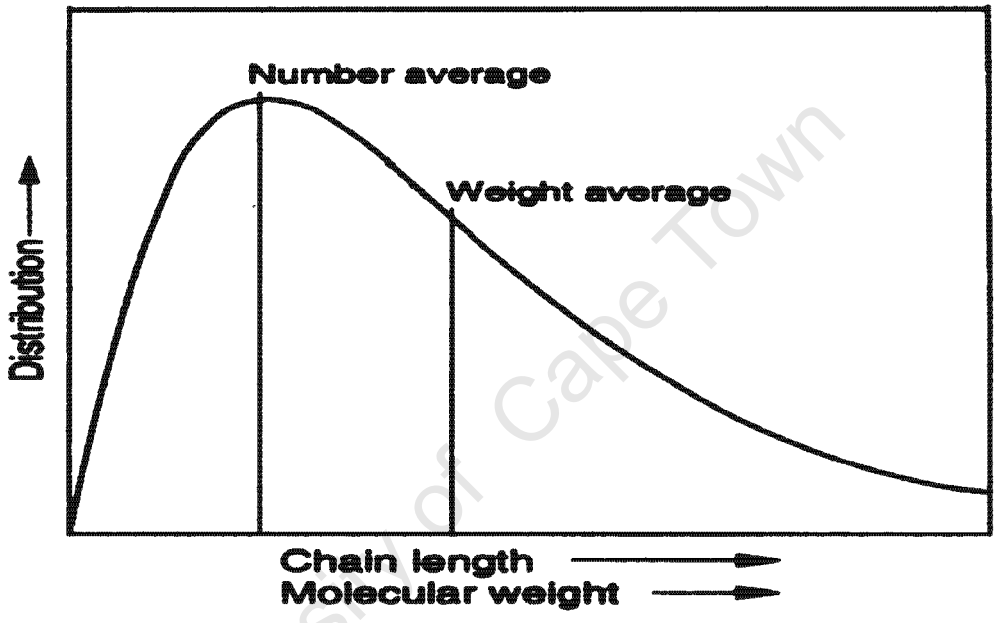

Figure 2.1: *Typical molecular weight distribution of a polymer*[8].

Various properties are affected by the magnitude of the molecular weight, e.g. the melting or softening temperature. The melting temperature, stiffness and strength increase with increasing molecular weight. However, the processing of the polymer becomes difficult with increasing molecular weight[6,8].

2.1.2 Polypropylene

Polypropylene is a homopolymer made by polymerisation of propylene monomers using co-ordination chemistry. The synthesis of polypropylene is facilitated by the introduction of a Ziegler-Natta catalyst (an organo-metallic catalyst based on titanium and aluminium) to produce a semi-crystalline linear polymer (see Figure 2.2). The automotive industry extensively uses polypropylene in the production of components such as car bumpers and dashboards[9]. Compared with other thermoplastics polypropylene has properties and low cost that make it the most widely used thermoplastic worldwide. Some of the properties include its low density, high toughness and durability, water resistance, excellent electrical properties and long flex life [5].

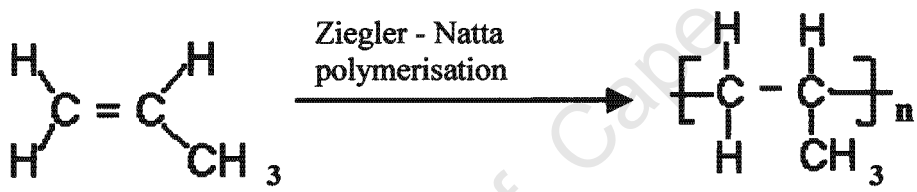

Propylene Polypropylene

Figure 2.2: *Polymerisation of propylene monomer to form polypropylene.*

There are various types of polypropylene that are distinguished by the special arrangement of the methyl group (-CH_3) around the polymer chain. These types of polymers are called stereoisomers[10]. There are three stereoisomers of polypropylene, namely, isotactic, syndiotactic and atactic (see Figure 2.3). Isotactic polypropylene results from the head-to-tail addition of the polypropylene monomers with a characteristic of having all the methyl groups on the same side of the polymer chain (i.e. the monomers are oriented in the same way). Syndiotactic polypropylene differs from isotactic in that it has alternating

orientations of the methyl groups while the atactic polypropylene has no consistent placement of the methyl group about the backbone.

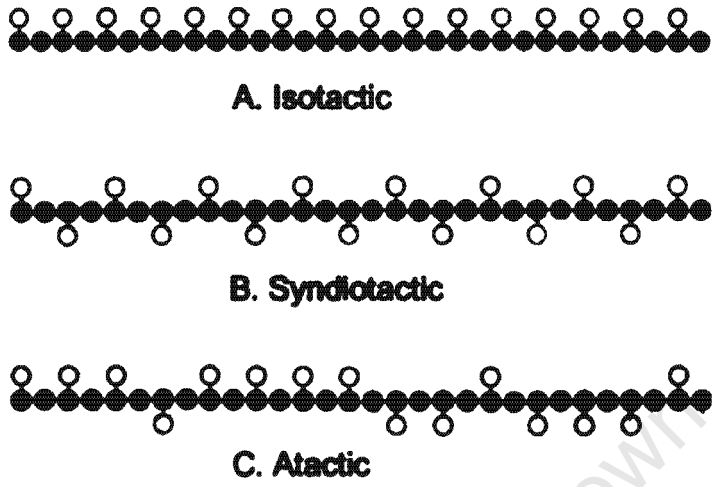

Figure 2.3: *Schematic representation of the stereo-chemical configuration of polypropylene[11]. The open circles represent the methyl (CH_3) groups along the carbon-carbon backbone.*

The level of tacticity determines the degree of crystallisation of the polymer. Higher crystallinity requires higher tacticity in the polymer chain. A reduction in the tacticity along the polymer chain results in a decrease in the crystallinity. The mechanical properties of polypropylene are affected by the stereo-chemical configuration. Isotactic and syndiotactic polypropylene chains can have higher degree of crystallinity (40% to 70%) while atactic polypropylene has almost no crystallinity[11].

The properties of polypropylene and other thermoplastic polymers can be enhanced to meet specifications for the designed part by incorporation of additives, reinforcing agents and fillers. Fillers such as calcium carbonate and talc and reinforcing agents like glass fibre are mostly used. These enhancements increase the use of polypropylene in load bearing applications.

Other polymers can be combined with polypropylene to form types of polymers called copolymers. There are different types of copolymers viz. alternating, random, block, graft and random terpolymer copolymer. This thesis is focused only on the homopolymer form of polypropylene.

2.1.3 Polyamide 6-6 (Nylon 6-6)

Polyamide 6-6, unlike polypropylene, is made from different monomers. Nylon 6-6 is an aliphatic polymer produced from a diacid (adipic acid) and diamine (hexamethylene diamine). Adipic acid and hexamethylene diamine chemically react to produce polyamide 6-6 by a condensation reaction (Figure 2.4) [5,12,13].

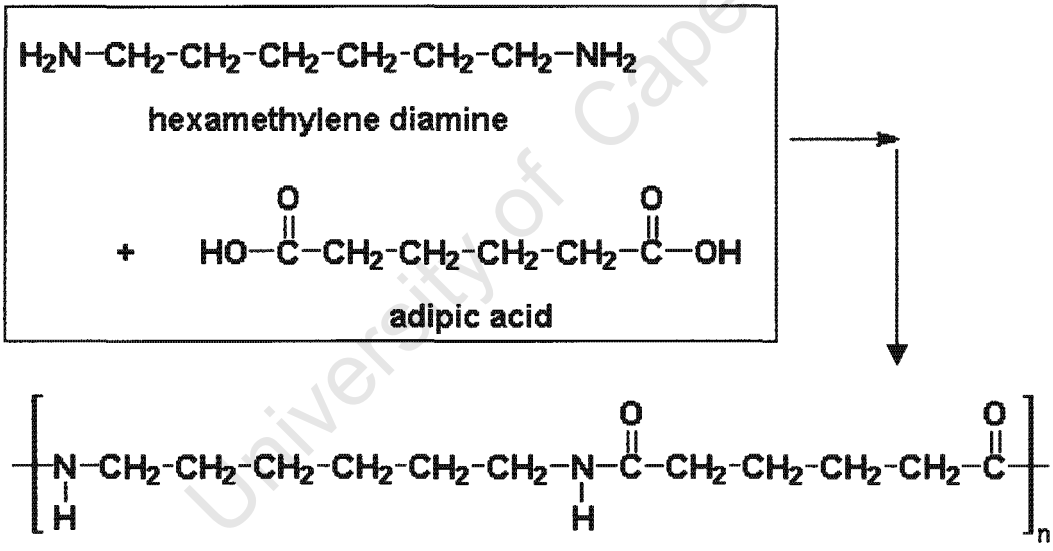

Figure 2.4: *Chemical reaction for the synthesis of polyamide 6-6*[12].

There are other types of polyamide that differ from polyamide 6-6 in their molecular structure and the packing of the side groups, e.g. polyamide 6 and

polyamide 6-10. These differences are caused by the positioning of the –NH group in the polymer chain. Stereo-regularity and the hydrogen bond between the polymer chains determine the crystallinity and result in the higher melting point of polyamides[6]. Figure 2.5 shows the stereo-regularity and hydrogen bonding in polyamide 6 and polyamide 6-6, where polyamide 6-6 has more hydrogen bonding and therefore has higher melting point than polyamide 6.

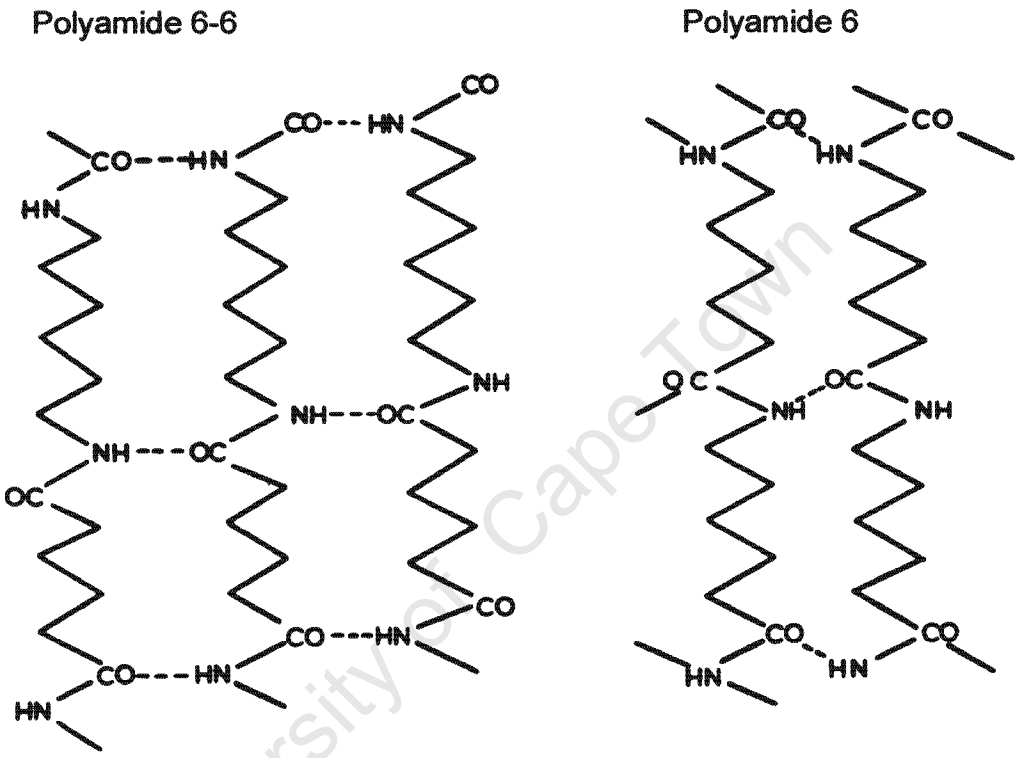

Figure 2.5: *Stereo-regularity and hydrogen bonding in polyamide 6-6 and polyamide 6[6].*

2.1.3.1 Polyamides and Moisture Absorption

Most thermoplastics when exposed to certain environmental conditions such as elevated temperature and moisture lose their dimensional stability. Temperature is the main cause of dimensional changes in other thermoplastics in service but in polyamides both temperature and moisture are involved. The mechanical

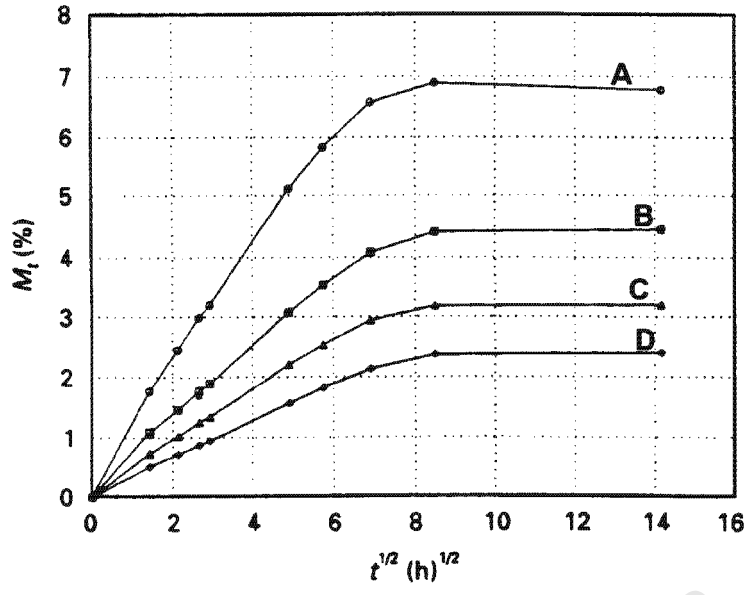

Figure 2.6: *Effect of glass fibre volume fraction on the moisture uptake of polyarylamide (PAR). (A) pure PAR, (B) 16 vol%, (C) 27 vol% and (D) 32 vol% glass fibre reinforced PAR* [13].

2.2 POLYMER MODIFICATION

2.2.1 Fillers

Incorporation of fillers in polymer matrices can serve to enhance the mechanical properties. Fillers have various categories and they influence the mechanical properties of composites differently. These categories are spherical fillers (e.g. calcium carbonate, glass sphere and silica flour), lamellar or platy fillers (e.g. mica, talc and glass flake) and cylindrical fillers (e.g. whisker, wollastonite and chopped fibres) [15]. Incorporation of different fillers in the polymer matrix imparts different mechanical responses. Polymer modification by filler addition was mainly directed on enhancing the strength and stiffness of the composite. It was later realised that not all fillers have a reinforcing effect in the composite.

Fillers such as fibres play a major role in enhancing the strength of polymer composites materials while fillers such as mica, calcium carbonate and talc improve a range of properties including shrinkage, moulding cycle time, stiffness and creep resistance [16]. The impact strength of thermoplastic polymers is negatively affected by the addition of mineral fillers. Two types of fillers of interest for this research work are chopped glass fibres and platy talc fillers.

2.2.1.1 Glass Fibres

Glass fibres are the most widely used reinforcing agents in the composite industry. This is due to a wide variety of properties that different types of glass fibres provide. There are various types of glass fibres commercially available for specific properties for a particular application[17,18,19,20]. Examples of commercially available glass fibres are A-glass, C-glass, D- glass, E-glass, ECR-glass, AR-glass, R-glass and S-glass.

E-glass is the most commonly used type of glass for fibre manufacturing. One type of glass differs from the other by the percentage composition. E-glass has a low electrical conductivity whereas C-glass has a high chemical resistance. The designation letter is given to a particular glass because of its superior properties. Glass fibres have no crystallinity or long-range order and they are silicates[19]. Silica forms a three-dimensional network of Si-O bonds from the building block of the $[SiO_4]^{4-}$ tetrahedral. Glass fibres are isotropic, i.e. their Young's modulus and thermal expansion coefficients are the same along the fibre axis and perpendicular to the fibre axis. Figure 2.7 shows (A) a scanning electron microscope (SEM) micrograph representing the fracture surface of a short glass fibre polymer composites and (B) a simplified two-dimensional internal structure of glass.

Glass fibres are manufactured by drawing molten glass through platinum bushings at high speed and immediately cooling them in a spray of water. The glass surface does not bond well with many matrix resins because they are non-compatible with the matrix resin. It is crucial that the coupling agent is applied on the surface of glass fibre not only to improve the compatibility with the matrix resins but also to protect them during handling. The coupling agent is applied immediately after cooling with spray water.

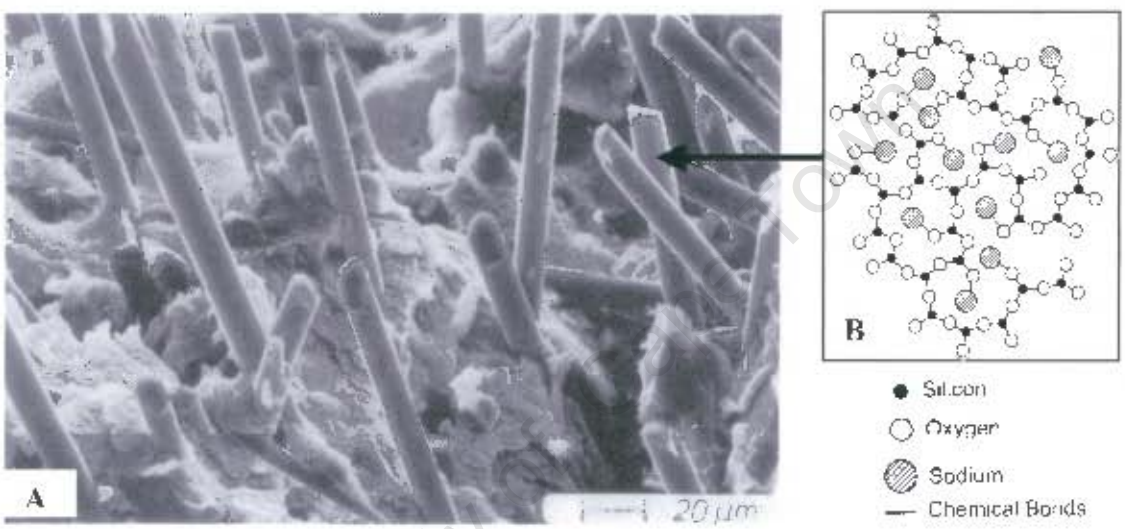

Figure 2.7: *SEM micrograph of the fracture surface of: (A) short glass fibre polyphenylene sulfide composite and (B) the internal structure of glass fibre*[19,21].

2.2.1.2 Talc Fillers

Talc is a low cost magnesium silicate filler originally used in polymers to reduce cost. This is a natural, hydrated magnesium silicate that appears in different particle shapes but commercially manufactured in a lamellar form. Talc has the chemical formula $3MgO{\bullet}4SiO_2{\bullet}H_2O$[22]. An octahedral layer of oxide and magnesium hydroxide is sandwiched between two tetrahedral layers of silicon

oxide to form the structure of talc in platy form (see Figure 2.8). Platy talc fillers have a soft slippery feel with a sandwich structure that easily slides and delaminate because of the outer oxide surfaces that only form weak Van der Waals forces with the composite resin[23].

Polymers such as high-density polyethylene have high gas permeability, which limit their use in certain industrial and packaging applications. The addition of platy talc fillers reduces the gas permeability and the total weight of the component. Other uses of talc in thermoplastics are to:-

- Increase flexural strength.
- Reduce creep tendency.
- Reduce shrinkage and warping.
- Increase stiffness and flexural modulus.
- Increase surface hardness of moulded parts.
- Can act as a nucleating agent to increase the clarity and stiffness in polymer films.

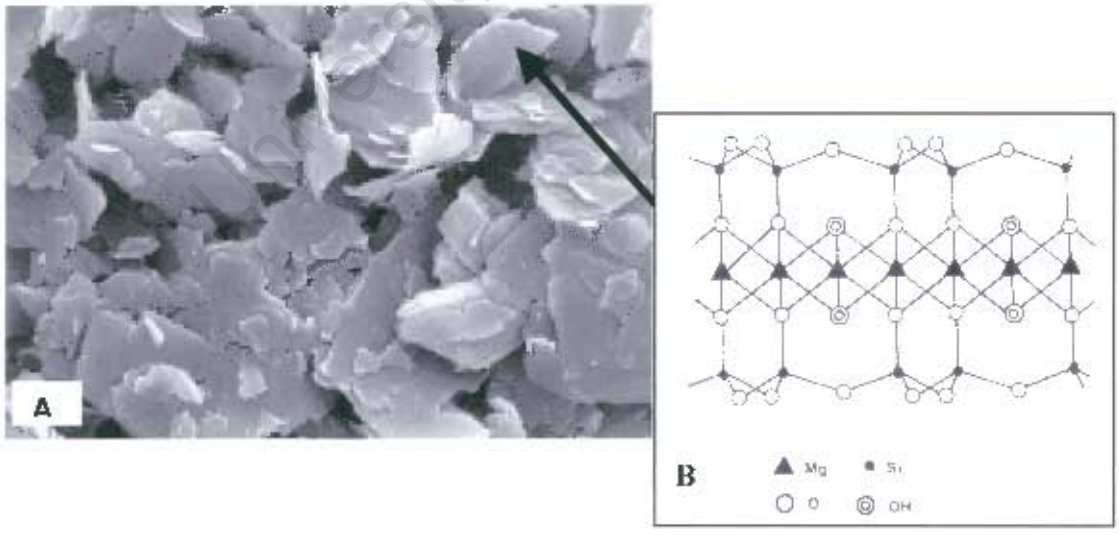

Figure 2.8: *Typical structure of platy talc filler*[23,24].

2.2.2 Composites

2.2.2.1 Polymer Composites

Composites materials are designed to combine different desired superior properties from different materials for a particular specification. This research work is focused on two types of thermoplastic polymer matrix composites, namely fibrous and mineral filled composites. Short glass filled fibrous and talc mineral filled composites will be studied for micro mechanical failure mechanisms and for processing effects. It is of fundamental importance to understand the behaviour of filled thermoplastic composites materials, mainly short glass fibre reinforced thermoplastics, since they are increasingly used. Short fibre reinforced thermoplastic composites are advantageous in their ease of manufacture by processes such as injection moulding where fast cycle times and lower operating costs are typical.

The polymer resins, glass fibres and talc fillers have been discussed in the preceding sections above. Polymer resins and fillers are not always compatible and therefore require a bond strengthening technique. Many polymers, mainly thermoplastics, do not naturally form strong chemical bonds with inorganic surfaces. Coupling agents such as organosilanes are used as adhesion promoters in polymer composites. Coupling encourages a good bond between the polymer resin and fillers to ensure effective load transfer between the matrix and the reinforcing fibres[25,26]. In mineral particle filled polymer composites, coupling agents are not only necessary for filler-matrix resin bond strengthening but also to increase particle dispersion in the matrix[27]. The mechanical properties of composite materials are therefore enhanced by the addition of coupling agents[28]. Without coupling agents fillers, fibres or mineral particles, act as stress raisers within the continuous polymer resin.

Organosilanes are multifunctional groups with two parts, one part has a group which bonds strongly to the surface of the filler and the other part has a group that is compatible with the polymer matrix. The silane part of the organosilane molecule attaches to a reinforcing fibre or mineral particle surface, while the organic part is compatible with the polymer matrix. Figure 2.9 shows the reaction mechanism between the coupling agent and the glass/polymer network.

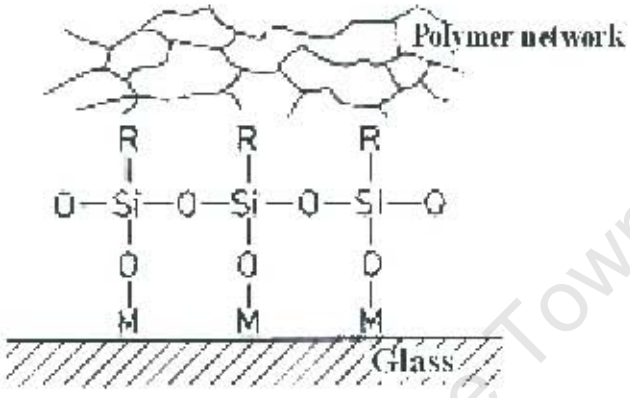

Figure 2.9: *Representation of the coupling agent located between the polymer resin and glass fibre*[17].

2.2.2.2 Filler-matrix Interface

An interface can be defined as a binding surface where a discontinuity in material parameter, such as crystal structure, elastic modulus, density or coefficient of thermal expansion take place. Coupling agents are used to strengthen the fibre/matrix interface. This makes a very thin and rough layer between the filler and the matrix. Figure 2.10 represents an uneven sizing layer on the fibres.

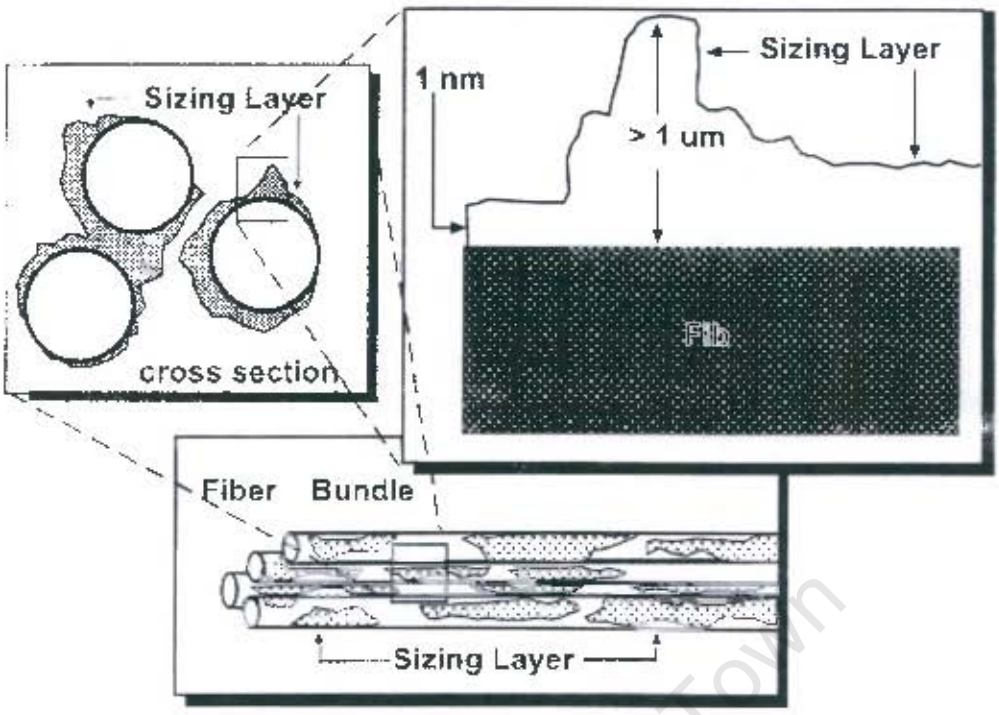

Figure 2.10: *Idealized sketches of the non-uniform distribution of a sizing layer on glass fibres*[19].

A strong interface is one where the polymer resin wet a large area of the filler. Coupling agents enhance the wettability of the fibre by the matrix resin thereby enabling load transfer from the matrix to the fibres. The interface plays a major role in determining the mechanical behaviour of the composite material[29]. It is therefore essential to understand the nature of the bonding at the interface, i.e. whether it is mechanical and/or chemical bonding [7].

Mechanical bonding occurs during curing where the matrix contracts thereby gripping the reinforcing fibre. This kind of bonding is not enough on its own for a strong interface but is efficient in load transfer when the load is applied parallel to the interface. Chemical bonding is divided into two types, dissolution and wettability bonding and reaction bonding. Dissolution and wettability bonding involve a short-range electronic interaction of components where atoms from

different components, matrix and fibre surface come into intimate contact. The fibre surface must be free of contaminants and air bubbles to ensure a strong contact. Reaction bonding refers to the actual transport of atoms from one or both components to the reaction site by the process of diffusion. In the case of glass filled polymer composites atoms diffuse from the matrix resin and from silane to the reaction site resulting in a strong interface.

2.3 PROCESSING

2.3.1 Methods

Various techniques used to process thermoplastics and thermoplastic composites include extrusion, blow moulding and injection moulding. Injection moulding is the most commonly used processing method in the polymer composite industry. This can be attributed to the shorter cycle time (in the range of 20-50s), higher level of automation and the ability to produce complicated shapes with much better surface finishes. Although injection moulding has been proven to be the best method for processing thermoplastic composites, it has some drawbacks. The flow of the melt inside the mould cavity has a considerable influence on fibre orientation and anisotropy of strength in the moulded component[30]. The average fibre length can also be reduced as a result fibre breakage during injection moulding. Figure 2.11 shows a typical injection-moulding machine.

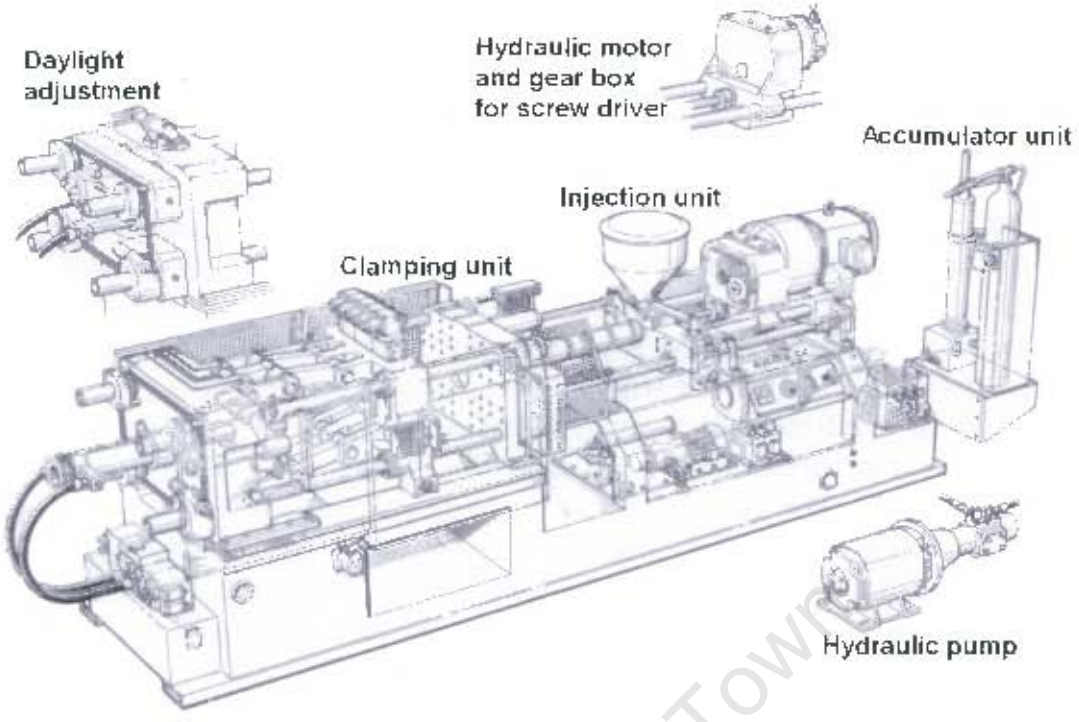

Figure 2.11: *Typical injection moulding machine for thermoplastics* [31].

Injection moulding machines for commercial use are automated and easy to operate. The injection unit and the clamping unit are the two important units of the machine. Most injection machines are horizontal with the injection unit on the right and the clamping unit on the left of the support. There are machines with vertical clamping and horizontal injection unit[31].

During processing, the polymer composite material is fed into the hopper (Stage 1 in Figure 2.12) in the form of pellets (for thermoplastics). The pellets proceed to the heated barrel where they melt and transform into a viscous melt. The resin is then injected into the mould cavity using the screw until cavity is full (Stage 2). The pressure on the screw is maintained until the moulded component has solidified. Fresh melt is conveyed towards the front of the screw and the screw rotate backwards to prepare for the next shot. When the moulded component is cool enough the nozzle breaks off, the mould opens up and the ejector pins eject

the component (Stage 3). The cycle repeats itself to produce more components. The barrel and mould temperatures are different for different polymer resins according to their melting temperature. Other settings include the injection speed and pressure, screw back speed and pressure, and holding pressure and time.

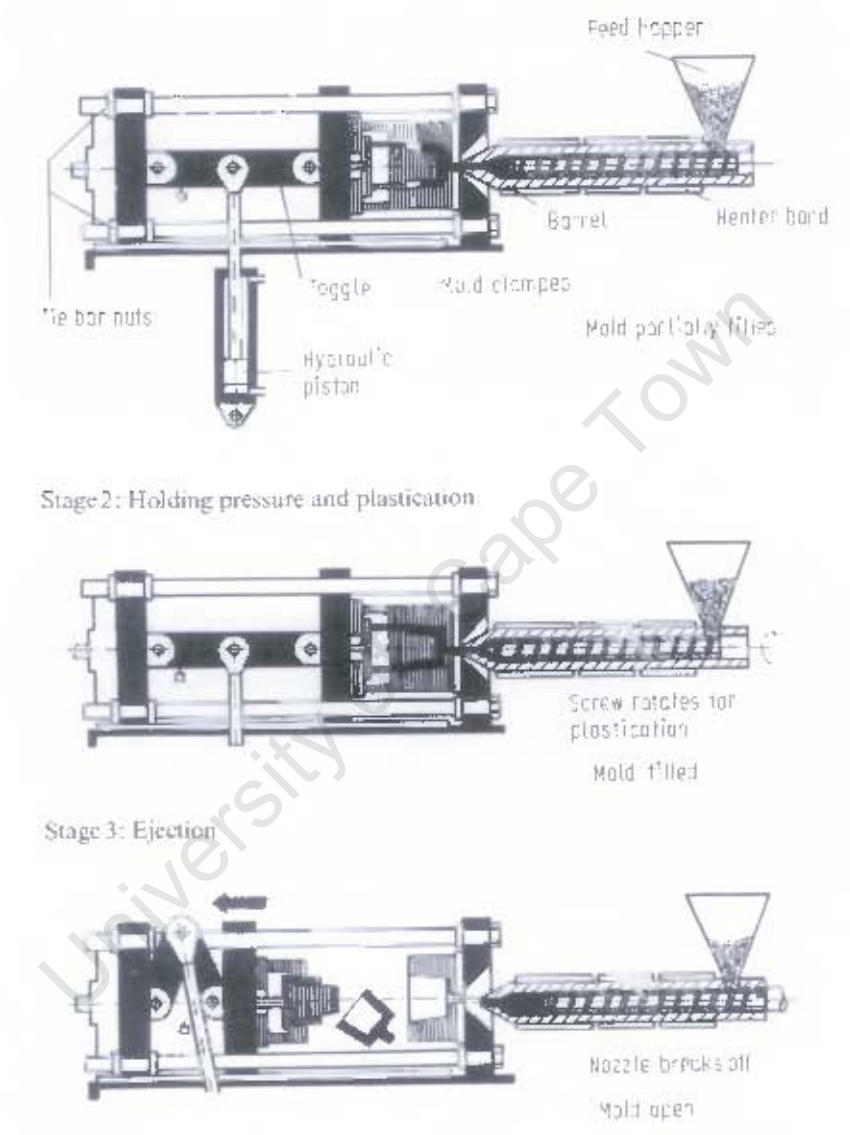

Figure 2.12: *Schematic representation of the screw injection moulding machine-inset operation cycle*[30].

The solidification of the melt inside the mould is different in different areas of the mould cavity. The subject of solidification and cooling of the melt is strongly related to the manner in which the melt flows in the mould. The flow of the melt along the streamlines is divided in to three types: shearing, converging and diverging flows. The flow profile is shown in Figure 2.13 below. The melt enters the mould through the gates and flows down the cavity i.e. converging flow. When it reaches the fountain flow region (see Figure 2.13) it stretches out (diverging flow) and lays down against the mould walls. Heat is extracted from the material in contact with the mould wall behind the moving melt front resulting in a solid layer of material building up[30]. The layer grows in thickness to a constant thickness that is maintained during the mould-filling phase. The velocity profile indicates that the maximum shear rate occurs a small distance from the solid layer due to the non-isothermal flow nature. When the mould cavity is full the cooling process continues and the material at the centre of the mould cavity cools and solidifies. Solidification happens during the holding time with a constant holding pressure that prevents the moulded component from shrinking by further movement of the core material. It is not often that one gets to identify all the layers shown in Figure 2.13. In most moulded components three layers are observed: the two solid layers and the core. The thickness of these layers can be altered by changing the melt temperature, mould temperature or injection speed.

Fibre orientation is affected by the flows that happen in the mould and results in anisotropy of mechanical properties. Fibres frequently align in the flow direction (along the length of the mould) in the solid layers while the orientation is random in the core with some fibres aligned along the fountain flow. The diverging flow encourages fibres to orientate transverse to the mould flow. Fibre orientation is also dependent on the component geometry, fibre length and fibre concentration[32]. Mechanical properties are strongly affected by fibre orientation, hence it is important to be able to predict fibre orientation in moulded components.

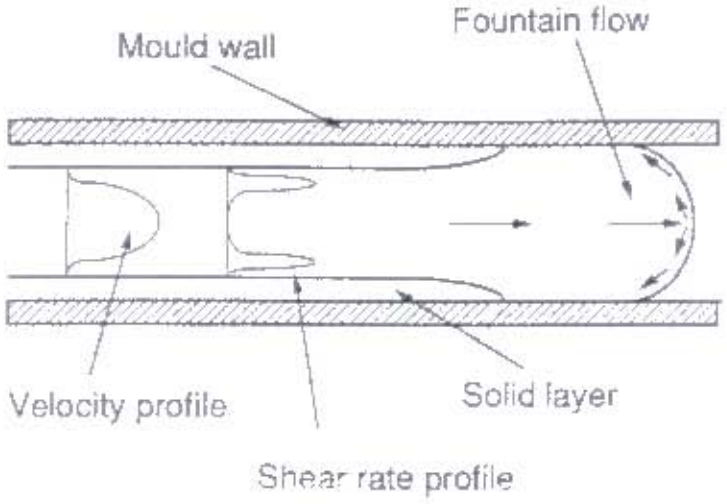

Figure 2.13: *Schematic representation of the flow profile, velocity and shear rate patterns in the mould filling stage*[16].

The fibre length influences the orientation of the fibres depending on the fibre concentration and the component geometry. There are different regions of fibre concentration in the moulded component: dilute region, semi-concentrated region and concentrated region. Mechanical properties increase with an increase in the fibre concentration to a saturation point. As the fibre concentration increases more fibres break because of increased fibre-fibre and fibre-mould wall interactions. Fibre breakage is high in the concentrated region and low in the semi-concentrated region. Fibres rotate in the melt and interact with each other and with the mould wall. However, in the dilute region there are less fibres and enough space for fibres to rotate without interacting with each other. The shorter the fibres the more chances there are to execute a free rotation without hitting the mould wall.

2.3.2 Mould Construction

The design and construction of injection moulds are based on product specifications. Material characteristics also influence the design of the mould.

The mould design for reinforced polymers must ensure minimum possible fibre breakages and mould wearing[16,33,34]. The design process is vital since it determines the quality of injection-moulded component[35]. Polymers and polymer composites shrink when cooling causing a mismatch in the assembly of the moulded parts. The shrinkage effect can be minimised if included in the design stage i.e. mould cavity design dimensions have to be larger than the actual component dimensions.

One major defect that is encountered with bad designs is jetting (see Figure 2.14) caused by die swelling[16]. Jetting is the major source of weld lines in moulded components. Unlike bad positioning of injection points in the component, jetting produces a multiple of unwanted weld lines. The designer should design to prevent jetting in the components to avoid a compromise in the mechanical properties. Increasing the diameter of the sprue and designing moulds with large gates can minimise or eliminate jetting in moulded components.

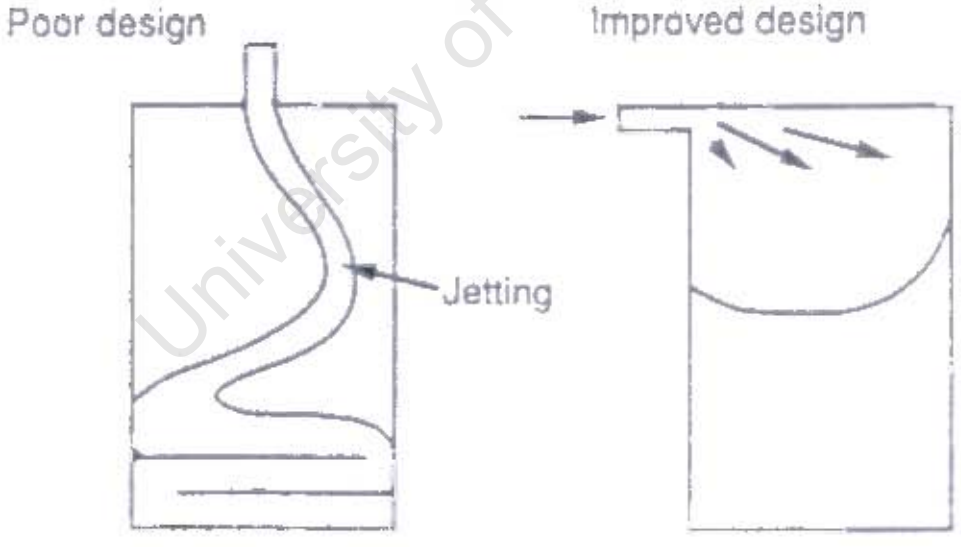

Figure 2.14: *Mould modification to eliminate jetting*[16].

Other defects are a result of a combination of performance of the injection-moulding machine, mould design, and processing conditions. These include dimensional and functional failures due to shrinkage, warpage and twist due to high temperature differences at the end of filling, cracking and distortion due to residual stresses, and flashes due to poor mould control.

2.3.3 Component Cooling Time

In addition to good mould design and processing conditions, the cooling time is the most commercially important aspect in the production of injection-moulded components. Mould design and the injection moulding conditions are planned around the component cooling time since it affects the productivity and the quality of the moulded components[36]. The injection speed and the holding time are the main factors that determine the cooling time of the moulded component. Residual stresses are formed in the moulded component as a result of differential cooling in various layers of the component part[31]. Components that are cooled rapidly form rigid layers in the surface while the core is still warm. This puts compressive stresses in the surface of the component and tensile stresses in the core. Residual stresses are also formed during mould packing as a result of excessive holding pressures. This can cause overloading in the core of the component part, which can lead to stress cracking after the component has cooled. Stress cracking is induced by the cooling of the component under high internal pressures and tensile stresses in the skin surface[31]. It is vital to regulate cooling time control during injection moulding processes.

2.4 MECHANICAL TESTS

All materials require some degree of standard testing to ensure the fitness for the desired application. There are various standard test methods introduced to determine the mechanical behaviour of materials. This section will briefly discuss some of the test methods mostly used, namely: tension testing, 3-point bend testing, Izod and Charpy impact testing, and drop weight impact testing. These methods are employed in industry to develop mechanical property data mainly taken at a short period of time at standard temperature and strain rates[6]. However, the testing conditions are dependent on the end requirements of the design. Tests can be conducted at room temperature, elevated temperatures, low temperatures and at low and high strain rates[5].

2.4.1 Tension Testing

The tensile test is a common deformation test used to measure the strength of material. This is a measure of the resistance of material to stresses pulling in opposite directions. This test is not a true depiction of the force that is subjected on materials in existing everyday situations but it is mainly used for material characterisation. The test specimens are dumbbell shaped which induces failure to occur at the gauge length preferentially at the middle of the specimen. The stress, strain, modulus and elongation are the material parameters obtained from the tensile test. The plot in Figure 2.15 represents the important parameters in the stress-strain relationship. The straight-line section represents the elastic region beyond which permanent deformation in the material occurs. The specimen gets longer and narrower (necking) when pulled in tension. Errors can be obtained in the measured elongation of the specimen, depending on the efficiency of the clamps. Movement in the clamping region lead to error in elongation and the error can be large when the overall elongation in the

specimen is small[37]. Figure 2.15 shows the stress-strain curves of long chain high crystallinity polypropylene (iPP-L), low crystallinity polypropylene (PP-L) and ethylene-propylene di-block copolymer (EP-L). It can be seen that the stress-strain properties change with material structure.

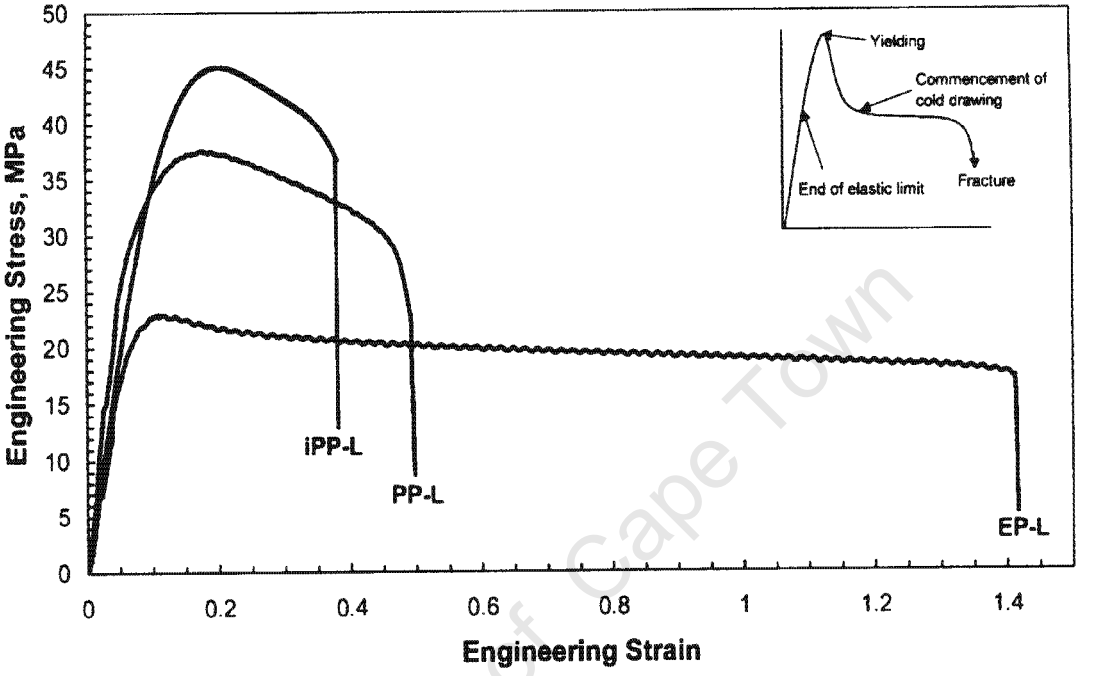

Figure 2.15: *The engineering stress-strain curves for long chain polymers, iPP-L for isotactic polypropylene; PP-L for low crystallinity polypropylene and EP-L for ethylene-propylene di-block*[38].

2.4.2 Flexural Testing

Materials are subjected to flexural testing in order to determine the mechanical behaviour when a combination of tensile and compressive forces is applied [4]. The test specimen used is a rectangular bar, which is placed on fixed supports near each end. The load is applied from the top at the middle of the specimen.

The top part of the specimen is under compression and the bottom part is under tension. There are two types of flexural tests, namely, 3-point and 4-point bend tests. These tests give the flexural stress (σ), deflection and the flexural modulus (E) of the material and the following equations are used to calculate these parameters.

$$\text{Flexural stress, } \sigma = \frac{3WL}{2bd^2} \quad (1)$$

$$\text{Flexural modulus, } E = \frac{L^3 m}{4bd^3} \quad (2)$$

where, W, L, b, d and m are the load, support span, specimen width, specimen thickness and slope of the load vs. deflection curve, respectively.

2.4.3 Impact Testing

Impact tests are used to measure the ability of a material to withstand a sudden sharp blow[37]. The damage that occurs after the blow is strongly dependent on the: shape, density, mass, hardness, velocity, and initial height of the impacting object as well as the properties of the target material[39]. There are four standard impact tests, viz. Izod, Charpy, drop weight, and tensile-impact, used to compare the impact behaviour of materials. The Izod, Charpy and tensile-impact tests are performed using the same machine with different pendulums and clamps.

The Izod and Charpy tests cannot be completely considered as different tests. The two tests differ in the manner in which the specimens are positioned and the direction of the notch during testing. The Izod specimen is clamped vertically at

its lower end with a notch facing the pendulum while the Charpy specimen is not clamped and it is positioned horizontally with the notch facing away from the pendulum[40]. Errors associated with these two tests result from the clamping pressure and the sharpness of the notching tool[37].

The tensile-impact specimen, unlike the Izod and Charpy specimens, is clamped and notched at both ends. One side of the specimen has a special shaped clamp on which the pendulum impacts thereby deforming the specimen in tension. Errors occur at the clamping region where there are rapid acceleration and momentum transfer between the clamp and the striker.

The drop weight impact test is different from the three impact tests described above. During drop-weight testing, the specimen is clamped horizontally and struck by a weight falling vertically (free fall) from a certain height guided by a rail[40]. This test is performed to simulate the impact that the material experience when struck by a dropped tool or by runway debris[41]. The velocity of the falling weight depends on the height while the energy and momentum are dependent on the mass. This test can be applied on moulded components ready for use. The load on the specimen is measured continuously as function of time or deflection for the entire duration of impact[42]. This can be seen in Figure 2.16 where the plot of load versus deflection shows fluctuations in the load when the crack propagates through fibres and matrix for 50% w/w long fibre reinforced polyamide 6-6 (50LFPA). The unfilled polyamide 6-6 (PA 6-6) plot shows less fluctuation since it constitutes only of polymer resin. The arrow in the graph indicates crack initiation[43].

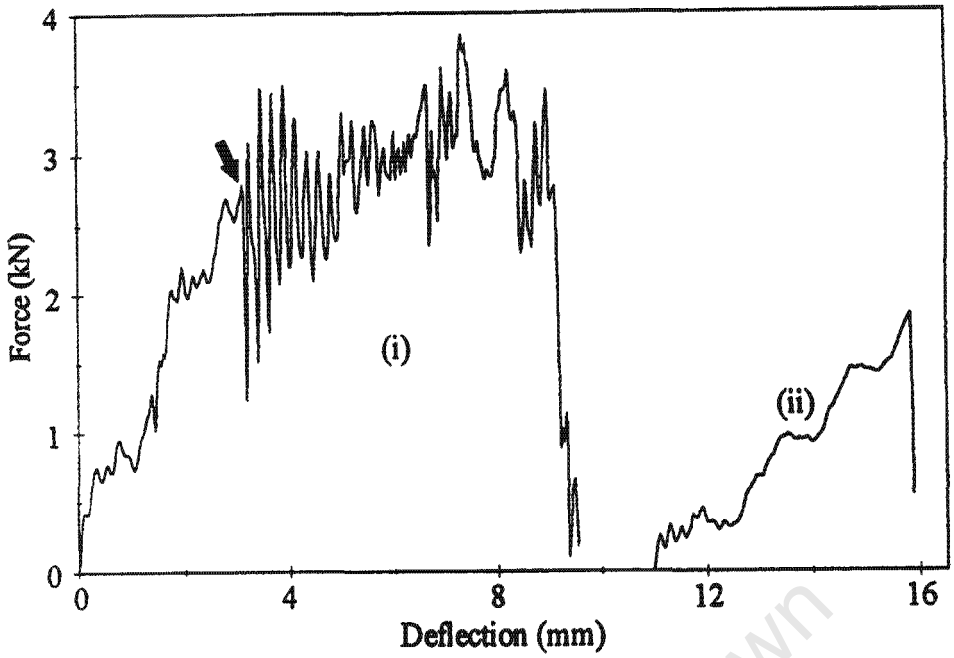

Figure 2.16: *Force vs. deflection curves for (i) 50LFPA and (ii) PA 6-6*[43].

2.5 FAILURE MECHANISMS

The mechanisms by which composites fail are complex due to the anisotropy and heterogeneity of the material. The properties of the constituents, bonding efficiency across the interface, fibre volume fraction, fibre length and fibre orientation are some of the factors that influence failure in polymer composites[32,39]. The mechanisms of failure are mostly studied based on crack propagation resulting in fracture of the component. These mechanisms can be divided into matrix related and fibre related failure.

- Matrix related failure mechanisms are:
  - Crazing.
  - Voiding.

- Shear yielding.
- Matrix fracture.
- Plastic deformation.

- Fibre related failure mechanisms.

  - Debonding.
  - Pullout.
  - Fibre fracture.

2.5.1 Matrix Related Failure Mechanisms

These failure mechanisms cannot be separated since they occur at the same time or one causes the other. Crazing is caused by the plastic deformation in glassy polymers. This is the formation of thin sheets perpendicular to the principal stress axis, which contains fibrils[44]. Crazing lead to cracking and breakage of the specimen and is largely seen in rubber toughened plastics. Shear banding refers to the local deformation of the materials at 45 ^{0} to the stress direction. This results in a high degree of polymer chain orientation. These mechanisms start by plastic deformation and can result in matrix cracking leading to the complete failure of the material[44]. Voids on the other hand can occur in unfilled and filled materials. Voids are normally processing defects and can also be found at the fibre end in short fibre composites. This is because the broken fibre ends in short fibre composites are not sized so they cause localized stresses. Voids can lead to a catastrophic failure of the material by void coalescence.

2.5.2 Fibre Related Failure Mechanisms

For short fibre composites, there is a critical fibre length l_c below which the fibre does not carry the load. Fibres with lengths less than the critical length do not break when the load is applied. For short fibres the applied stress might not reach the fibre fracture stress and failure will occur by fibre-matrix debonding and fibre pullout. The diagram in Figure 2.17 shows that the stress increases from each end of the fibre. If the fibre length is greater than or equal to l_c the fracture stress (σ_f) will be reached between B and C resulting in failure along the fibre length. For a fibre with cross sectional area d and length l that is loaded through the surrounding matrix, with shear strength τ at the interface and the longitudinal tensile stress σ in the fibre, the fracture strength is only reached when:

$$\frac{l_c}{2} = \frac{d\sigma_f}{4\tau} \Rightarrow l_c = \frac{d\sigma_f}{2\tau}, \left(\frac{l_c}{2} \text{ is the transfer length}\right)^{45}.$$

The stress transfer from the fibre to the matrix occurs by a shear transfer mechanism. The efficiency of the transfer is dependent on the shear strength and the orientation of the fibre relative to the stress direction[46]. The stronger the interfacial bond the more stress transfer from the matrix to the fibre. This implies that the value of l_c depends on the shear strength. In situations where the fibre is orientated parallel to the tensile stress direction, fibre fracture and fibre-matrix debonding will take place. When the fibre is aligned transverse to the tensile stress direction, there is no fibre fracture that occurs but matrix cracking takes place.

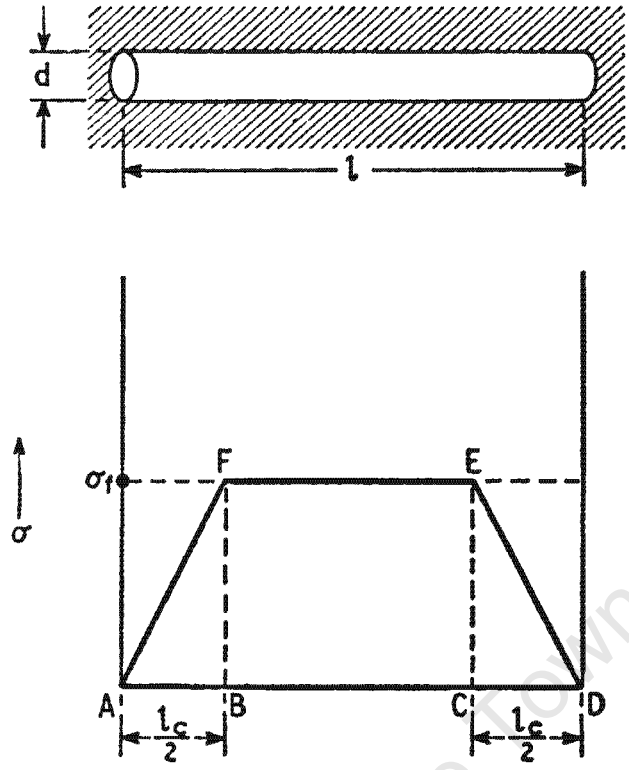

Figure 2.17: *A diagram representing the stress distribution on transfer length of the fibre*[45].

2.5.3 Theoretical Models for the Prediction of the Elastic Properties

The elastic properties of the composite can be predicted by the rule of mixtures. The rule of mixture is based on the assumption that the strain ε_1 in the matrix will be the same as that in the fibre if the bond between the fibre and the matrix is perfect[17]. The stresses in the fibres and the matrix σ_f and σ_m, respectively, are given approximately by:

$$\sigma_f = E_f \varepsilon_1 \qquad (3)$$

and $\sigma_m = E_m \varepsilon_1$ (4)

The elastic modulus of the fibre E_f is greater than the elastic modulus of the matrix E_m. Therefore, the stress in the fibres is greater than the stress in the matrix (the underlying basis of fibre reinforcement). For a composite with total cross-sectional area A, the rule of mixture is expressed as:

$$E_c = E_f V_f + E_m V_m \quad (5)$$

where V_f and V_m are the fibre volume fraction and the matrix volume fraction, respectively. Since $V_m = 1 - V_f$,

$$E_c = E_f V_f + E_m (1 - V_f) \quad (6)$$

Equation (5) is applicable in the prediction of the elastic modulus of long fibre composites because it assumes that the fibres are so long that the effects of the fibre ends can be neglected. Fibre length and fibre orientation play an important role in short fibre composites. Therefore, the rule of mixture needs to be modified to include the fibre length correlation factor and the fibre orientation factor. However, the reinforcing efficiency of short fibres is less than that of long fibres[47].

The elastic properties of isotropic and homogeneous composites can be predicted using the Kerner equation (see equation 7). It is assumed that the included components are spherical and uniformly distributed in a uniform medium[7].

$$E_c / E_m = 1 + [15(1 - \nu_m)/(8 - 10\nu_m)][V_f /(1 - V_f)] \quad (7)$$

where ν_m is the Poisson's ratio for the matrix.

Equation 7 was modified to include a factor (ϕ), which is based on the maximum volumetric packing fraction for spheres in a matrix. Lewis and Nielsen modified the Kerner equation and expressed it as:

$$E_c / E_m = (1 + ABV_f)/(1 - B\phi V_f)] \quad (8)$$

where $(A = (7 - 5\nu_m)/(8 - 10\nu_m)$

and $B = [(E_f / E_m) - 1]/[(E_f / E_{m)}) + A]$

Modification of the Kerner equation was also done to include the geometry of the reinforcing component. Ramsteiner and Theysohn showed that a good approximation of the experimental results for the Young's Modulus can be achieved if the shape factor is introduced. The shape factors are 2, 7 and 16 for spherical fillers, fibrous wollastonite and the platy talc fillers, respectively (in ref 7).

2.5.4 Crack Propagation and Void Formation

Figure 2.18 summarises the mechanisms of failure in discontinuous fibre reinforced thermoplastic composites. However, failure in thermoplastic

composites does not always occur by way of propagation of a single crack across the component part. Composite materials often accumulate damage in a general rather than localized way. Figure 2.19 shows an example of the mechanism of failure that occurs by void formation, void coalescence and fracture. A polymer composite under applied load fail by filler-matrix debonding resulting in void formation (I. in Figure 2.19). The voids formed around the fibres or particulate fillers grow in the stress direction forming dimple-like holes, which then coalesce due to plastic deformation and shear conditions resulting in fracture (II. and III.). The interface plays a major role in this kind of mechanism. Strong interfaces will lead to a catastrophic failure, i.e. the composite will fail by matrix failure in the case of particulate filled composites while fibre breakage in addition to matrix cracking will occur in the case of fibre reinforced composites.

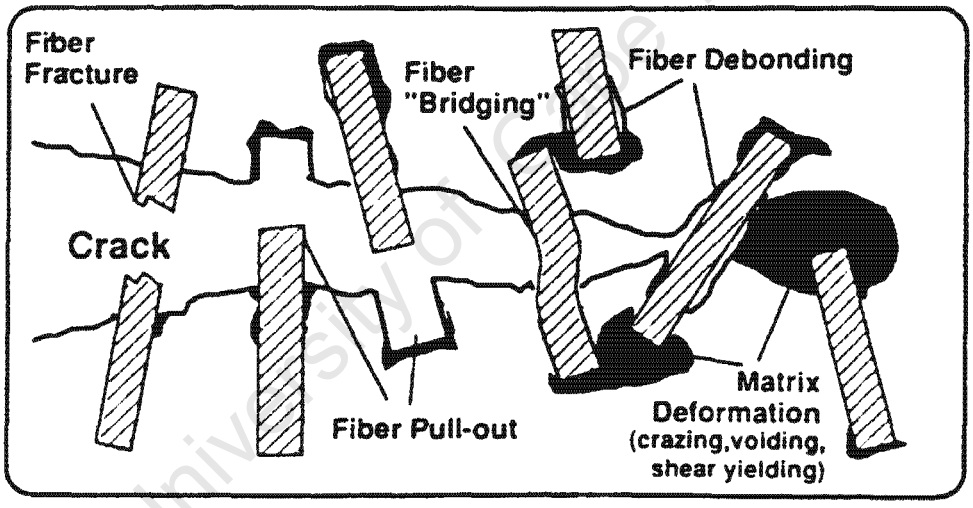

Figure 2.18: *Failure mechanisms in short fibre reinforced thermoplastics*[15].

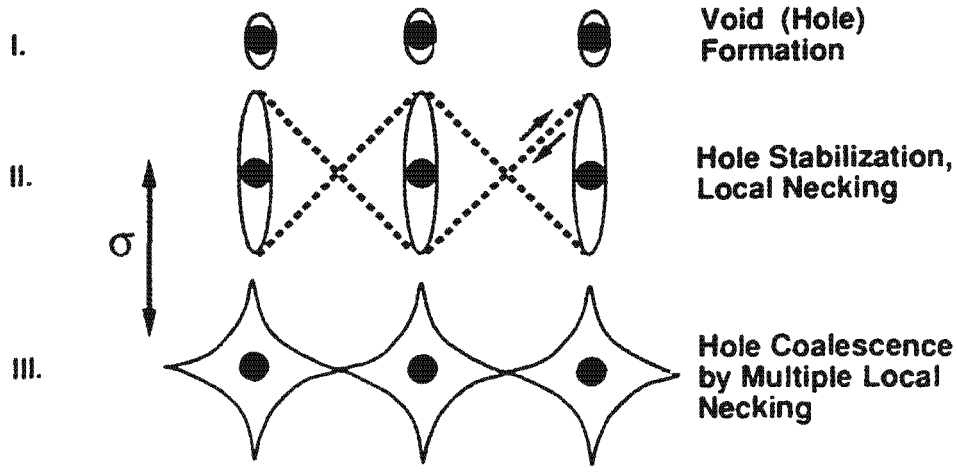

Figure 2.19: *Crack initiation in ductile matrix composites*[15].

2.5.5 Fibre Volume Fraction and Fibre Length

Long fibre composites have higher tensile, flexural and impact strengths compared to short fibre composites. However, short fibre composites are gaining interest in the rapid mass production engineering industries. This can be attributed to their ease of processing by processes such as extrusion compounding and injection moulding[48]. It is therefore said that fibre lengths influence the mechanical properties (strength and modulus) of composite materials. Fibre length, however, has a combined effect with fibre volume fraction on the properties of the materials since it decreases with an increase in fibre volume fraction[48,49,50,51,52]. The decrease in fibre length is a result of an increase in interaction between fibres as their concentration is increased. This interaction leads to an increase in fibre breakage hence the decrease in the fibre length. Figures 2.20, 2.21 and 2.22 show the relationship between the fibre length, fibre volume fraction, composite modulus and failure strain. It was also established that the impact energy is dependent on the fibre length and volume fraction[51].

Figure 2.20 shows the increase in the tensile modulus as a result of an increase in both the fibre length and the fibre volume fraction. The increase in the modulus is minimal when the fibre lengths are very small (< 0.1 mm) or large (> 10 mm). There is a critical length after which the modulus reaches a saturation level (± 1 mm in Figure 2.20).

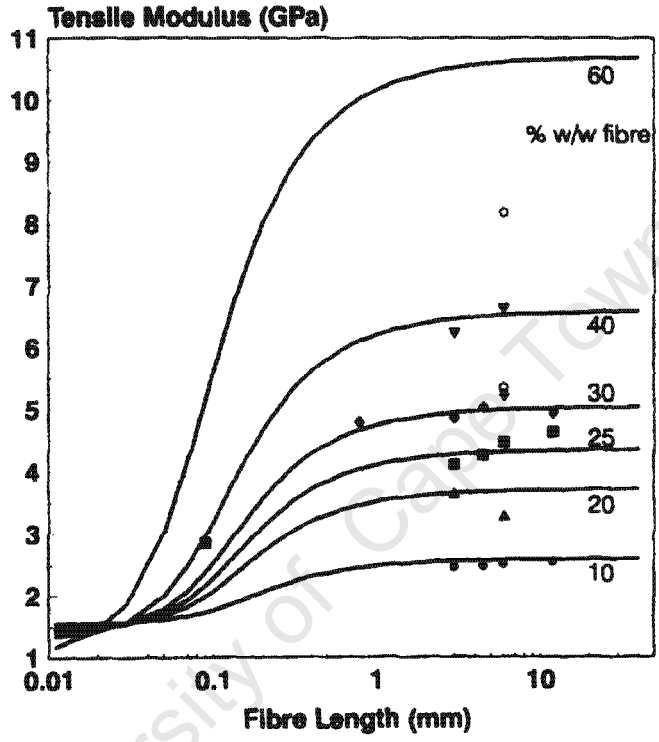

Figure 2.20: *Plots indicating the increase in tensile modulus with fibre length and fibre volume fraction*[49].

As mentioned in the paragraph above, the fibre length is related to fibre volume fraction (see Figure 2.21). The mean fibre length decreases with the fibre volume fraction. The stiffness of the material increases as the fibre volume fraction is increased. This can be seen in Figures 2.20 and 2.22 where the modulus is increasing and the failure strain of the composites is decreasing, respectively, with an increase in the fibre volume fraction. In many cases the flexural modulus and strength are higher than the tensile modulus and strength[53].

Higher flexural moduli and strengths could be a result of the different forces that the material is subjected to in bending, i.e. the top part of the material is in compression while the bottom part is in tension. In fibre-reinforced materials, fibre orientation also plays a major role. Fibres are aligned transverse to the flexural stress in the skin of the bar specimen and randomly aligned in the core. Higher stresses are therefore required for a crack to propagate through the skin of the bar specimen[54]. The relationship between the flexural and tensile strength and the flexural and tensile modulus can be seen in Figures 2.23 and 2.24, respectively. It is apparent that the flexural properties are higher than the tensile properties.

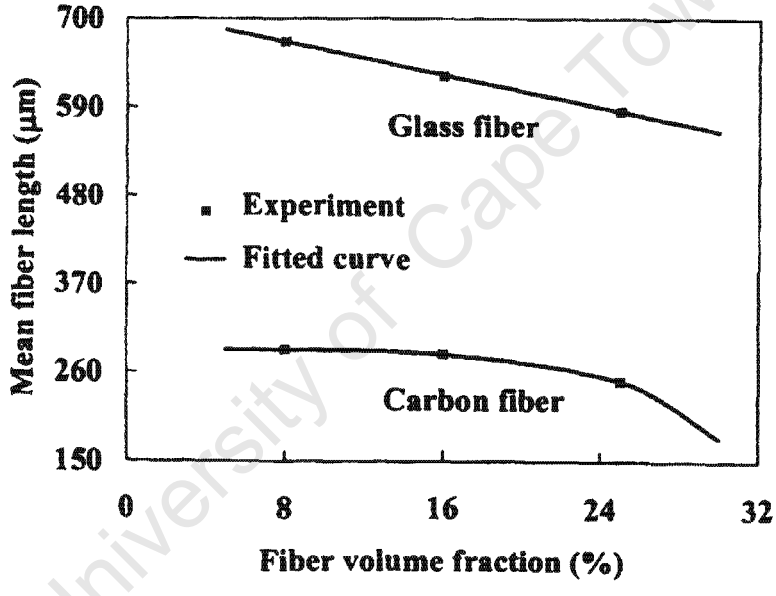

Figure 2.21: *Mean fibre length vs. fibre volume fraction for short glass fibre-reinforced polypropylene and short carbon fibre reinforced polypropylene*[48].

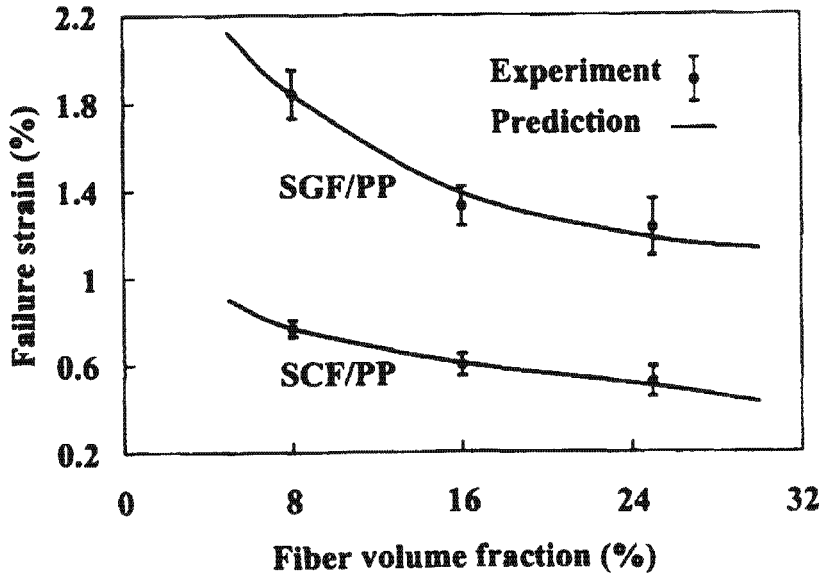

Figure 2.22: *Failure strain vs. fibre volume fraction for short glass fibre-reinforced polypropylene and short carbon fibre reinforced polypropylene*[48].

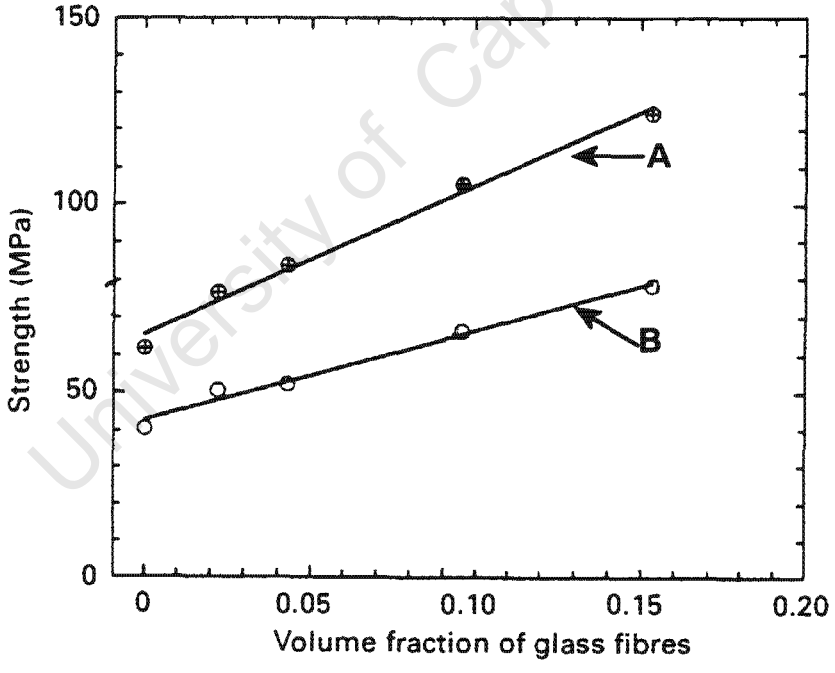

Figure 2.23: *(A) Tensile and (B) flexural strength vs. the volume fraction of glass fibres*[13].

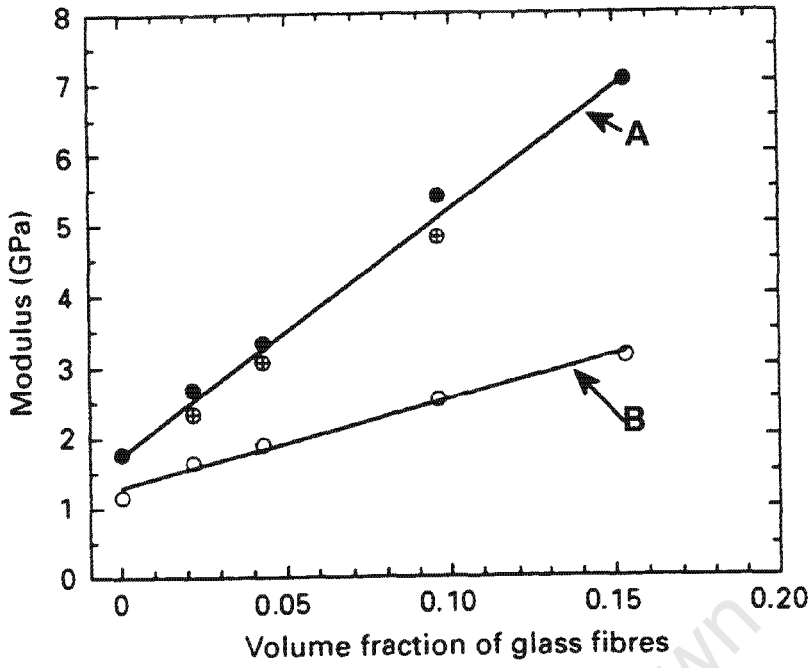

Figure 2.24: *(A) Tensile and (B) flexural modulus vs. the volume fraction of glass fibres*[13].

2.5.6 Strain Rate and Temperature

Strain rate has an influence on the failure mechanisms and the mechanical properties of composites materials[55,56]. The increase in the strain rate results in an increase in the strength and the impact energy of the material[51]. This behaviour can be attributed to the embrittlement of the matrix resin due to high velocity conditions[13]. Temperature has also been proven to cause mechanical property changes in composites materials. The change in test temperature, however, only affects the matrix and the fibre-matrix interface properties[57]. The mechanisms of failure can change from crazing or cracking to plastic deformation by increasing the test temperature. This results in an increase in the impact strength but a reduction in the tensile strength. The effect of strain rate and temperature can be seen in Figures 2.25 and 2.26, respectively.

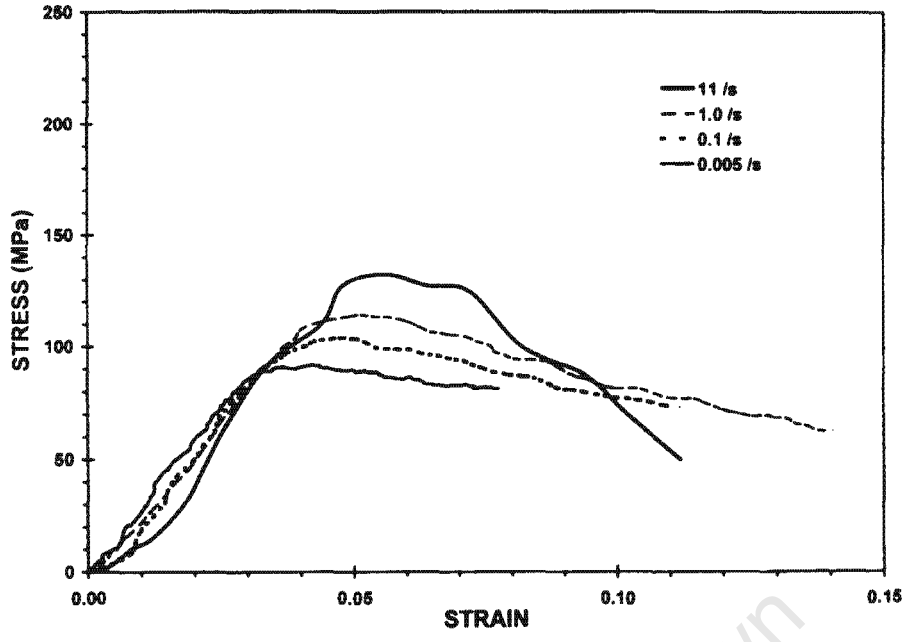

Figure 2.25: *Variation of stress with strain for the short fibre composite with vinylester resin at various strain rates*[55].

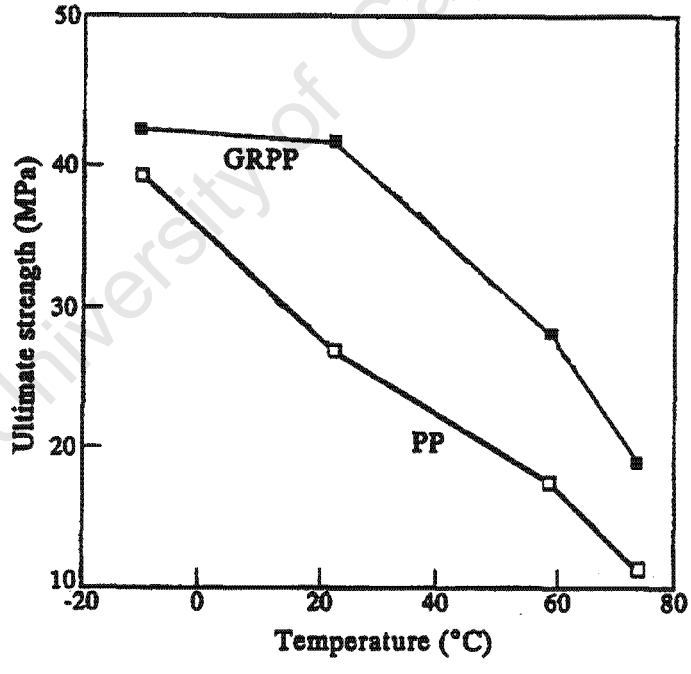

Figure 2.26: *Ultimate tensile strength vs. temperature for polypropylene and short glass fibre-reinforced polypropylene*[46].

2.5.7 Fractographic Studies

Micro-structural elements such as fibre orientation, matrix deformation and the fibre-matrix interface can be investigated by making use of light and scanning electron microscopy[44,58,59]. The microstructure of polymers changes with the addition of fillers, impact modifiers and test conditions. Fractographic features and cracking mechanisms can be revealed by microscopy[60]. The micrographs in Figures 2.27 and 2.28 were taken using a light- (LM) and a scanning electron microscope (SEM). Figure 2.27 shows the mechanism of crack propagation by interfacial voiding, matrix failure and fibre breakage for short glass fibre reinforced poly (ethylene terephthalate) composite. If the stress required for fibre breakage is higher than the interface strength, the crack will propagate by fibre-matrix debonding or matrix tearing resulting in fibre pullout in the composite. It can also be seen in Figure 2.27 that a notch acts as a site of crack initiation.

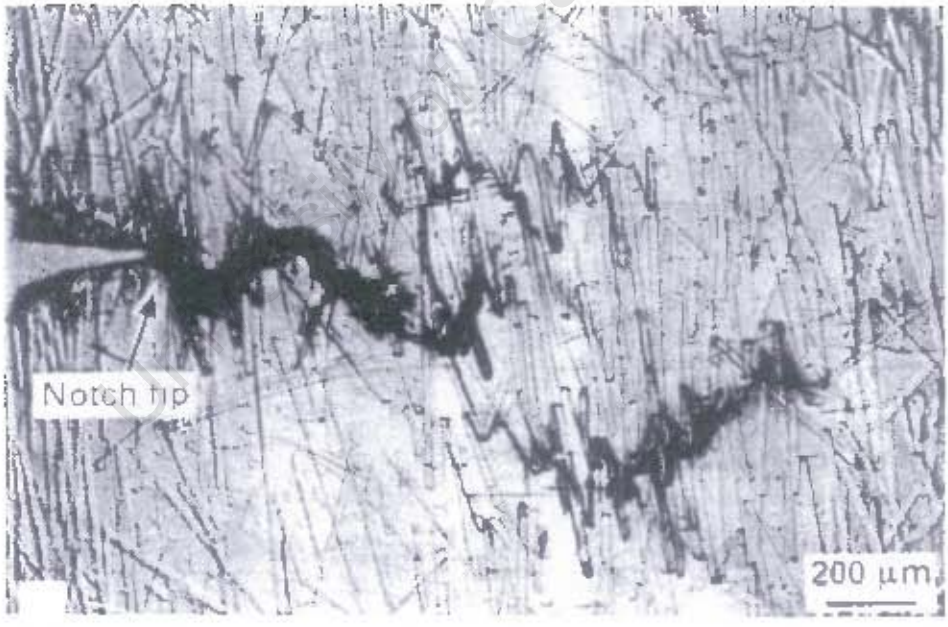

Figure 2.27: *Micrograph showing the fracture pattern of short glass fibre reinforced poly (ethylene terephthalate) composite taken under the light microscope*[61].

Figure 2.28 shows SEM micrographs of the fractured surfaces of two short glass fibres reinforced composites with different matrix adhesion properties. The nature of the fibre and the matrix and the fibre-matrix bond are the major factors that affect the fracture behaviour of composite materials. Fractographic studies are vital in determining the modes of failure such as matrix cracking, fibre breakage, fibre-matrix interface bond failure and void growth[44]. These modes of failure are easily observed using SEM, however, their initiation is not easily identified. The micrographs (A) and (B) in Figure 2.28 show a relatively weak interface as can be see by the clean glass fibres that indicate failure at the fibre-matrix interface. The holes are a result of the fibre pullout mechanism of failure. A different failure mode is observed in micrographs (C) and (D) where the fibres are still covered with the resin after the composite failure. This is indicative of a strong interface between the fibres and the matrix. There are other types of fractures such as cone fracture, radial cracking that can seen with the naked eye on drop-weight impact test plate specimens[62].

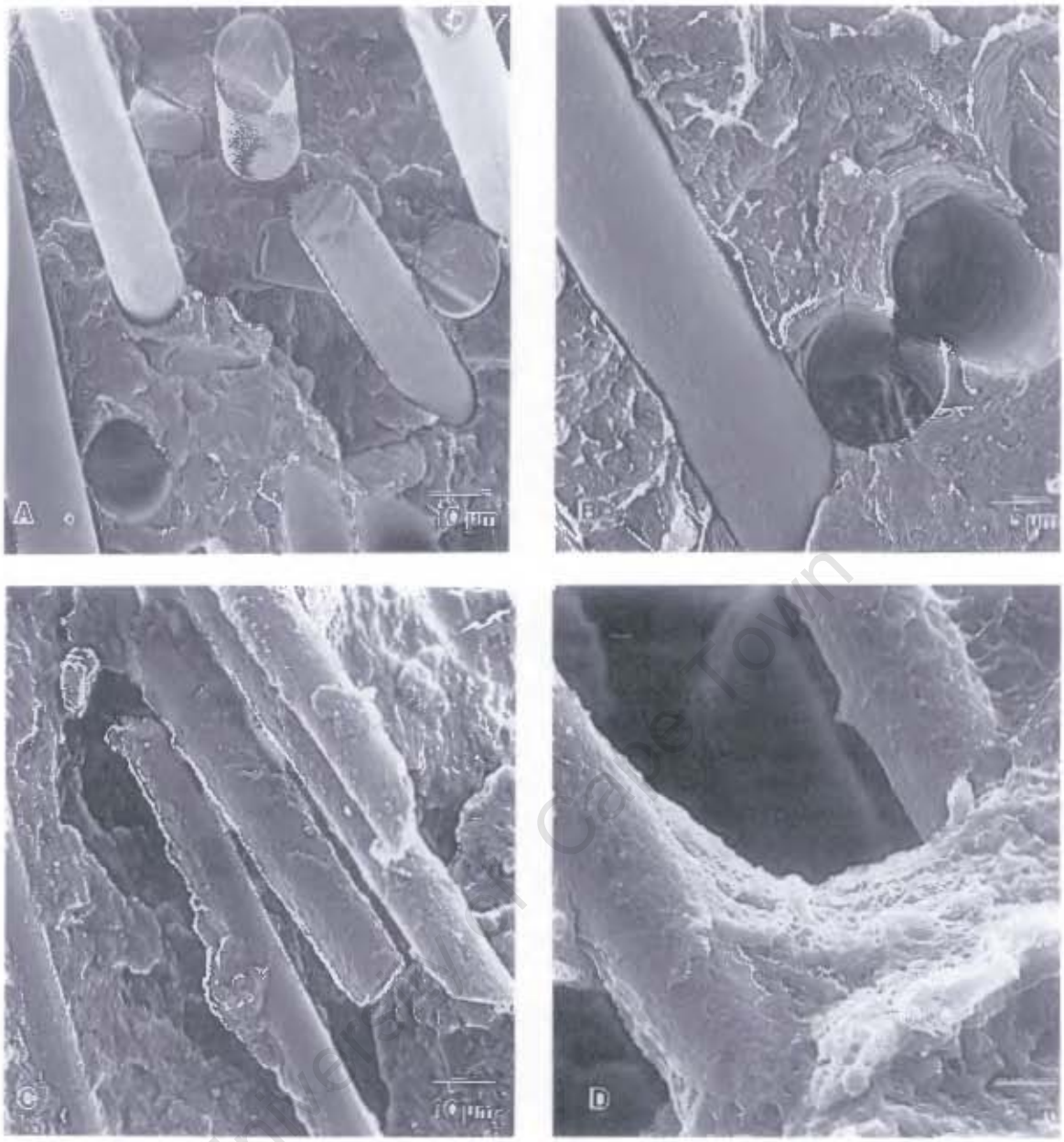

Figure 2.28: *SEM micrographs of the fracture surfaces showing the two glass fibre composites [(A and B) and (C and D)] with different adhesion properties*[40].

CHAPTER 3

EXPERIMENTAL TECHNIQUES

This chapter gives an outline of all the experiments conducted for the purpose of this research project. Several mechanical tests were conducted in order to carry out the objectives of this research work. The polymer composite specimens were subjected to tensile, flexural (three-point bend) and impact (Izod, Charpy and drop-weight) tests. The fractured specimens were observed under the light and scanning electron microscope to investigate the fractographic features and to study the mechanisms of failure. The experimental procedure followed when conducting the mechanical tests and microscopic examinations, are discussed. This chapter is aimed at equipping the readers with an understanding as to how the results of this research work, outlined in chapter four, were obtained.

3.1 MATERIALS INVESTIGATED

This research study involved five different types of materials that allowed for a comparison between polypropylene and polyamide 6-6 composites. Table 3.1 below gives a summary of the materials used including their industrially designated names. These materials were used to determine the mechanical response and to investigate the failure mechanisms of thermoplastic composites at various test conditions. The same base grades were used in the composite formulations. All the materials were provided in the form of pellets and the composites materials were already compounded into 30% short glass fibre or talc filled composites. The physical and mechanical properties of the materials in Table 3.2 were provided by PLASTAMID Pty Ltd. The tensile strength of the materials was obtained at a test speed of 50 mm/min. The test speed used to obtain the tensile modulus was 1 mm/min. Properties that are not provided in Table 3.2 were not available from PLASTAMID Pty Ltd.

Table 3.1: *Materials investigated.*

Description	***Grade***	***Designation***
Unfilled polypropylene	PP1100M	PP1100M
Unfilled polyamide 6-6	Zytel EFE1147	EFE1147
30% w/w talc filled polypropylene	PH3030 (A Blend of PH3020 and PH3040)	30Talc/PP
30% w/w short glass fibre reinforced polypropylene	PH2130	30SGFRPP
30% w/w short glass fibre reinforced polyamide 6-6	Zytel 70G30	30SGFRPA 6-6

Table 3.2: *Physical and mechanical properties of materials*

	PP1100M	EFE1147	PH3030	PH2130	ZYTEL 70 G30
Physical properties					
Mass density (g/cm^3)	0.91	1.14	1.15	1.14	1.37
Melting point (^{o}C)	163	261	163	163	263
MFI (g/10 min)	8.5	-	5	3	-
Mechanical properties					
Tensile strength (MPa)	35	77	33	?	192
Elongation to break (%)	-	>20%	-	4%	3.3%
Elongation @ yield	9%	-	6%	-	-
Tensile Elastic modulus (GPa)	1.5	1.6	1.9	4.8	10
Izod impact (notched) (kJ/m^2)	3.5	5.8	45 J/m	55 J/m	13
Flexural modulus (GPa)	1.7	2.6	2.3	3.9	9.4

Mechanical tests, namely tension and impact (Izod, Charpy and drop-weight), were conducted for this purpose. These tests were performed at room temperature except for the drop-weight tests that were conducted at –35 ^{O}C and 20 ^{O}C to simulate different environmental conditions. The drop-weight test was also conducted at various test speeds to determine the influence of strain rate on the behaviour of thermoplastic matrix composites. Unfilled thermoplastic polymers were used to investigate the influence of fillers on the mechanical properties and on the mechanisms of failure.

3.2 SPECIMEN PREPARATION

All the specimens used in this research work were manufactured by an injection moulding process. Two different injection moulding techniques were used for the

specimen preparation. An automated injection moulding machine and a manually operated injection moulding machine were used in order to determine the effect of processing technique on the mechanical properties of the moulded components. The automated injection moulding machine was used for moulding polypropylene- and polyamide-based materials while the manually operated machine could only be used for the moulding of polypropylene-based materials. This is because the manually operated injection moulding machine has a maximum temperature that is lower than the polyamide 6-6 moulding temperature. For this reason, a comparison of the mechanical properties of the materials prepared by the two injection moulding machines was only done on polypropylene-based materials.

Polyamide required to be treated before moulding to reduce moisture since it is known to absorb up to 10% moisture. The polymer was dried in an oven before injection moulding in order to remove the absorbed moisture. Experiments were conducted to determine the moisture uptake of polyamide 6-6 and short glass fibre reinforced polyamide 6-6. The equipment used was a Karl Fischer titration machine. A small piece of material was placed in a small beaker containing a solution of methanol 205 and hydranol composite 5. The percentage moisture uptake was monitored over a particular time interval. These experiments were performed at PLASTAMID (Pty) Ltd.

3.2.1 Automated Injection Moulding Machine

The machine used was a commercial injection moulding machine used for the preparation of tests specimens at PLASTAMID (Pty) Ltd. This machine was used to mould dumbbell shaped tensile test specimens and circular drop weight test plates. Specimens for Izod and Charpy impact tests were cut from the gauge section of the tensile dumbbell shaped specimens. The polymer materials required specific machine settings during injection moulding since the melt

temperatures and melt flow indices are different. Different settings were tried to obtain the proper settings that give the best moulded specimens free of flash and warping. The machine settings in Table 3.3 below show the processing conditions for polypropylene and polyamide 6-6 composites. After injection moulding, the polyamide specimens were stored in a desiccator to avoid moisture absorption that may cause changes in the mechanical response.

Table 3.3: *Injection mould machine settings.*

Parameters	***Polypropylene-based materials***	***Polyamide 6-6 based materials***
Temperature profile (°C):		
Mould	40	100
Nozzle	220	290
Metering zone	240	295
Transition zone	230	295
Feed zone	200	290
Injection speed (mm/s)	55	60
Injection pressure limit (100 bar)	120	100
Injection time (sec)	1.29	3.34
Maximum injection speed (160 mm/s)	113	160
Holding pressure (bar)	50	45
Post injection pressure time (sec)	40	16
Cooling time (sec)	20	12

3.2.2 Manually Operated Injection Moulding

A HERCUS PIM 20 injection moulder was used to prepare unfilled polypropylene, 30% w/w talc filled polypropylene and 30% w/w short glass fibre reinforced polypropylene. Figure 3.1 shows the non-commercial manually operated injection moulding machine available at the University of Cape Town. Polymer or polymer composite pellets were fed into the hopper (A) and the material was then heated to the required temperature in the barrel (B). The machine is fitted with a thermostat which prevents the barrel from overheating. Before moulding, the mould was placed in a bucket of boiling water to keep it hot and ready for moulding. Once the material in the barrel has reached the moulding temperature, the mould, which was placed on the stage (C), was filled with molten material from the nozzle of the machine through the sprue.

Two moulds were not available and were specifically designed and machined for the dumbbell tensile specimens and impact bar specimens. The moulds were made of mild steel (see Figure 3.2) and the design drawings appear in Appendix A. During injection moulding the melt enters the mould through the sprue, passing through the gates to fill the cavities. A constant pressure was maintained until the moulded component had solidified. The barrel temperature was set to 240 ^{O}C. The mould temperature, injection time and the holding time were estimated to be 60 ^{O}C, 3 seconds and 20 seconds, respectively. The mould is kept intact with eight screws to prevent it from opening due to the melt pressure during moulding. When the moulding cycle was complete, the mould was opened and the moulded component was ejected from the mould. The moulded component was released by pushing on the ejector plates thereby exposing the ejector pins and forcing the component out of the mould cavity. The specimens were separated at the gate section. The thickness of the gates was less than the specimen thickness to allow easy separation by breaking.

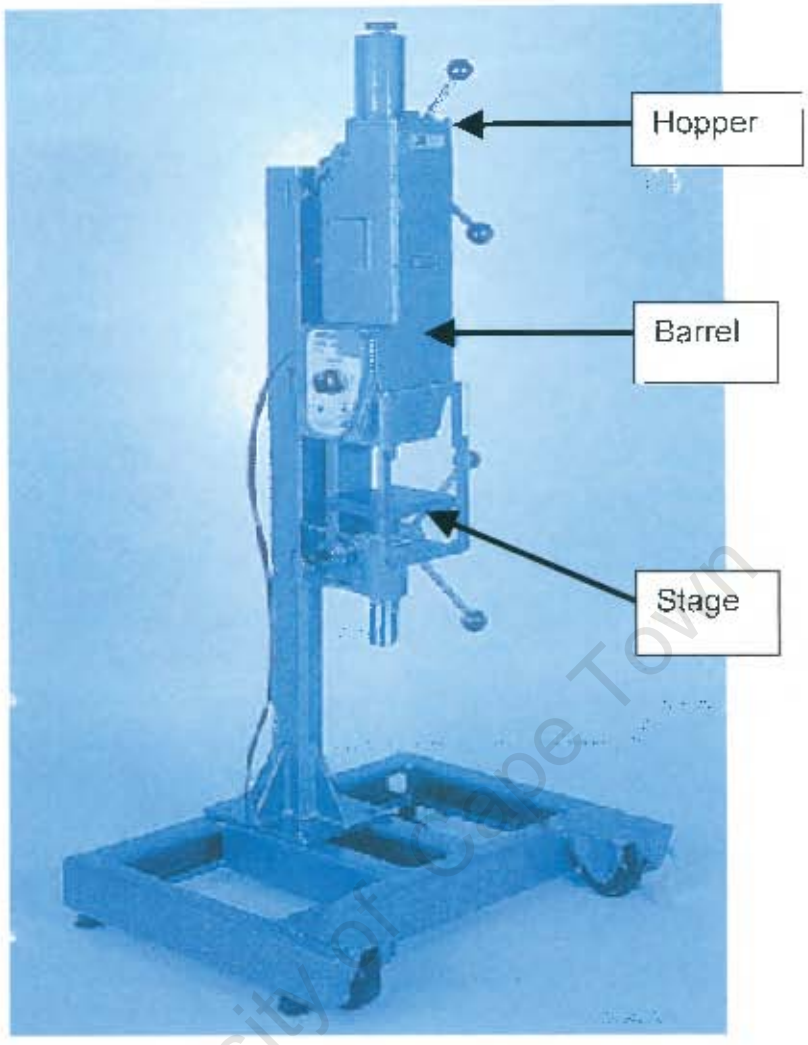

Figure 3.1: *HERCUS PIM 20 manually operated injection moulder.*

Figure 3.2 represents the impact bar and the dumbbell shaped tensile specimen moulds machined for injection moulding using the manually operated machine. The two moulds are almost identical with their mould cavities making the only distinction. The sprue (see Figure 3.2 A) and the gates (see Figure 3.2 B) in the two moulds were machined to the maximum possible size. The diameter of the sprue was limited by the nozzle diameter. The gates were large enough to ensure minimum fibre breakage and prevent jetting when the melt enters the mould cavities.

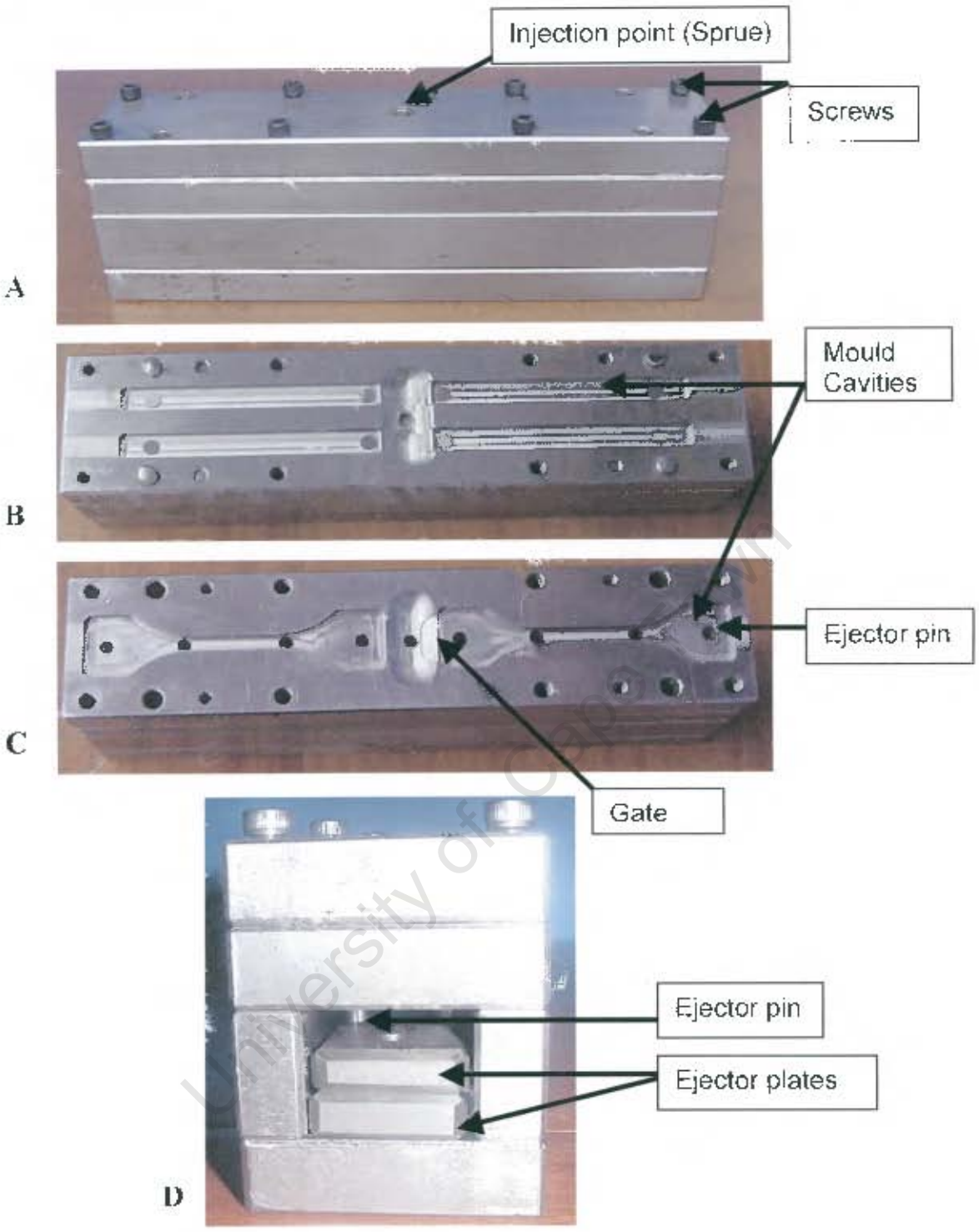

Figure 3.2: *Photographs of the moulds showing: (B) the impact bar and (C) tensile specimen moulds. (A) and (D) are the side views of the moulds. (B) is the inner section of the impact bar mould, (C) is the inner section of the tensile specimen mould.*

3.3 MECHANICAL TESTING

Several mechanical tests were conducted at room temperature to determine the mechanical properties of the polymer composites. The polymer composites were tested for tensile strength, tensile modulus, flexural strength, flexural modulus, Izod, Charpy and drop weight impact energy. All the tests were conducted at the University of Cape Town with the exception of the Izod and Charpy impact tests which were conducted at PLASTAMID (Pty) Ltd. The American Standard of Testing Methods (ASTM) was followed when conducting all the mechanical tests with the exception for the Charpy impact test. The pendulum for the Charpy test was used according to the International Standard Organisation (ISO). The fractured parts of the specimens were examined under light and scanning electron microscopy for the investigation of micro-structural features and failure mechanisms of thermoplastic matrix composites.

3.3.1 Tensile Testing

The tensile tests were performed by pulling the dumbbell shaped specimens in tension to the point of failure using the Zwick tensile tester (Figure 3.3). The ASTM standard D 638M was used. This test is mainly used for material characterisation. Tensile specimens prepared by the automated and manually operated injection moulder were tested. The dimensions of the specimens prepared using the automated machine were different from those prepared by the manually operated machine (see Table 3.4). Specimen parameters were entered into the computer and the software calculated the force and displacement of the material. The force and the displacement were used to calculate the stress and the strain in the material. The test speed was set at 50 mm/min for all types of specimens. Ten specimens were tested for each type of material. Figure 3.3

shows the tensile apparatus after performing a test on unfilled polypropylene (PP1100M).

Table 3.4: *Tensile specimen dimensions.*

Specimen parameter	***Automated machine (mm)***	***Manually operated machine (mm)***
Width (mm)	10	6.1
Thickness (mm)	4	3.3
Gauge length (mm)	85	41
Length (mm)	172	118

Figure 3.3: *Photograph of the Universal Zwick 1484 set-up after testing PP1100M material.*

3.3.2 Three Point Bend Testing

The Zwick 1484 machine was also used for three-point bend testing by replacing the tensile grips with suitable 3-point bend fixtures (see Figure 3.4). The ASTM standard D 5023 was used for conducting the three-point bend test. This test was used to determine the mechanical properties of the materials subjected to flexural forces. The test specimens were cut from the gauge section of the tensile specimens prepared by the automated injection moulder while other bars were prepared using the manually operated injection moulder. The dimension of the specimens used for these tests were 80 mm x 10 mm x 4 mm for the length, width and thickness, respectively. The 3-point bend test was performed by placing the specimens on a support span of 60 mm in length. Each specimen was subjected to a flexural load at the centre by means of a loading nose that flexes the specimen between the two lower stationary supports. The test speed was set at 5 mm/min. Ten specimens were tested for each type of material.

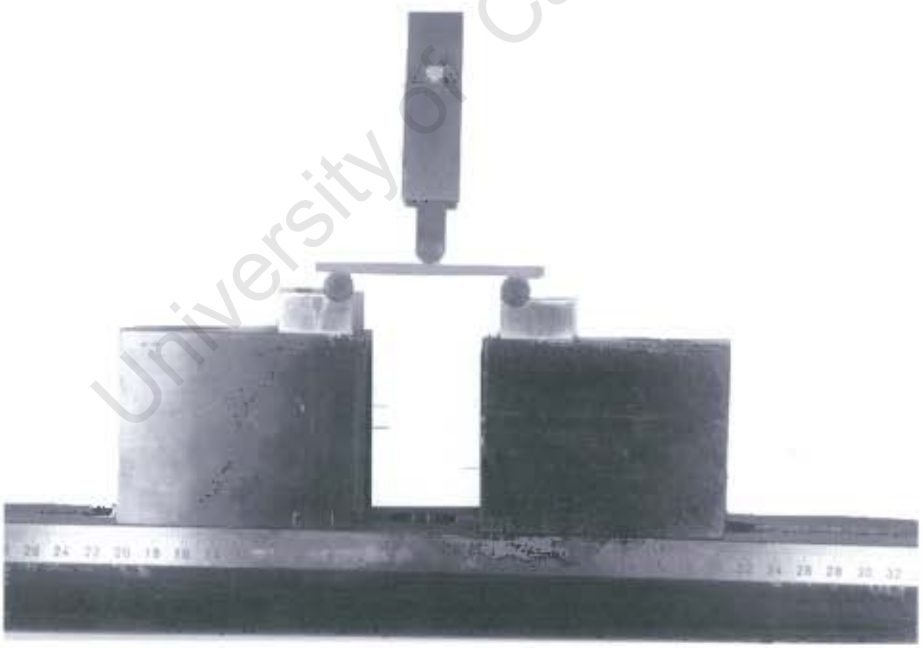

Figure 3.4: *Three-point bend test set up on the Universal Zwick tensile testing machine.*

3.3.3 Impact Testing

Impact tests were used to determine the energy utilized to cause deformation in the specimen and the material resistance to impact. These tests were also used for material ranking as well as determining the effects of sharp impactors of the designed part. There are several types of impact tests, however three types of impact tests were performed for the purpose of this research work. These were the Izod, Charpy, and drop weight impact tests. The Izod and Charpy impact tests were performed using the Zwick impact tester (Figure 3.5 below). A specific pendulum and a clamp were fitted on the machine for a particular test. The drop weight test was performed using a different machine from that of the Izod and Charpy tests.

Figure 3.5: *The Zwick impact tester for Izod and Charpy testing.*

3.3.3.1 Izod and Charpy Impact Testing

The Izod impact test was used to measure the impact energy required for the specimens to fail when they are impacted on the free end while the other end is clamped. The Izod tests were performed following the ASTM standards D256. All the specimens tested were notched (see Table 3.5 for the notch size) at the centre with the notch facing the pendulum. A 5.5 J pendulum was released from 124 $^{\circ}$ to strike the specimen at the free end. The impact energy (J) and the impact resistance (kJ/m^2) were recorded. The Charpy impact test is comparable to the Izod impact test with few differences viz. the placement of the specimen and the notch direction. The Charpy specimen was placed horizontally, unclamped, against the anvil with a notch facing away from the pendulum. The pendulum used for the Charpy test was a 7.5 J for ISO 179 standards. It was released from an angle of 160 $^{\circ}$ to strike the specimen at the middle directly opposite the notch. The dimensions of the specimens used are shown in Table 3.5 below.

Table 3.5: *Specimen parameters for the Izod and Charpy tests.*

Parameter	*Izod Test*	*Charpy Test*
Length (mm)	62	80
Width (mm)	10	10
Thickness (mm)	4	4
Notch length (mm)	2	2
Notch angle (degrees)	30	30
Notch radius (mm)	0.25	0.25

3.3.3.1 Drop-weight Impact Testing

The drop-weight impact tester, unlike the Zwick impact tester, was an in-house built apparatus. It was used to obtain the impact energy and the impact resistance of the materials at various rates of strain and temperatures. The drop weight impact test is unidirectional with no preferred direction of failure. This test, unlike Izod and Charpy impact tests, can be applied to moulded parts ready for use and measures the load on the specimen, continuously, as a function of time and deflection for the entire period of impact. The dimensions of the specimens used were 100 mm x 3.2 mm for the diameter and the thickness, respectively.

A 3.14 kg weight was dropped, guided by a rail, in a free fall from a pre-determined height to strike at the centre of the specimen clamped in a horizontal plane (Figure 3.6). The striker had a hemispherical nose with a diameter of 8.2 mm. The impact height was varied, which in turn changed the impact velocity and therefore subjected the material to different rates of strain. Specimens were tested at 300, 600 and 1200 mm heights to determine the material response to increasing rates of strain. The height was measured from the initial position of the weight on the guide rail to the position of the optical switch (Figure 3.7). The optical switch was used to measure the time taken for the velocity flag to pass through the optical sensor. The software uses this time to calculate the velocity of the falling weight at the time of impact. The velocity was measured immediately after the second arm of the velocity flag had passed through the optical switch.

Tests were performed at -35 ^{0}C and 20 ^{0}C to simulate different environmental conditions. Liquid nitrogen was used to reduce the temperature of the specimen to –35 ^{0}C. This was done by circulating liquid nitrogen from the dewar through the copper disc and from the copper disc back to the dewar (see Figure 3.8). The liquid nitrogen was transferred from the dewar to the specimen by pumping it

through silicon tubes to the disc specimen using a Unipump (see Figure 3.8 A). The temperature was controlled by varying the flow rate of the liquid nitrogen and by heating the copper disc using the power supply (Figure 3.8 A) and cartridge heater (Figure 3.8 B), respectively. Before testing, the desired temperature was set on the temperature control device (Figure 3.8 A). When the desired temperature was reached during cooling, the cartridge heater maintained this temperature by regulating the temperature of the copper disc. A thermocouple, which was attached on the copper disc was used to measure the test temperature. For each type of material, four tests were performed at a particular temperature.

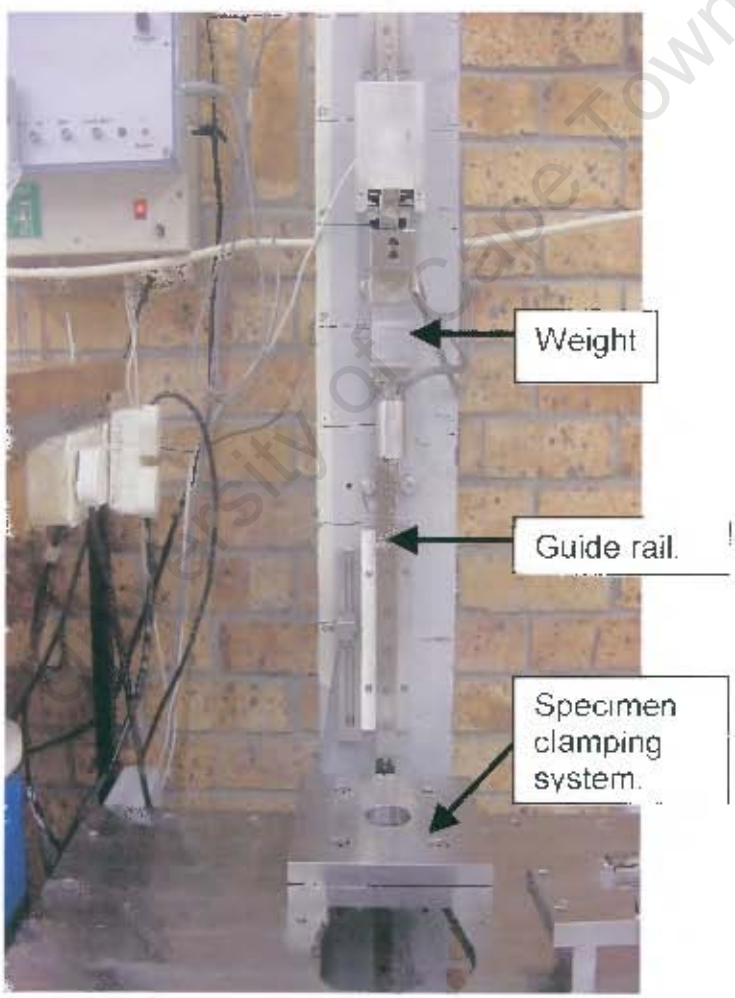

Figure 3.6: *The in-house built instrumented drop-weight tester.*

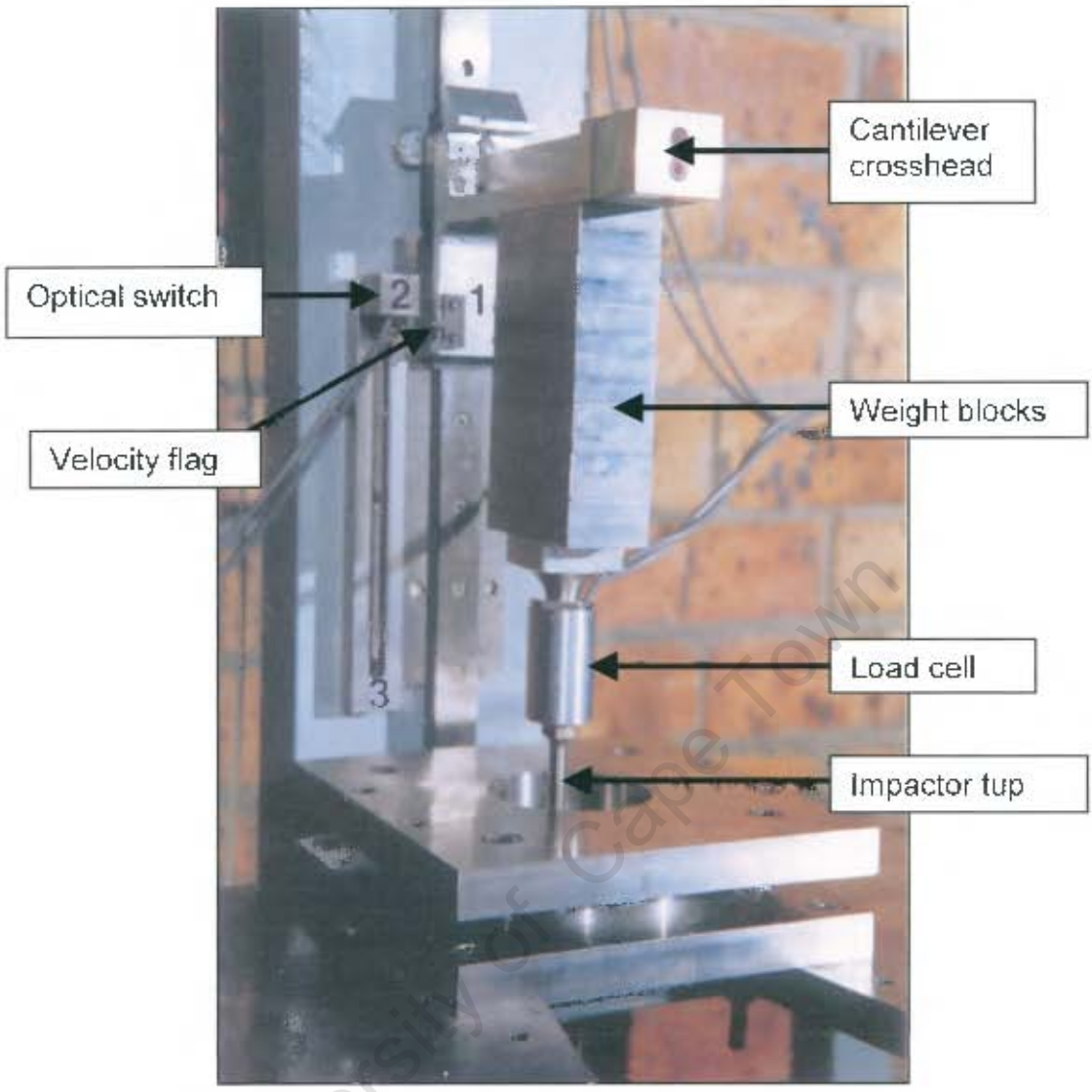

Figure 3.7: *A close-up view of the experimental set-up showing the velocity-measuring device for drop-weight testing.*

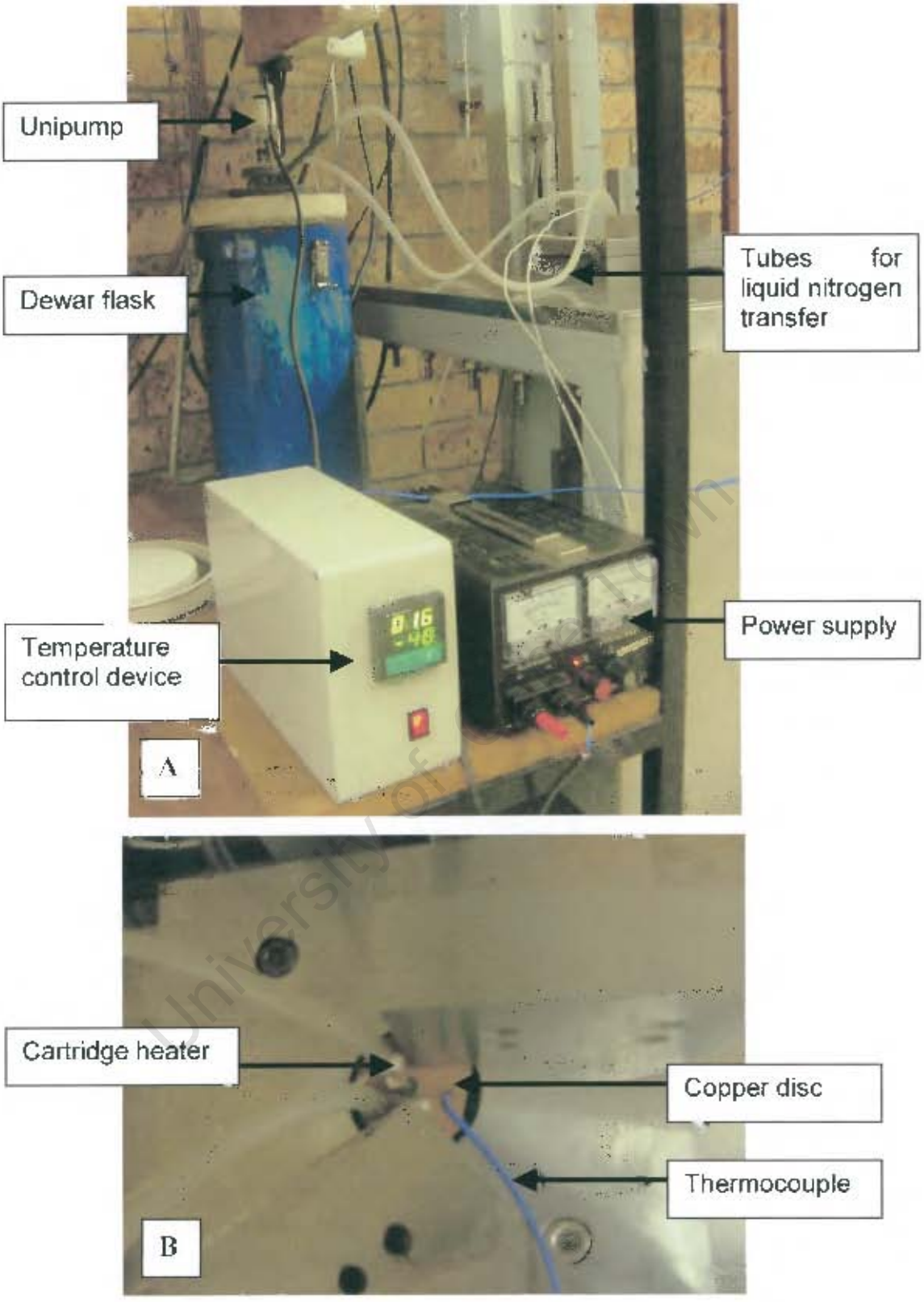

Figure 3.8: *Low temperature drop-weight test set-up (A) and the top view of the copper disc attachment on the specimen (B).*

3.4 FILLER ORIENTATION DETERMINATION

The fibre orientation was investigated in different areas of the moulded bar specimen. A rectangular piece of a composite specimen was mounted in a thermosetting resin. The specimen was then ground and polished to 0.25 μm before it was washed in methanol. The polished surface was observed under light microscopy to determine the fibre orientation at different locations in the specimen, for example, at the centre and near the surface. The point of polymer injection for the disc specimens meant that the fillers spreads out from the single injection point. However, the orientation of the glass fibre and talc fillers was not measured at different locations in the disc specimens.

3.5 FRACTOGRAPHY

Fractographic studies were carried out using the scanning electron microscope (SEM). The fracture surfaces of all the test specimens were examined in order to investigate the failure mechanisms of composite materials such as matrix plastic deformation, fibre breakage and fibre-matrix debonding. The fractured parts of the specimens were mounted on aluminium stubs and sputter coated with a thin layer of gold-palladium alloy to avoid electrical charging caused by polymeric materials during SEM observations. Micrographs of the fracture surfaces were taken. These micrographs were used to study the failure mechanisms and the nature of the interfacial bond in the various polypropylene and polyamide 6-6 composites.

CHAPTER 4

EXPERIMENTAL RESULTS

The results of all the experiments outlined in chapter three are reported in this chapter. Results obtained from the mechanical tests and micro-structural and fractographic investigations are outlined. The mechanical properties and the mechanisms of failure are compared between the materials studied in this research work. A comparison is also made in the processing conditions since the test specimens were made using two different injection moulding machines. These results will indicate the influence of fillers, matrix resin and poor processing conditions. Processing conditions will be compared in polypropylene based materials because polyamide 6-6 based materials could not be processed using the manually operated injection-moulder. These results will also show the extent to which fillers, strain rate and temperature affect the mechanisms of failure. Fracture surfaces are also shown revealing the fibre orientation and microscopic features such a matrix plastic deformation, matrix tearing, fibre-matrix debonding, fibre fracture and pullout. These features give an indication of the type of failure mechanism that has occurred.

4.1 PRE-TREATMENT OF POLYAMIDE 6-6 MATERIAL

Polyamide 6-6 is highly sensitive to moisture and therefore required to be treated before injection moulding. Since polyamide 6-6 (EFE1147) and short glass fibre reinforced polyamide 6-6 (30SGFRPA) are some of the materials investigated in this research, experiments were conducted to determine their moisture uptake (see Figure 4.1).

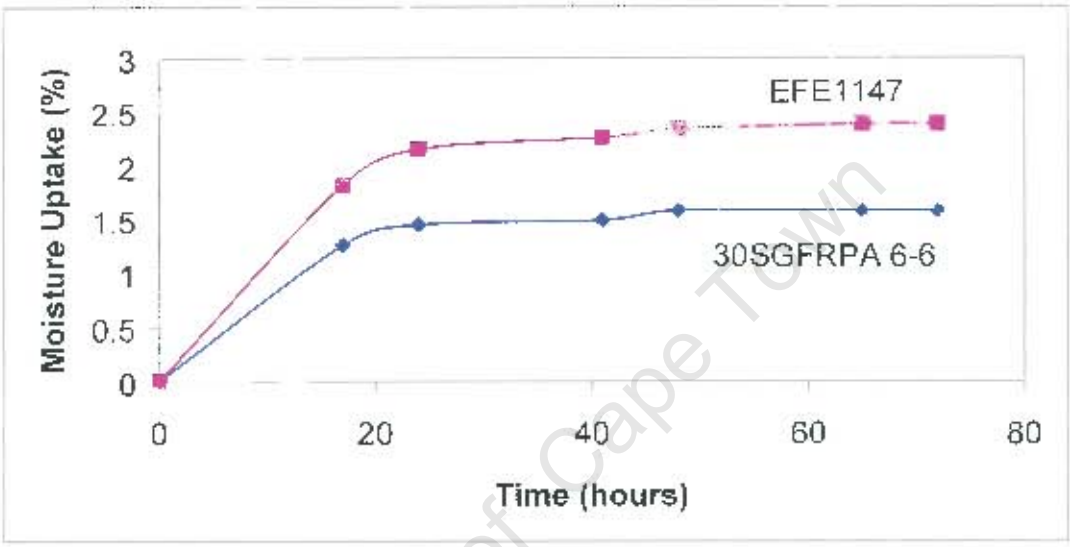

Figure 4.1: *Moisture uptake vs. time graphs for unfilled polyamide 6-6 (EFE1147) and glass fibre reinforced polyamide 6-6 (30SGFRPA 6-6).*

The results obtained in Figure 4.1 above represent the moisture uptake of EFE1147 and 30SGFRPA 6-6 as a function of time. The experiment was conducted over a period of 72 hours. It can be seen in Figure 4.1 that the moisture uptake in EFE1147 and 30SGFRPA 6-6 increases with time. However a saturation level is reached when the materials were left in a moist environment for a longer time. The two curves indicate that moisture absorption is higher for unfilled polyamide 6-6 than its glass filled composite. From these results it is apparent why polyamide need to be pre-treated before injection moulding.

4.2 MECHANICAL TESTING

Mechanical tests, namely tensile, flexural (three-point bend) and impact (Izod, Charpy and drop-weight) tests were conducted to determine the mechanical properties and further perform micro-structural and fractographic investigations. The mechanical properties obtained were compared for different materials to determine material compositions and processing effects on the mechanical properties.

Polypropylene based materials were used to determine processing effects. The instrumented drop-weight impact test was used to determine the material response at various rates of strains and temperatures. The results obtained are stress-strain curves, impact energy and impact resistance. Plots are often represented on the same set of axis to allow for easy visual comparison of material properties. Micrographs of the fractured surfaces are also presented.

4.2.1 Tensile Testing

The outcome of a tensile test is force versus elongation of the materials. This data was converted into stress-strain data in order to plot the stress-strain relationship. Plots obtained from the data of specimens prepared by an automated injection moulder are presented first. Graphs of polypropylene and filled polypropylene for specimens prepared by both injection-moulding machines are plotted for mechanical properties comparison. The changes in mechanical properties as a result of filler addition and processing conditions can be observed from the plots in Figures 4.2 to 4.6. Table 4.1 summarises the tensile results for materials processed by an automated and manually operated injection-moulding machine. The designations Au and Ma after the material's name stand for automated and manual, respectively.

Figure 4.2 shows tensile plots of (A) unfilled polypropylene and (B) unfilled polyamide 6-6 specimens. It can be seen from the graphs that the tensile stress of the unfilled polyamide 6-6 (EFE1147) is more than double that of unfilled polypropylene (PP1100M). However, PP1100M shows a ductile type of failure with extensive plastic deformation up to about 490% strain. The plastic deformation in EFE1147 is relatively minimal to about 40% strain. Addition of fillers in the polymer resins has altered the tensile properties. This can be seen in Figure 4.3 where the maximum stress of polypropylene and polyamide 6-6 is doubled with the addition of 30% short glass fibres. The ductility of the polymers is also reduced to less than 10%. Platy talc fillers have a decreasing effect on the tensile strength and modulus of polypropylene. The maximum stress of polypropylene was reduced to half when 30% platy talc fillers were added (see Figures 4.2 and 4.3 for comparison or Table 4.1).

The influence of processing conditions can be seen in Figure 4.4 where the comparison of tensile response is made between the specimens prepared by the automated and manually operated machine. The tensile stress of polypropylene and 30% talc filled polypropylene is higher for specimens prepared by the manually operated injection moulder when compared to those prepared by the automated injection moulder. However, the opposite is observed with 30% short glass fibre reinforced polypropylene, which shows lower stress and modulus for specimens prepared by the manually operated machine. The average elastic modulus of polypropylene is also lower for specimens prepared by the manually operated machine. The tensile properties of all the materials tested are summarised in Table 4.1. The tensile stress and modulus of the materials are compared in Figures 4.5 and 4.6, respectively.

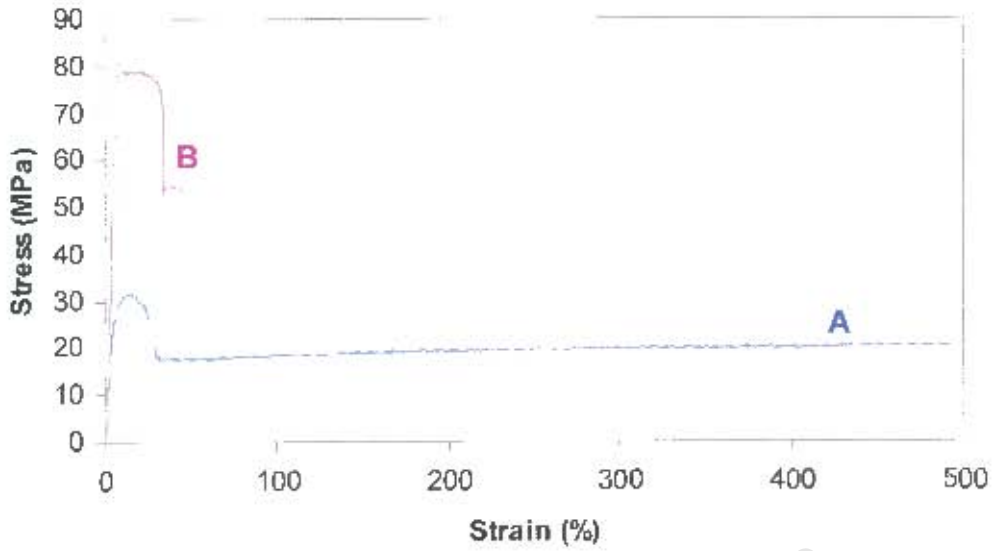

Figure 4.2: *Typical tensile stress/strain curves for (A) PP1100M-Au and (B) EFE1147-Au.*

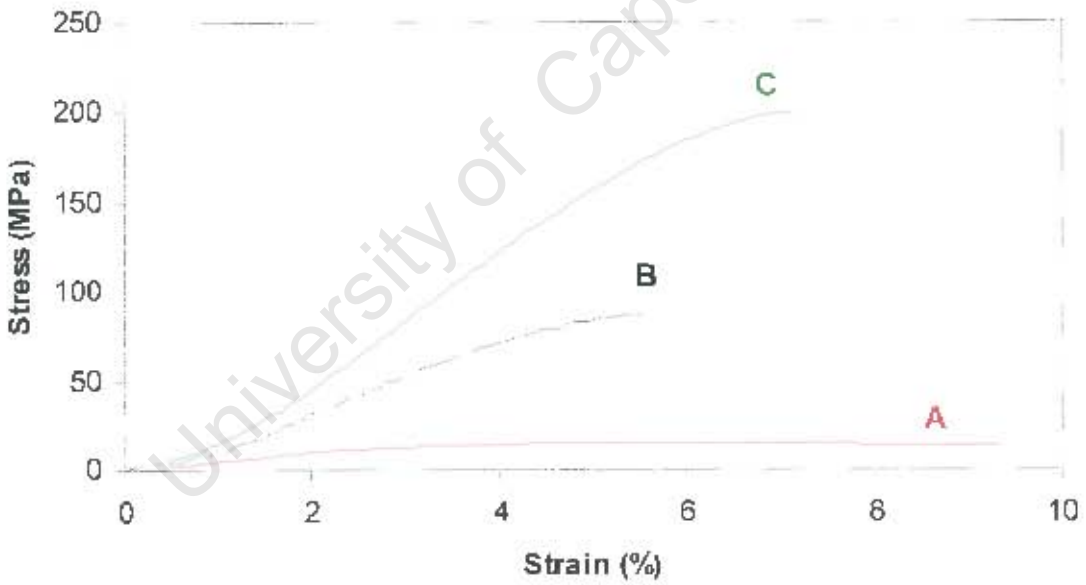

Figure 4.3: *Typical tensile stress/strain curves for (A) 30Talc/PP-Au, (B) 30SGFRPP-Au and (C) 30SGFRPA 6-6-Au.*

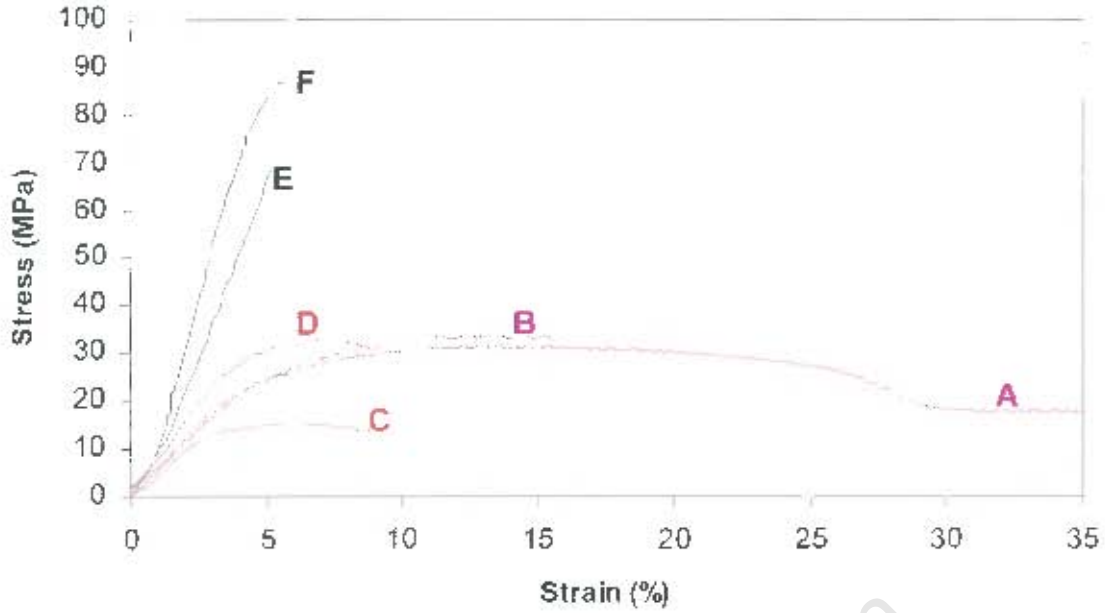

Figure 4.4: *Typical stress/strain curves for (A) PP1100M-Au, (B) PP1100M-Ma, (C) 30Talc/PP-Au, (D) 30Talc/PP-Ma, (E) 30SGFRPP-Ma and (F) 30SGFRPP-Au.*

Table 4.1: *Average tensile properties of specimens moulded by an automated and manually operated machine.*

Material	Automated Machine			Manual Machine		
	Stress (MPa)	Modulus (GPa)	Ductility %	Stress (MPa)	Modulus (GPa)	Ductility %
PP1100M	31.4 (±0.8)	0.54 (±0.002)	470 (±40)	34 (±0.02)	0.45 (±0.004)	20 (±4)
30Talc/PP	15.4 (±0.3)	0.5 (±0.007)	10 (±1)	33 (±0.3)	0.7 (±0.007)	10 (±1)
30SGFRPP	87 (±2)	2.1 (±0.08)	5 (±0.4)	68 (±4)	1.5 (±0.02)	5 (±0.5)
EFE1147	80.5 (±1.2)	1.4 (±0.04)	40 (±6)			
30SGFRPA 6-6	201 (±8)	3.8 (±0.03)	7 (±0.2)			

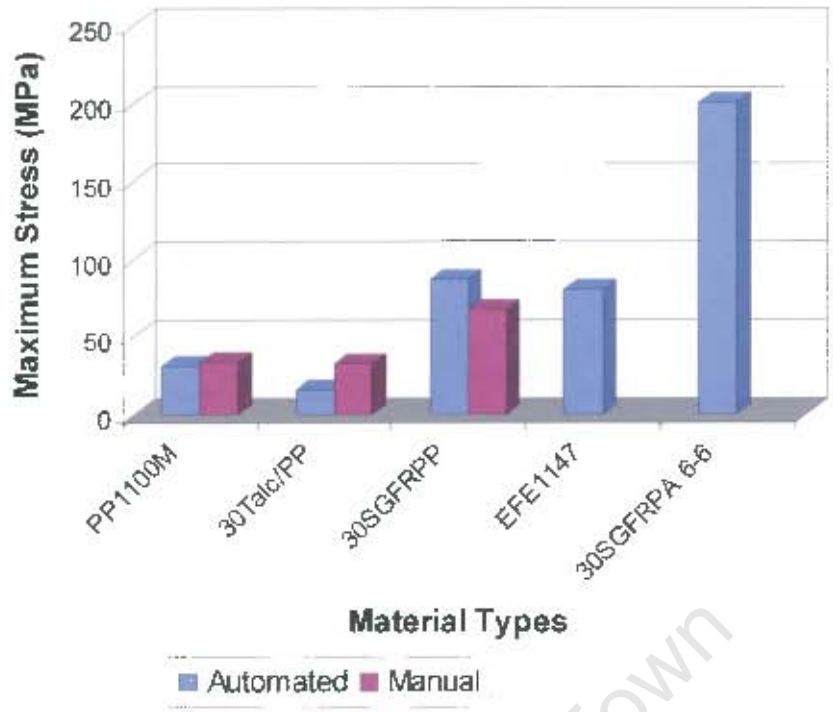

Figure 4.5: *Average tensile strength for specimens prepared using the automated and manually operated injection moulders.*

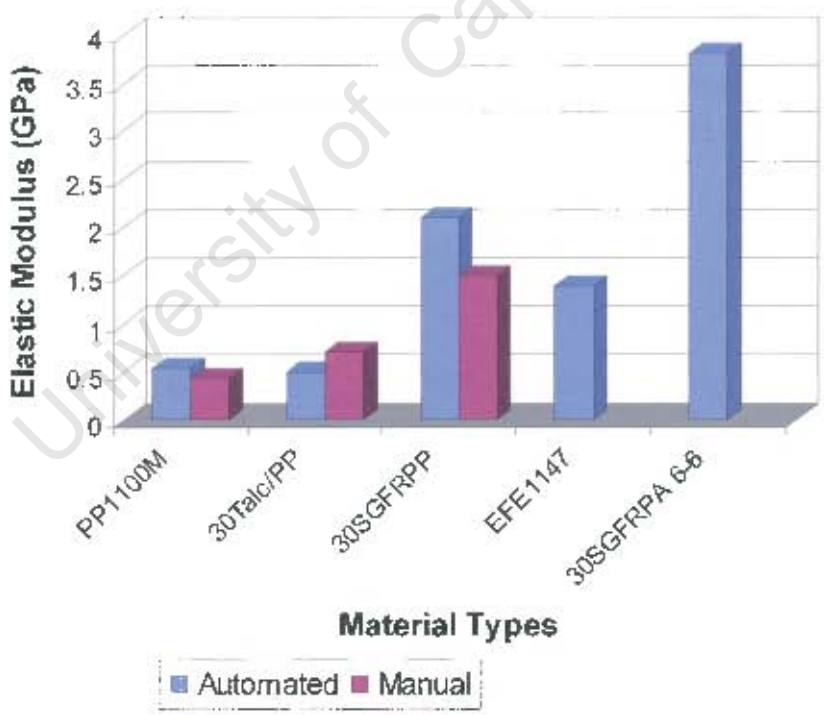

Figure 4.6: *Average tensile elastic modulus for specimens prepared using the automated and manually operated injection moulders.*

4.2.2 Three-point Bend Testing

The three-point bend test gives the applied force and the deflection of the material in flexure. The results of this test are represented by stress versus deflection curves where the stress was derived from the force using equations in section 2.4.2 in chapter 2. These results are presented similar to the tensile results in section 4.2.1. It is apparent in Figure 4.7 that talc fillers (curve A) do not have as significant an effect on the flexural strength of polypropylene as compared to glass fibres. This can be seen in curve (D) that shows much higher flexural stress and less deflection when compared to curve (B). The true failure stress and strain of the two thermoplastic resins (B and C in Figure 4.7) as well as 30% talc filled polypropylene (A) are not known since the tests were stopped before final failure. This was done because the three materials (A, B and C) were deforming plastically, continuously, during testing. Fibre reinforced materials (D and E) have reached their failure strain owing to the glass fibre additions in the thermoplastic resins.

All talc fillers and short glass fibres have an increasing effect on the flexural stress and modulus. This was not always true for the observations in the tensile stress. From the curves in Figure 4.7 and Table 4.2, it can be seen that polypropylene is more sensitive to glass fibres additions than polyamide 6-6. The maximum flexural stress of polypropylene was three times higher when the short glass fibres were added whereas that of polyamide 6-6 is doubled. Talc filler shows an increase in the maximum flexural strength and modulus.

The stress-deflection curves in Figure 4.8 show the influence of processing conditions by comparing the results of the materials prepared by two different injection-moulding machines. Notice the reduction in the ductility of unfilled polypropylene and 30% talc filled polypropylene (C and E in Figure 4.8) for specimens prepared by the manually operated machine when compared with the

automated machine (B and A). The maximum stress and modulus are higher for PP1100M and 30Talc/PP specimens prepared by the manually operated machine than those prepared by the automated machine. 30SGFRPP shows a lower stress and modulus for specimens prepared by the manually operated machine (see Figure 4.8 and Table 4.2). The comparison in the maximum stress and modulus can be made easily in Figures 4.9 and 4.10 where the flexural results are compared for the two processing machines. Figure 4.11 shows that the flexural properties are higher than the tensile properties for specimens prepared by the automated injection-moulding machine. Similar observations are seen, with an exception of 30SGFRPP, in Figure 4.12 where the flexural and tensile properties are compared for specimens prepared by the manually operated machine. For the 30SGFRPP, the flexural stress is lower than the tensile stress. The same trend was observed for the tensile and flexural modulus.

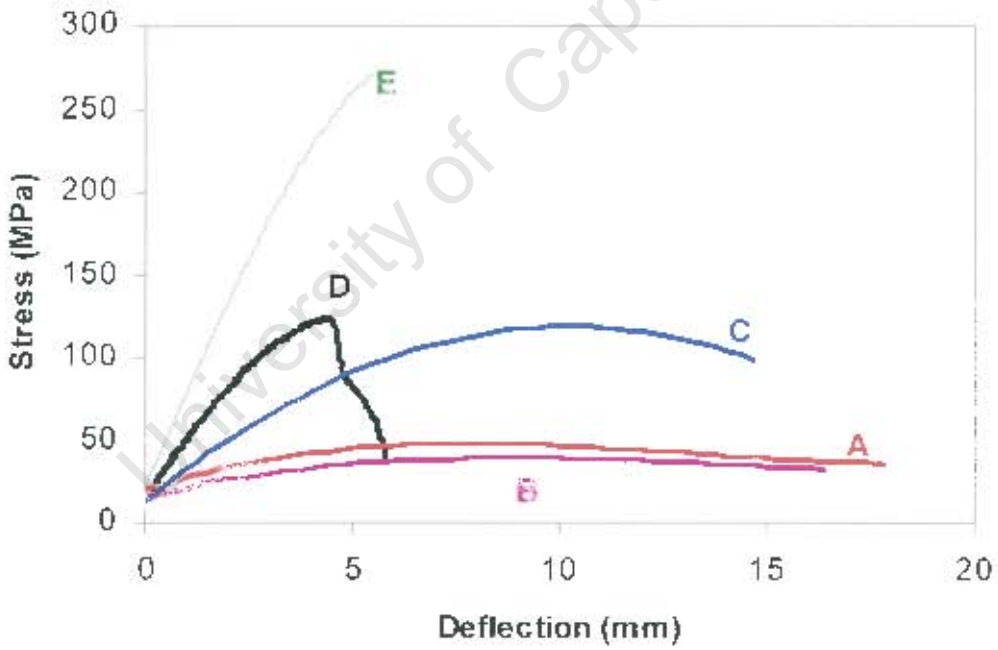

Figure 4.7: *3-point bend stress/deflection curves for (A) 30Talc/PP, (B) PP1100M, (C) Zytel EFE1147, (D) 30SGFRPP and (E) 30SGFRPA 6-6 for specimens prepared using an automated injection moulder.*

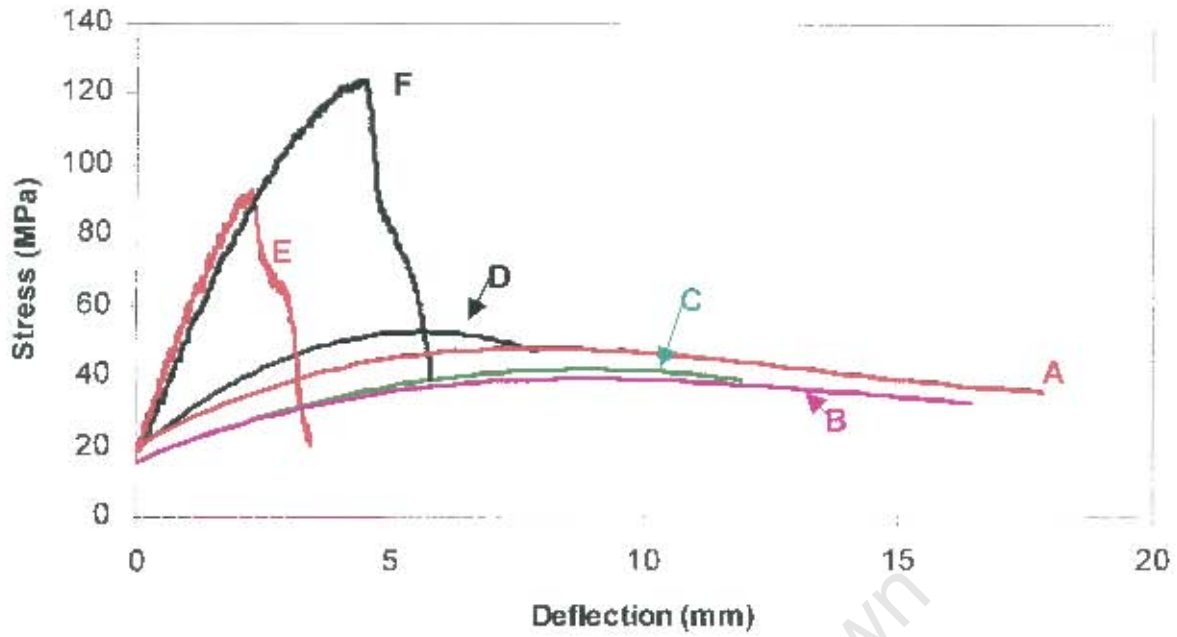

Figure 4.8: *Typical 3-point bend stress/deflection curves for (A) 30Talc/PP-Au, (B) PP1100M-Au, (C) PP1100M-Ma, (D) 30SGFRPP-Ma, (E) 30Talc/PP-Ma and (F) 30SGFRPP-Au.*

Table 4.2: *Average flexural stress and modulus for specimens moulded by an automated and manually operated machine.*

Material	Automated Machine		Manual Machine	
	Stress (MPa)	Modulus (GPa)	Stress (MPa)	Modulus (GPa)
PP1100M	41.8 (±1.4)	0.7 (±0.006)	42.4 (±1.1)	0.7 (±0.01)
30Talc/PP	52(±2)	1.5(±0.02)	92.6 (±1.2)	5.2 (±0.04)
30SGFRPP	128.8 (±2.4)	4.7(±0.05)	55 (±1)	1.1 (±0.02)
EFE1147	121(±3)	2.6 (±0.06)		
30SGFRPA 6-6	270.3 (±2.3)	8.1 (±0.01)		

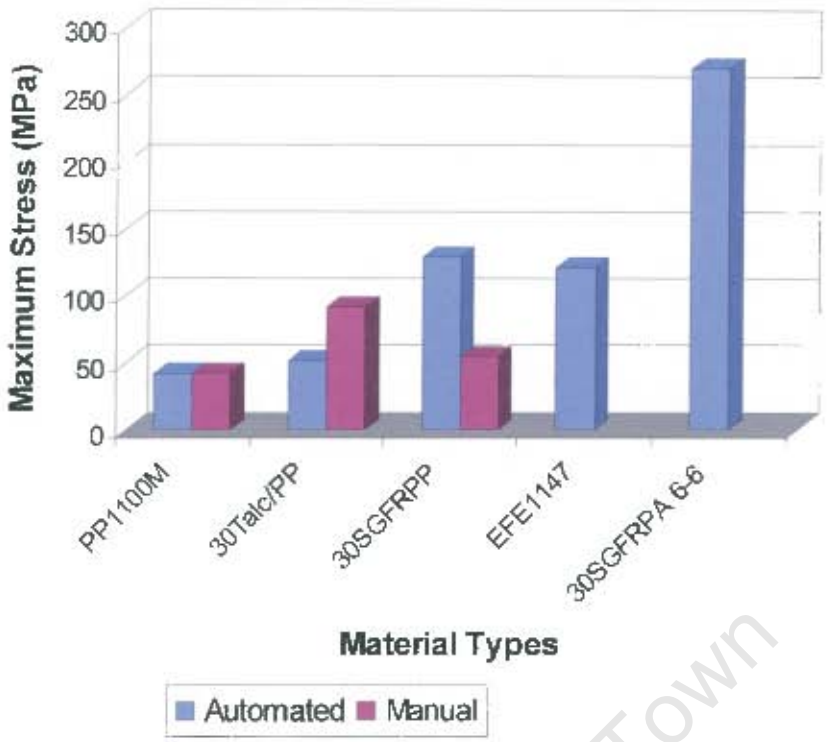

Figure 4.9: *Average flexural stress for specimens prepared using the automated and manually operated injection moulders.*

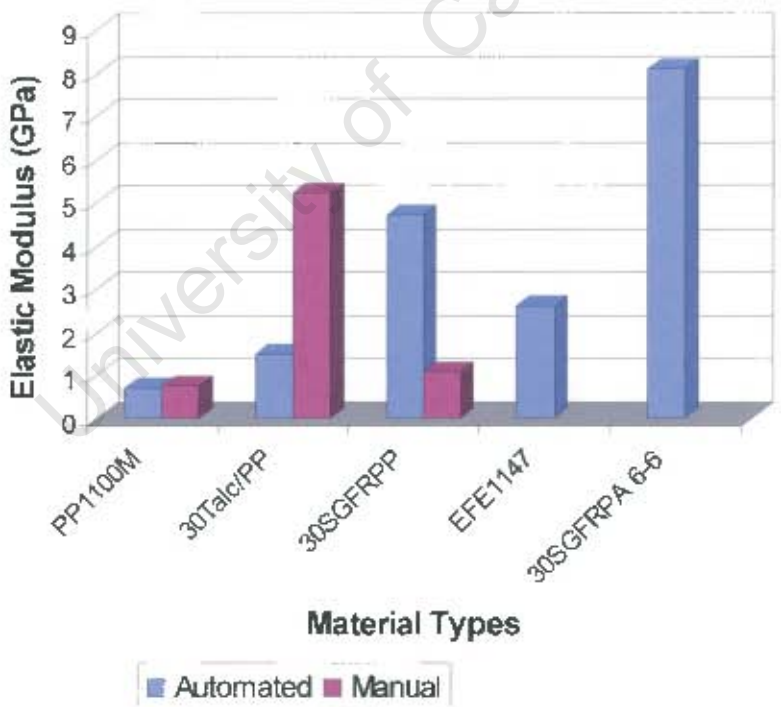

Figure 4.10: *Average flexural elastic modulus for specimens prepared using the automated and manually operated injection moulders.*

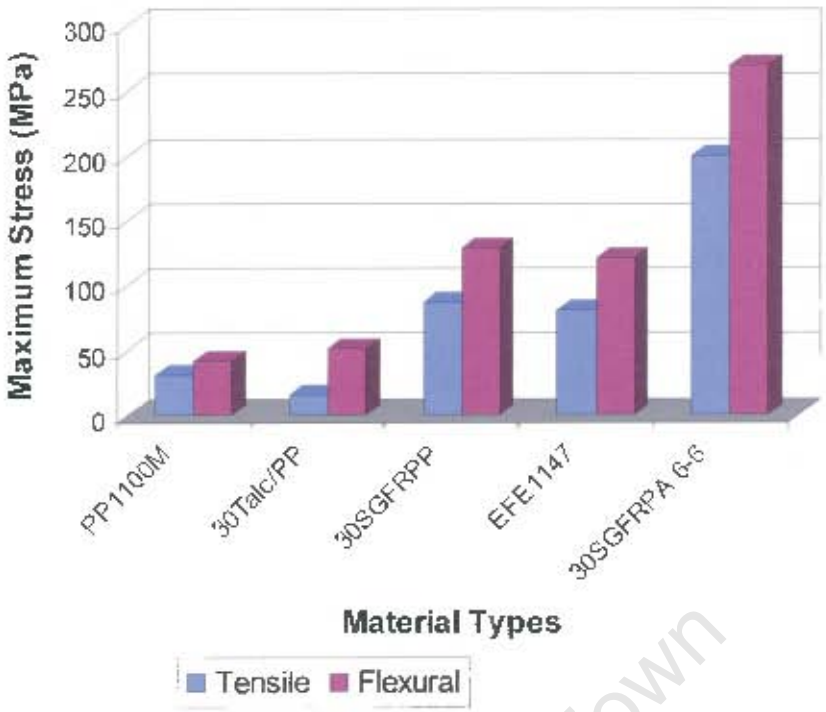

Figure 4.11: *Average tensile and flexural stresses for specimens prepared by the automated machine.*

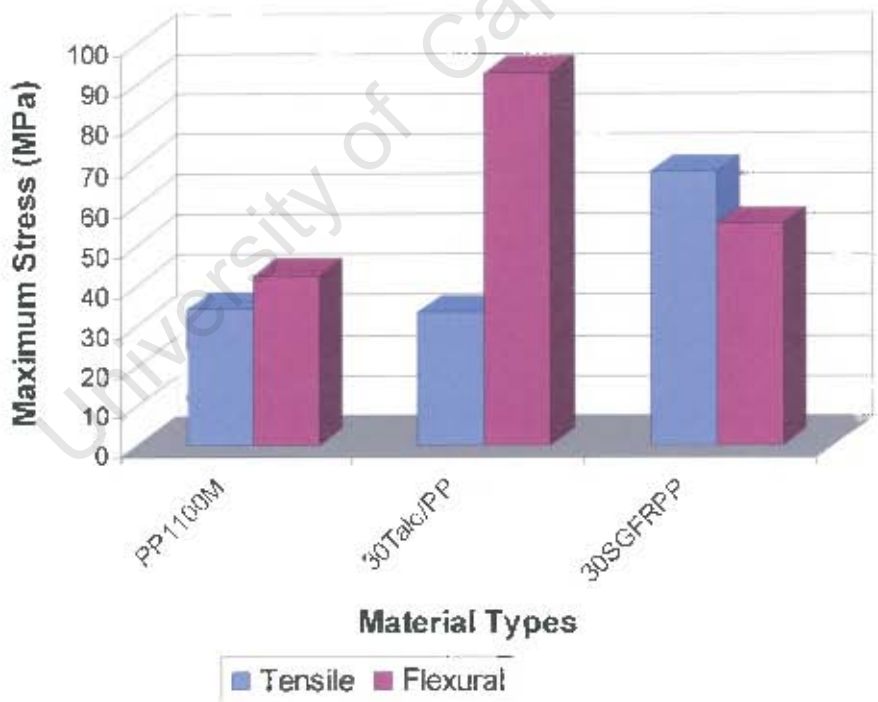

Figure 4.12: *Average tensile and flexural stresses for specimens prepared by the manually operated machine.*

4.2.3 Impact Testing

The results of the Izod, Charpy and drop-weight impact tests are outlined in this section. The Izod and Charpy results are presented together since a comparison is made between the two tests. The drop-weight test results are presented in a separate section (section 4.2.4).

4.2.3.1 Izod and Charpy Impact Testing

The results obtained from the two impact type tests are the impact energy and the impact resistance of the materials. The results of materials prepared by the automated and manually operated machine are presented in Table 4.3. These are the Charpy and Izod impact energy and the impact resistance of the materials together with their standard deviations. The Charpy and Izod impact results show a similar trend to that of the tensile stress and modulus. This can be seen in Table 4.3 where the impact energy and the impact resistance of 30SGFRPP and 30SGFRPA 6-6 are significantly higher than those of PP1100M and EFE1147, respectively. Talc fillers did not cause a reduction in the Charpy and Izod impact energy and impact resistance. Figures 4.13 and 4.14 show the Charpy and the Izod impact resistance of all the materials prepared by the automated injection-moulding machine. The Charpy impact resistance for 30SGFRPP is slightly higher than that of the EFE1147 whilst no difference is observed in the Izod impact resistance. The same trend was found in the impact energy of the materials.

The influence of processing conditions can be seen in Figures 4.15 and 4.16 where the Charpy and the Izod results of the two injection moulders are compared. The bar charts show that the Charpy and the Izod impact resistance are lower for specimens prepared by the manually operated machine when

compared to those prepared by the automated machine. The impact energies of the materials have shown the same trend (see Table 4.3).

Table 4.3: *The Charpy and Izod impact energy and impact resistance for specimens prepared by the automated and manually operated machines.*

Material	CHARPY (Automated)		CHARPY (Manual)		IZOD (Automated)		IZOD (Manual)	
	Impact Energy (J)	Impact Resist. (kJ/m^2)	Impact Energy (J)	Impact Resist. (kJ/m^2)	Impact Energy (J)	Impact Resist. (kJ/m^2)	Impact Energy (J)	Impact Resist. (kJ/m^2)
PP1100M	0.14 (±0.00)	4.23 (±0.14)	0.09 (±0.02)	2.87 (±0.49)	0.13 (±0.01)	4.06 (±0.37)	0.09 (±0.01)	2.80 (±2.80)
30Talc/PP	0.11 (±0.02)	3.51 (±0.51)	0.10 (±0.00)	2.99 (±0.11)	0.12 (±0.02)	3.59 (±0.67)	0.10 (±0.01)	3.13 (±0.29)
30SGFRPP	0.34 (±0.02)	10.55 (±0.60)	0.25 (±0.01)	7.79 (±0.32)	0.31 (0.01)	9.63 (±0.32)	0.22 (±0.01)	6.77 (±0.29)
EFE1147	0.24 (±0.06)	7.46 (±1.77)			0.33 (±0.11)	10.41 (±3.39)		
30SGFRPA 6-6	0.45 (±0.04)	13.98 (±1.15)			0.50 (±0.11)	15.52 (±3.35)		

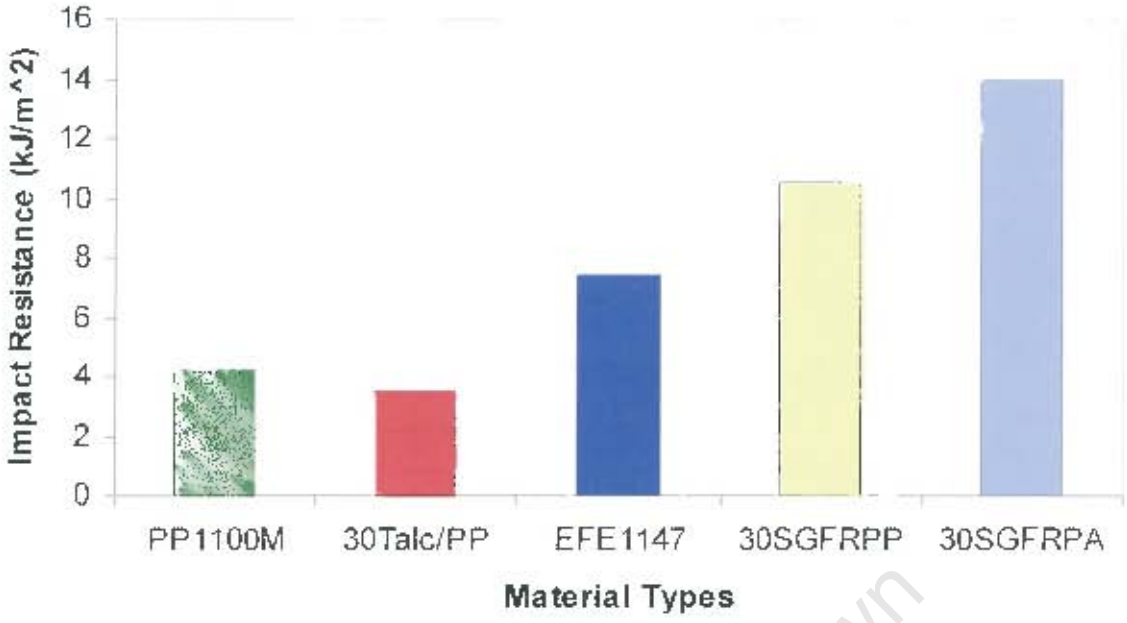

Figure 4.13: *Charpy impact resistance versus material types for automated moulded specimens.*

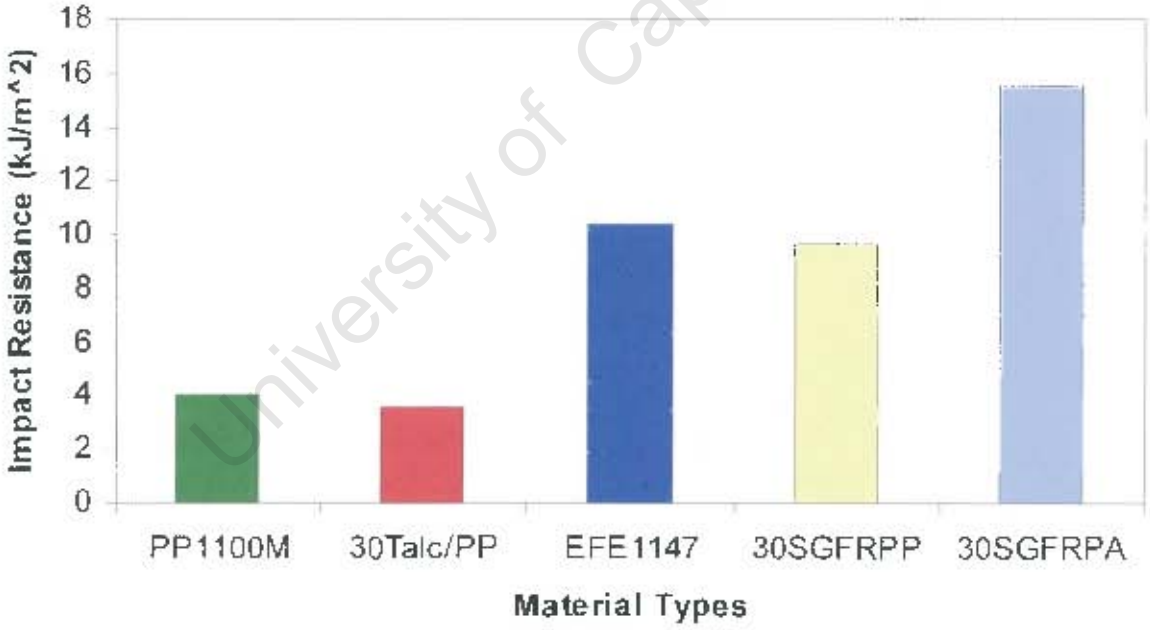

Figure 4.14: *Izod impact resistance versus material types for automated moulded specimens.*

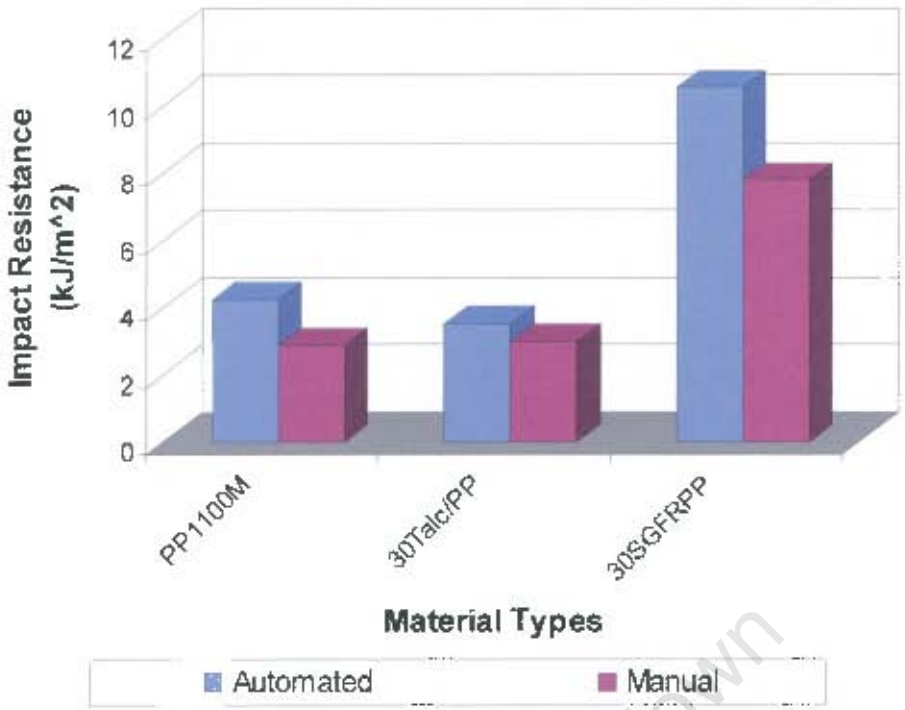

Figure 4.15: *Charpy impact resistance for the automated and manually operated injection moulded specimens.*

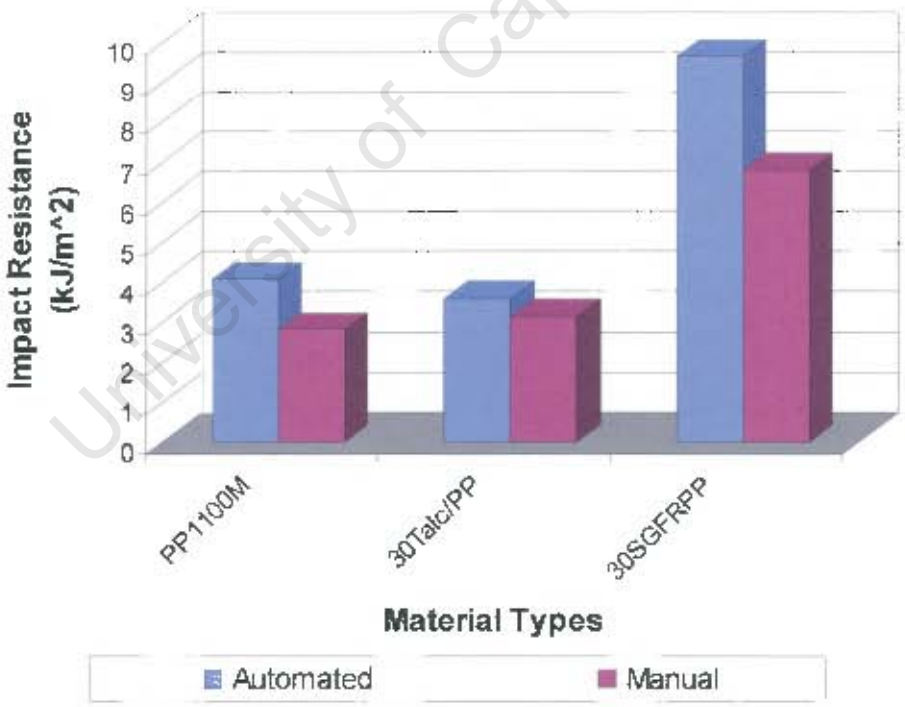

Figure 4.16: *Izod impact resistance for the automated and manually operated injection moulder specimens.*

4.2.3.2 Drop-weight Impact Testing

The drop-weight tests were performed at different test conditions that simulate various environmental conditions and rates of strain. Specimens were tested to investigate the strain rate and temperature influence on the mechanical properties and failure mechanisms by changing the drop heights and test temperatures, respectively. The dart was dropped from 300 mm, 600 mm and 1200 mm corresponding to impact velocities of 2.3 m/s, 3.3 m/s and 4.7 m/s, respectively. The test temperatures used were –35 ^{0}C and 20 ^{0}C. The drop-weight response is presented in terms of force versus deflection and energy versus deflection curves. The shape of the force versus deflection curve indicates the onset of the damage and its propagation. The energy versus deflection curve gives the impact energy absorbed by the specimen.

Figure 4.17 shows the force-deflection for (A) polypropylene and (B) polyamide 6-6 specimens tested at 20 ^{0}C and a drop height of 300 mm. At these test conditions the polyamide specimens did not break. The dart bounced on the specimen forming a small dent. Curve (B) in Figure 4.17 shows a gradual decrease in the force after the reaching the maximum. The unfilled polypropylene specimen (curve A) has a relatively lower maximum impact force and a sharp decrease in the force is observed after the maximum force was reached. This indicates that the polypropylene has a relatively brittle drop-weight failure while the polyamide 6-6 showed to be stronger by absorbing the applied force on impact without a catastrophic failure. An increase in the drop height causes a change in the force-deflection curve of polyamide 6-6 specimens. A sharp decrease in the force is observed when the drop height is increased from 300 to 1200 (see Figure 4.18). Figure 4.18 shows typical force-deflection and energy deflection curves for polyamide 6-6 (EFE1147) tested at 20 ^{0}C and 1200 mm drop height. The energy plots were used to estimate the drop-weight impact energy of the materials.

The plots (A) and (B) in Figure 4.19 show the force-deflection curves for 30SGFRPP and SGFRPA 6-6 specimens tested at 20 ^{0}C and 300 mm drop height. The maximum force and the deflection is higher for 30SGFRPA 6-6 than for 30SGFRPP. The curves in Figure 4.19 also show a sinusoidal behaviour, which was not observed in the unfilled materials in Figure 4.17.

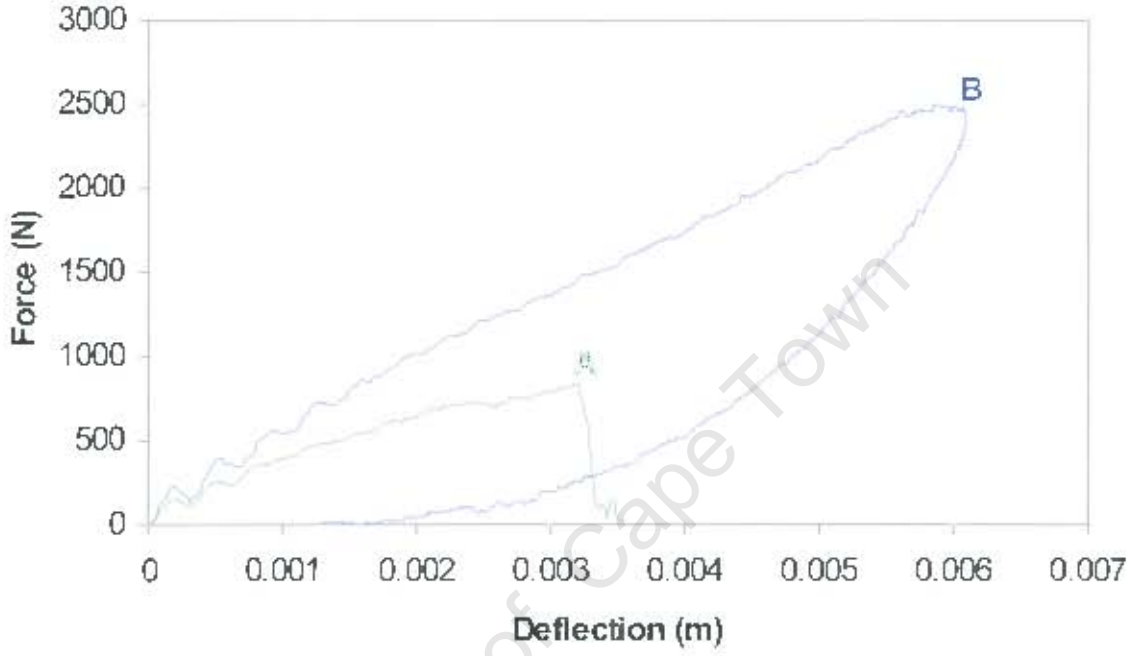

Figure 4.17: *Force versus deflection curves for (A) polypropylene (PP1100M) and (B) polyamide 6-6 (EFE1147) specimens tested at 20 ^{0}C and 300 mm drop height.*

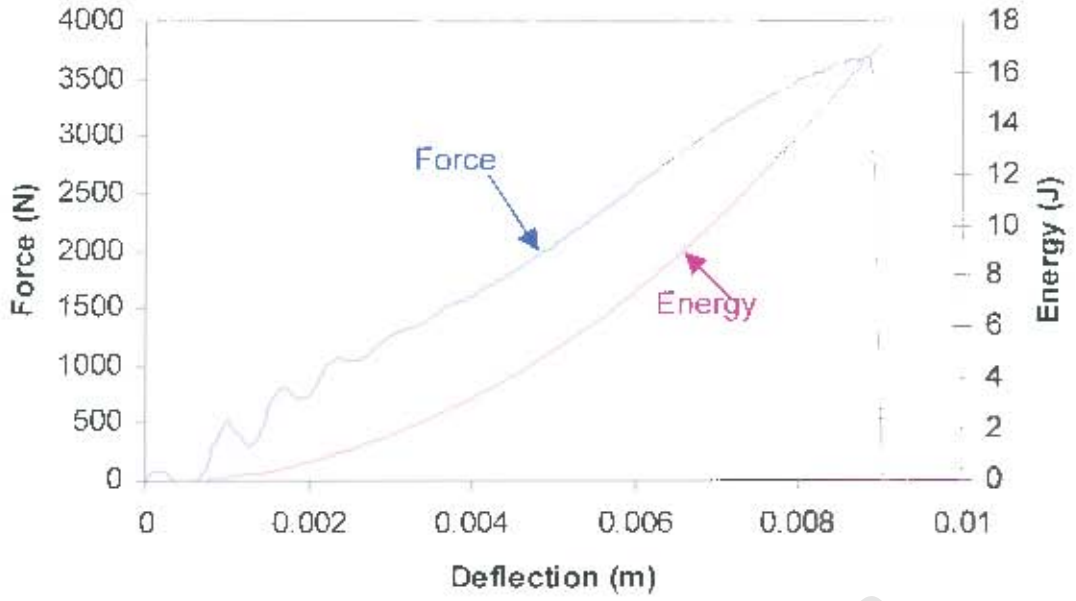

Figure 4.18: *Typical force versus deflection and energy versus deflection curves for polyamide 6-6 (EFE1147) specimens tested at 20 ^{0}C and 1200 mm drop height.*

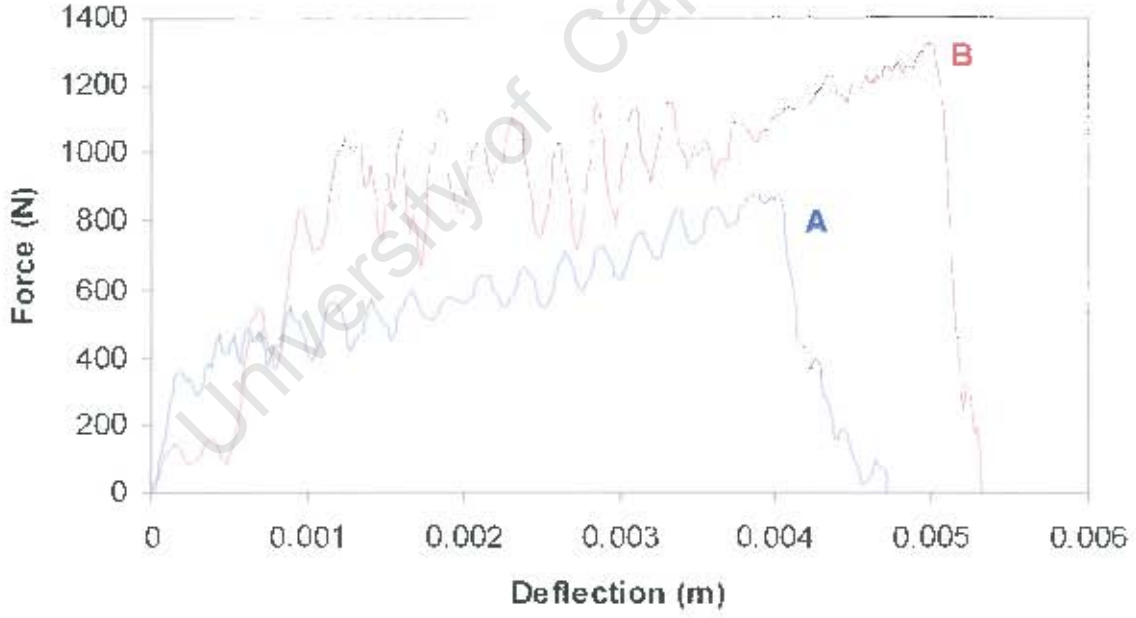

Figure 4.19: *Force versus deflection curves for (A) 30SGFRPP and (B) 30SGFRPA specimens tested at 20 ^{0}C and 300 mm drop height.*

4.2.3.2.1 Temperature Influence on the Drop-weight Impact Response

The plots in Figures 4.20 to 4.23 show the force-deflection curves of different materials tested at –35 ^{0}C and 20 ^{0}C. The polyamide 6-6 curve (b) for the specimen tested at 20 ^{0}C shows a gradual decrease in the force after reaching the maximum while a sharp decrease is observed in curve (A) when the temperature is reduced to –35 ^{0}C. The decrease in temperature also causes a reduction in the maximum force of the polyamide 6-6 (EFE1147). The EFE1147 specimens showed a small indent when impacted at 20 ^{0}C from a drop height of 300 mm. At –35 ^{0}C, the dart penetrated the EFE1147 plate specimen causing radial cracks spreading from the centre and circumferential cracks joining leaving pieces of the specimen to break off. Figure 4.21 shows the drop-weight force-deflection curves of 30SGFRPA 6-6 specimens tested at -35 ^{0}C and 20 ^{0}C. The results in Figure 4.21 show a decrease in deflection of the materials with a decrease in temperature. The amplitude of the fluctuations in the force also decreases with temperature. This can be seen in Figure 4.21 where the amplitudes of the sinusoidal curve (A) at –35 ^{0}C are lower than those in curve (B) at 20 ^{0}C. These fluctuations are due to the formation and propagation of circumferential cracks.

Polypropylene composites show a different response to polyamide 6-6 composites when the temperature was reduced from 20 ^{0}C to –35 ^{0}C. The deflection of 30Talc/PP and 30SGFRPP is reduced when the temperature was reduced (see Figures 4.22 and 4.23). However, an increase is observed in the maximum force at lower temperature (-35 ^{0}C). Figure 4.24 compares the impact energies of all the materials tested at –35 ^{0}C and 20 ^{0}C. It can be seen that reducing the test temperature results in a decrease in the impact energy of the materials. The drop-weight impact energy of EFE1147 is higher than that of 30SGFRPP and 30SGFRPA 6-6 at 20 ^{0}C but lower at –35 ^{0}C (see Figure 4.24). Additions of glass fibres reduce the impact energy of the polyamide 6-6

(EFE1147) at 20 ^{0}C while an increase is observed at –35 ^{0}C. Talc fillers and short glass fibres additions increased the drop-weight impact energy of polypropylene (PP1100M) at both temperatures.

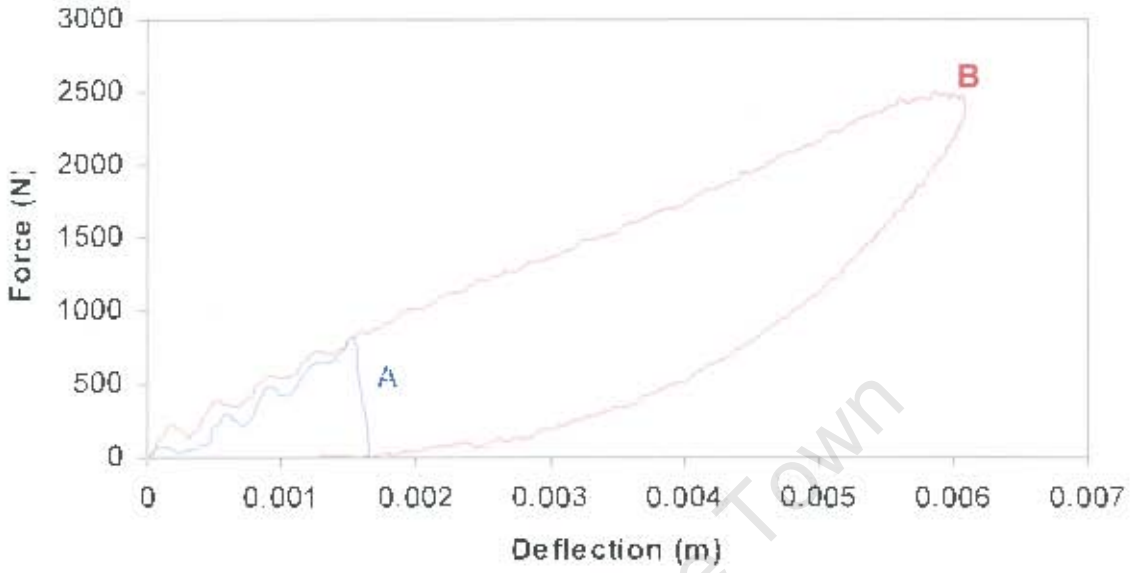

Figure 4.20: *Drop-weight force versus deflection curves for EFE1147 specimens tested at (A) –35 ^{0}C and (B) 20 ^{0}C.*

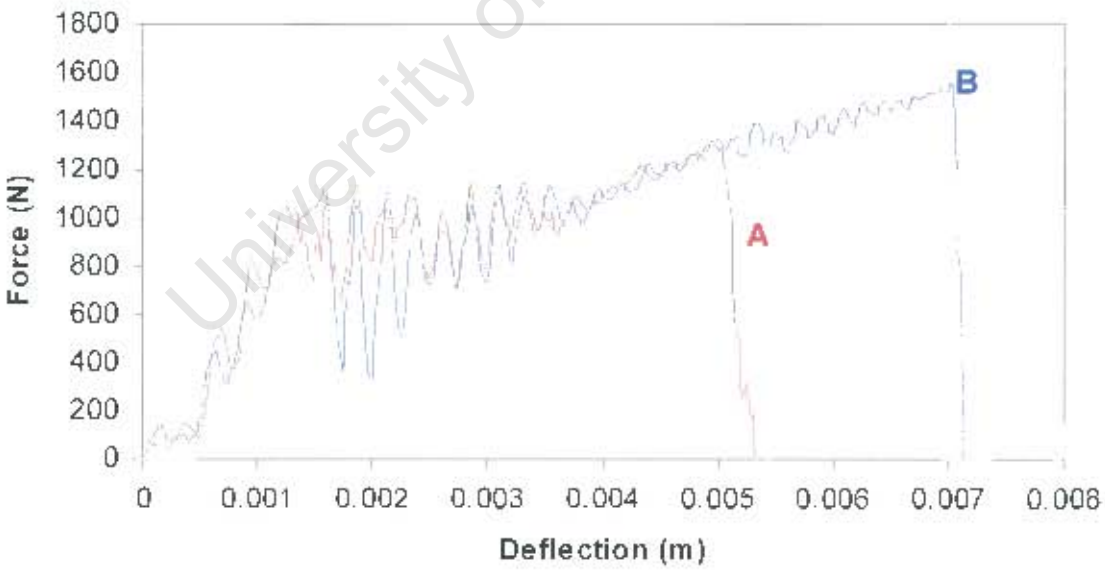

Figure 4.21: *Drop-weight force versus deflection curves for 30SGFRPA 6-6 specimens tested at (A) –35 ^{0}C and (B) 20 ^{0}C.*

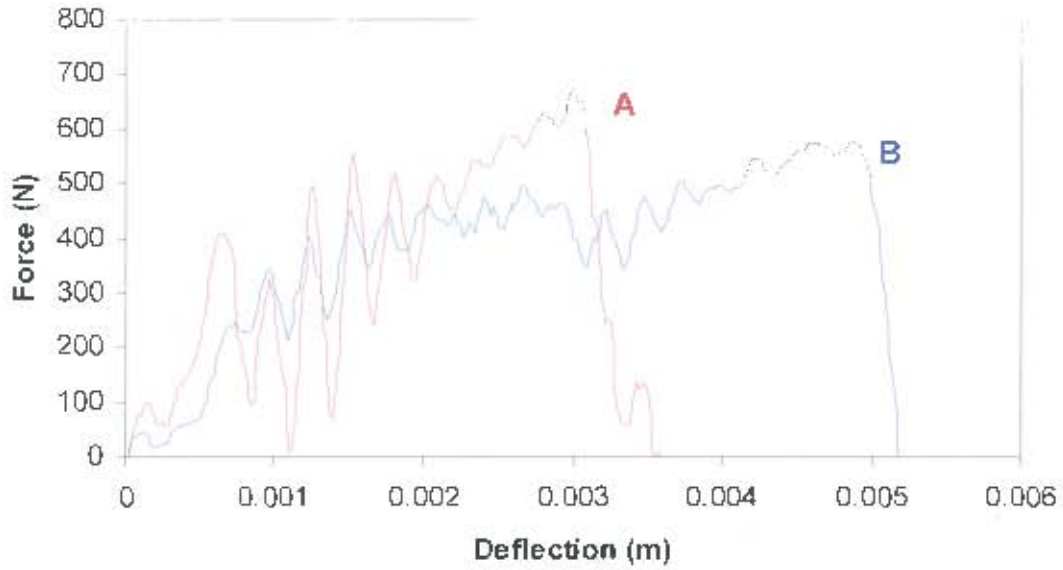

Figure 4.22: *Drop-weight force versus deflection curves for 30Talc/PP specimens tested at (A) –35 ^{0}C and (B) 20 ^{0}C.*

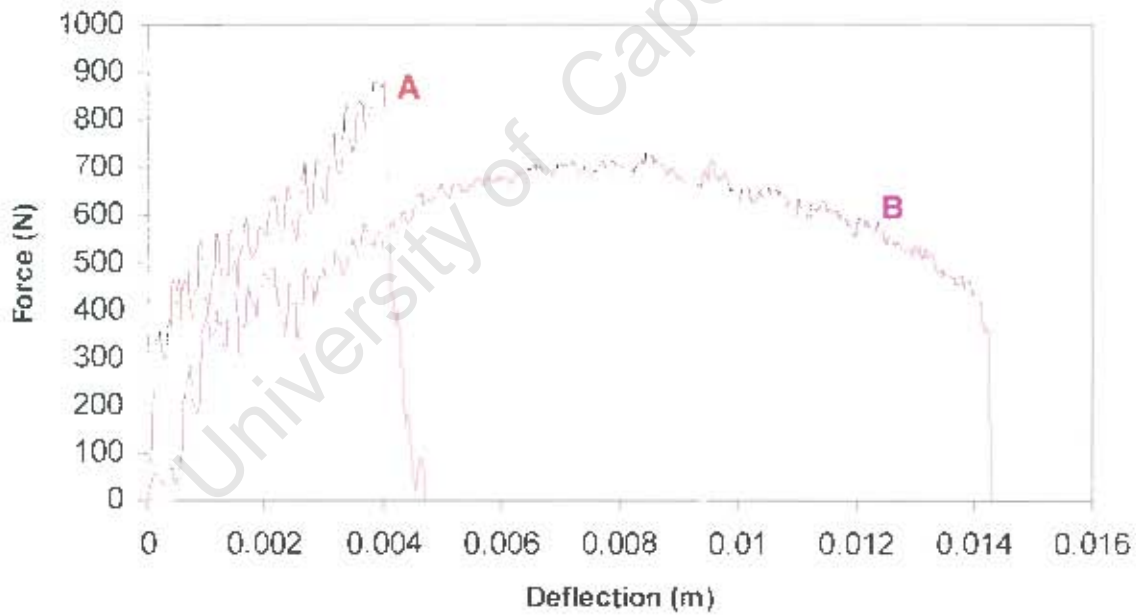

Figure 4.23: *Drop-weight force versus deflection curves for 30SGFRPP specimens tested at (A) –35 ^{0}C and (B) 20 ^{0}C.*

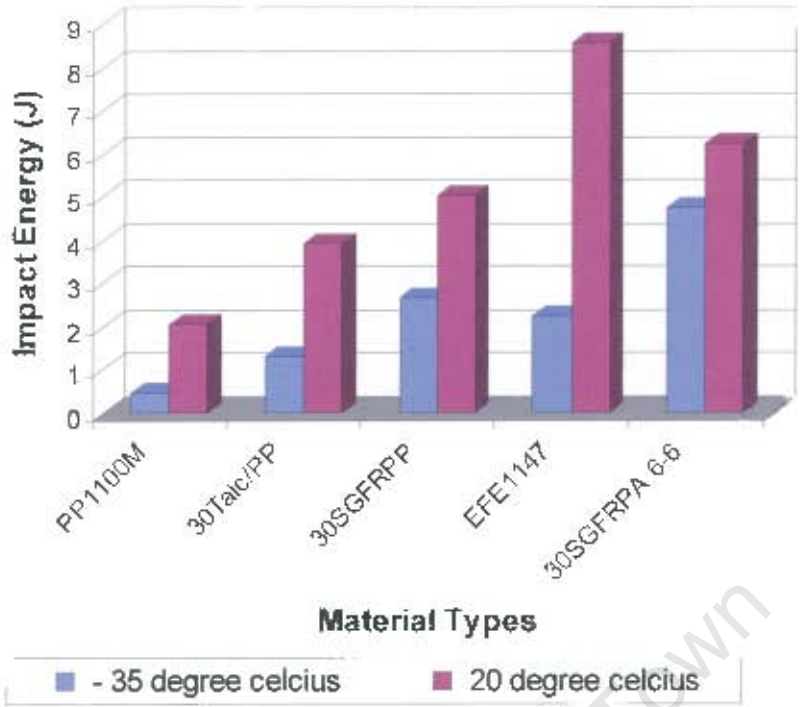

Figure 4.24: *Drop-weight impact energy of materials tested at -35 ^{0}C and 20 ^{0}C.*

4.2.3.2.2 Strain Rate influence on the Drop-weight Impact Response

The results in Figures 4.25 to 4.30 show the dependence of the polymer composites materials with strain rate. The strain rate was varied during drop-weight testing by changing the drop height on the drop tower. Variations in the drop height change the impact speed thereby subjecting the specimens to different rates of strain. The drop-weight energy response was observed under different impact velocities (or different rates of strain).

The graphs in Figure 4.25 show the drop-weight force-deflection curves of polyamide 6-6 (EFE1147) at different drop heights (or strain rates or velocities). Curve (A) shows a ductile response at 300 mm. When the polyamide specimen was impacted at 600 mm, the failure mode changed from ductile to brittle failure. A further increase in the drop height increased the impact force and the deflection of polyamide 6-6. The drop weight response for short fibre reinforced polyamide 6-6 (30SGFRPA 6-6) at the three drop heights is different from that observed for polyamide 6-6. Figure 4.26 show the decrease in the deflection of the material as the drop height is increased. The impact force increases when the drop height is increased from 300 mm to 600 mm and decreases with further increase in the drop height to 1200 mm. Figure 4.27 shows the impact response of polypropylene (PP1100M). It is clear from the graph that the deflection and the impact force increase with the drop height. This behaviour was observed for polyamide 6-6. However, polypropylene curves show a sharp decrease in the force after reaching the maximum at all three heights.

Polypropylene composites, like polyamide 6-6 composites, show a different response to that of unfilled polypropylene when the drop height is increased (see Figures 4.28 and 4.29). The curves show a decrease in the deflection when the drop height is increased. The impact force increases when the drop height is increased from 300 mm to 600 mm and decreases with a further increase in the

drop height to 1200 mm. The polymer composites show similar trends at the various heights while unfilled polymers also show similar trends.

The response of all the materials tested is summarised in Figure 4.30. The impact energy increases with increasing drop height for unfilled polypropylene and polyamide 6-6. Composites materials (30Talc/PP, 30SGFRPP and SGFRPA 6-6) show a slight increase in the impact energy when the drop height is increased from 300 mm to 600 mm. A decrease in the impact energy of composite materials is observed in Figure 4.30 when the drop height is further increased to 1200 mm.

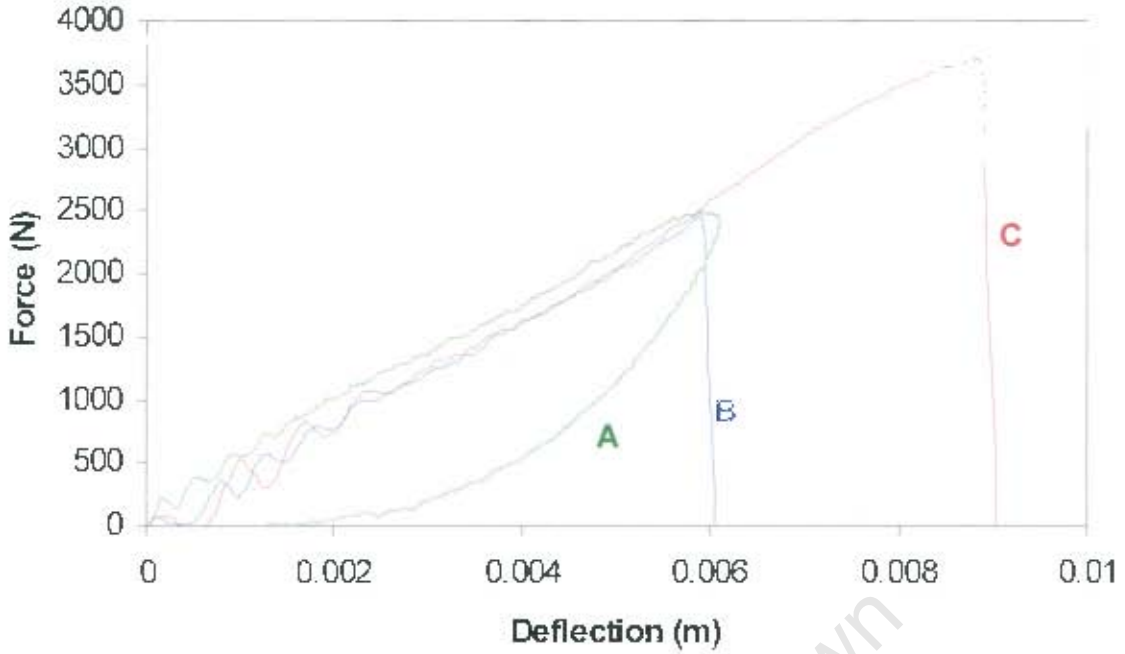

Figure 4.25: *Drop-weight force versus deflection curves for EFE1147 at (A) 300 mm, (B) 600 mm and (C) 1200 mm.*

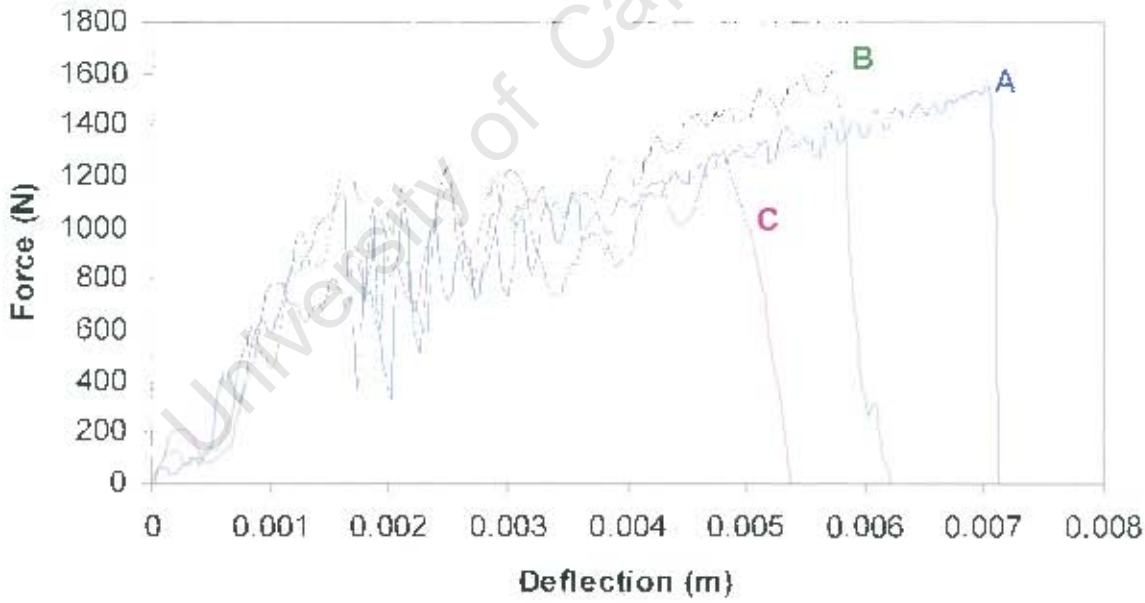

Figure 4.26: *Drop-weight force versus deflection curves for 30SGFRPA 6-6 at (A) 300 mm, (B) 600 mm and (C) 1200 mm.*

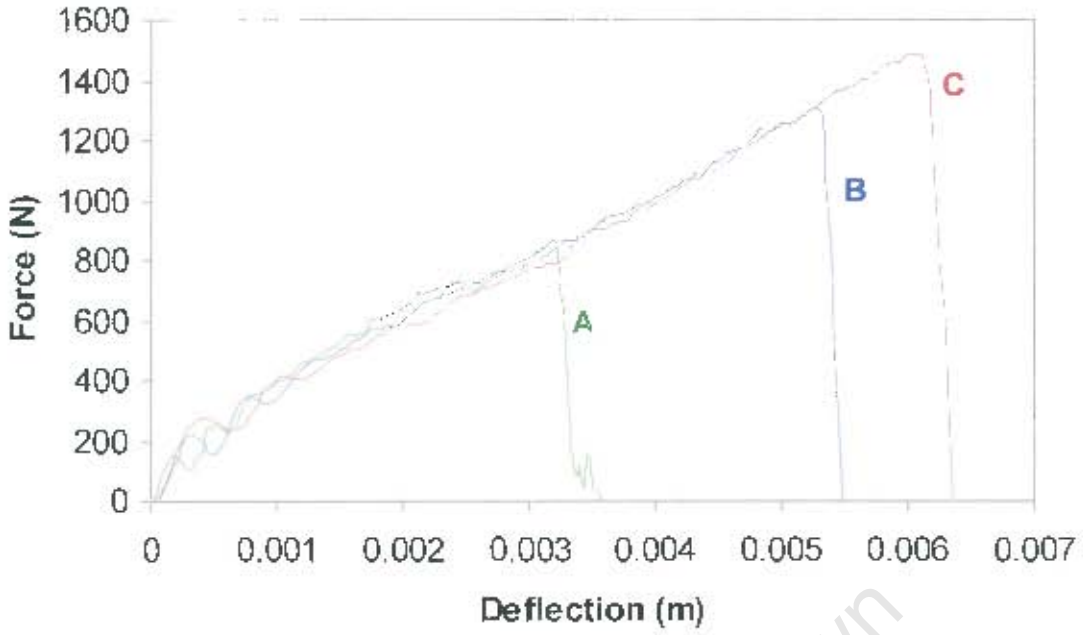

Figure 4.27: *Drop-weight force versus deflection curves for PP1100M at (A) 300 mm, (B) 600 mm and (C) 1200 mm.*

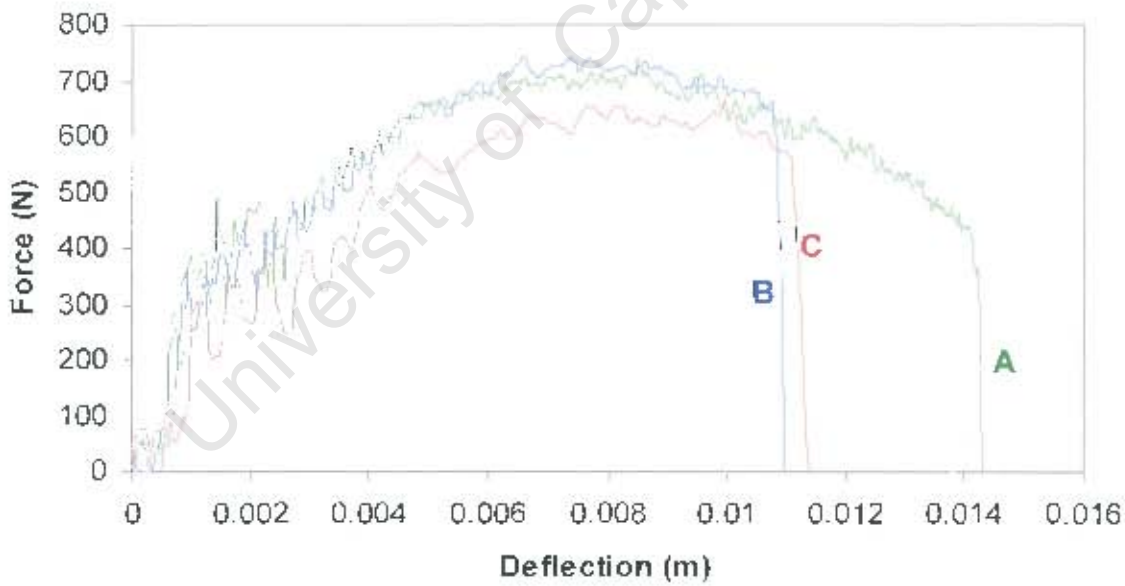

Figure 4.28: *Drop-weight force versus deflection curves for 30SGFRPP at (A) 300 mm, (B) 600 mm and (C) 1200 mm.*

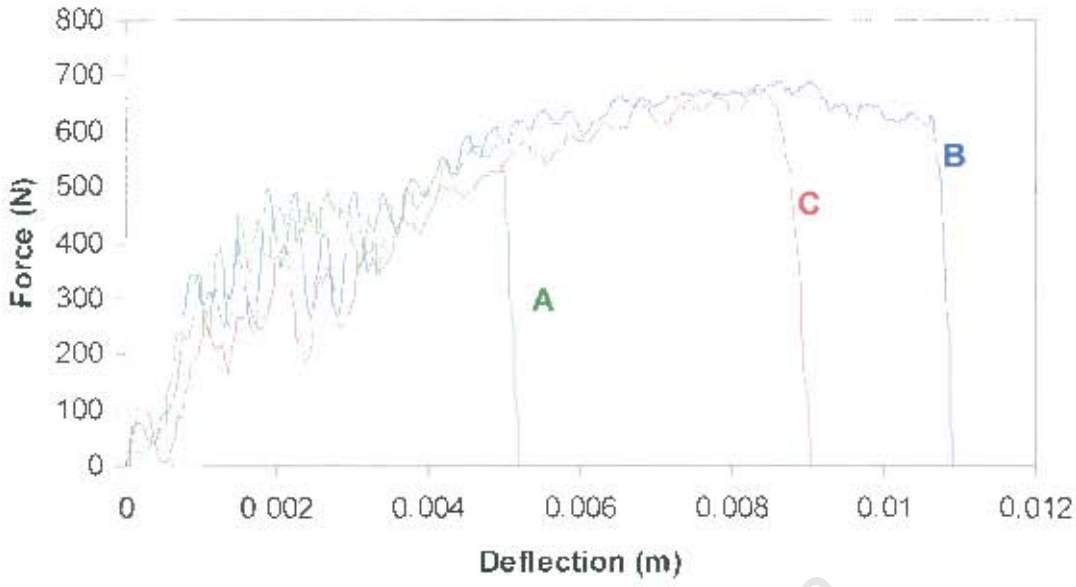

Figure 4.29: *Drop-weight force versus deflection curves for 30Talc/PP at (A) 300 mm, (B) 600 mm and (C) 1200 mm.*

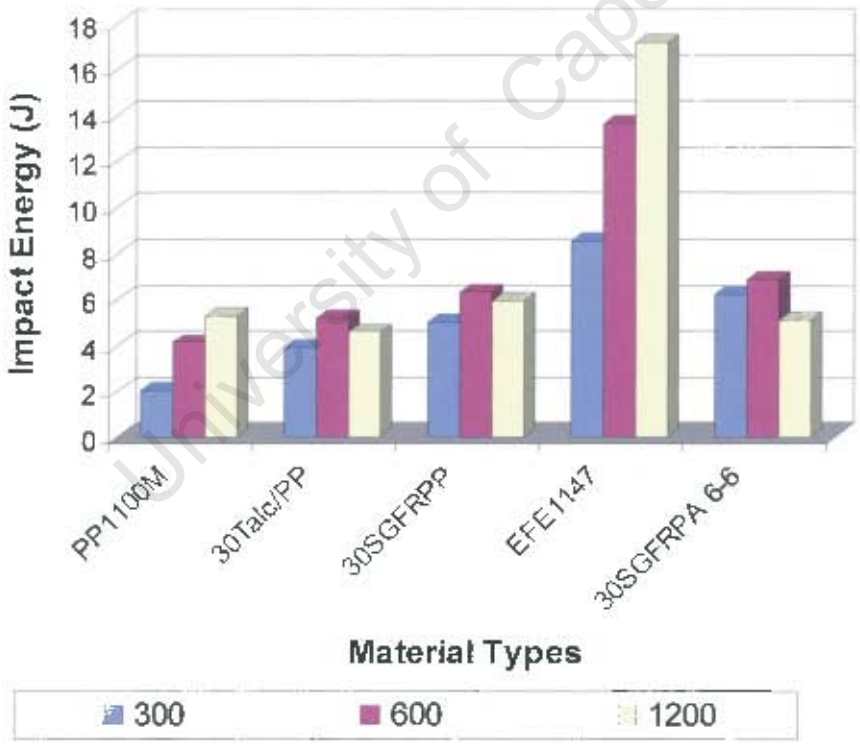

Figure 4.30: *Comparison of drop-weight impact test results for specimens impacted from different drop heights.*

4.3 FRACTURE MODES

Photographs of the fractured specimens were taken to observe the mode of fracture that occurs in the material during drop-weight testing. Different fracture modes were observed on the specimens. The most apparent modes were stress whitening, radial cracking and cone fracture. These fracture modes depend on the composition of the specimen. Unfilled polymers show multiple cracks radiating from the centre of the specimen. The common fracture mode that is visible in the composite materials under drop-weight impact is the cone fracture. This mode of fracture can be seen on the under side of the specimen.

The area of the specimen that revealed visible damage with the naked eye is shown in Figure 4.31. This shows the specimen that is supported horizontally by the clamp with a circular opening that exposes the specimen. Damage initiates at the centre of the specimen throughout the radius of the specimen. This damage, however, does not exceed the specimen-clamp contact point (A in Figure 4.31). The radial cracks are apparent in Figures 4.32 and 4.33 (see B and C). These cracks are radiating from the impacted area at the centre of the specimen. Polypropylene specimens (Figure 4.32) show less radial cracking than polyamide 6-6 specimens (Figure 4.33).

The effect of lowering the temperature to –35 ^{0}C can be seen in Figures 4.34 where a circumferential crack joins with the radial cracks separating out small pieces of the specimen. Higher strain rate effects are similar to low temperature effects. This can be seen in Figure 4.35 where a large hole is seen at the middle of the specimen as a result of the breaking off of the small pieces of the specimen during impact. Cone fracture is the most visible fracture mode on the underside of the short glass fibre reinforced thermoplastic specimens (see Figure 4.36). No radial cracking is visible with the naked eye. All the specimens have shown a brittle fracture mode at all testing conditions with the exception of the

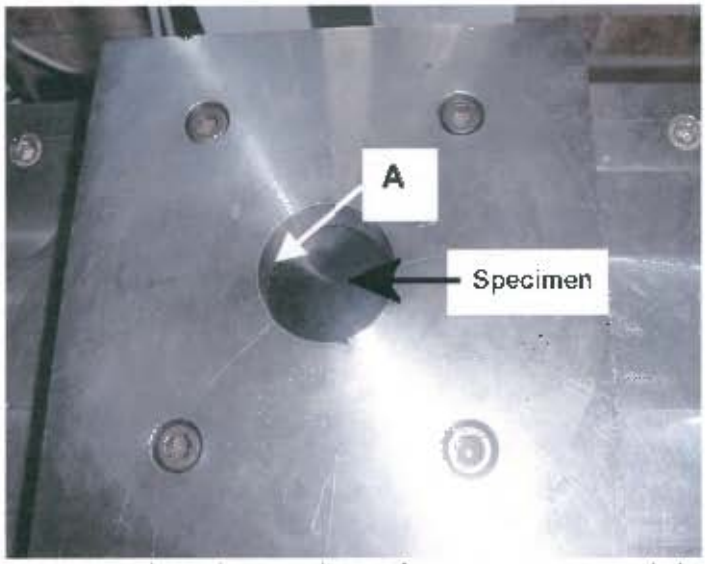

Figure 4.31: *Specimen clamping system of the instrumented drop-weight tower.*

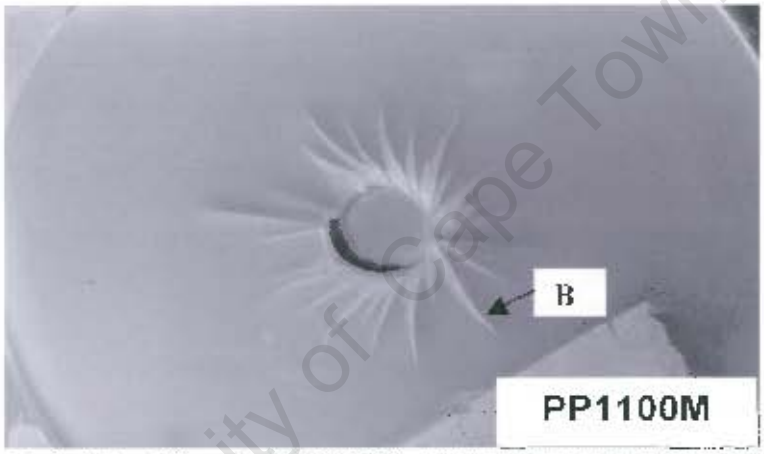

Figure 4.32: *Radial cracking in PP1100M after drop-weight impact.*

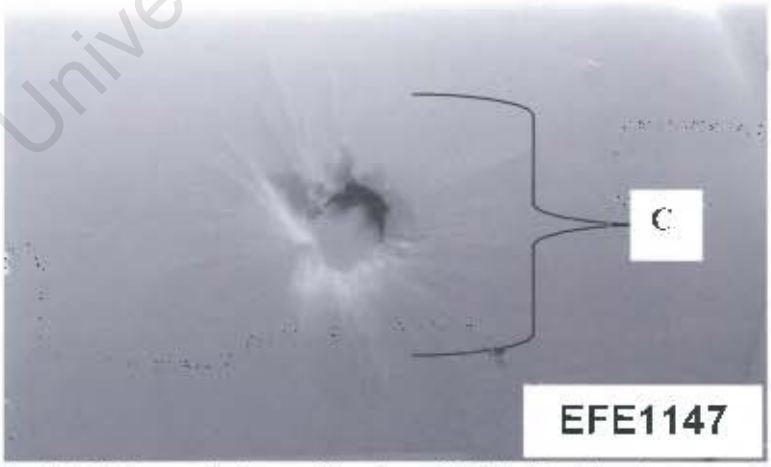

Figure 4.33: *Multiple radial cracking in EFE1147 after drop-weight impact.*

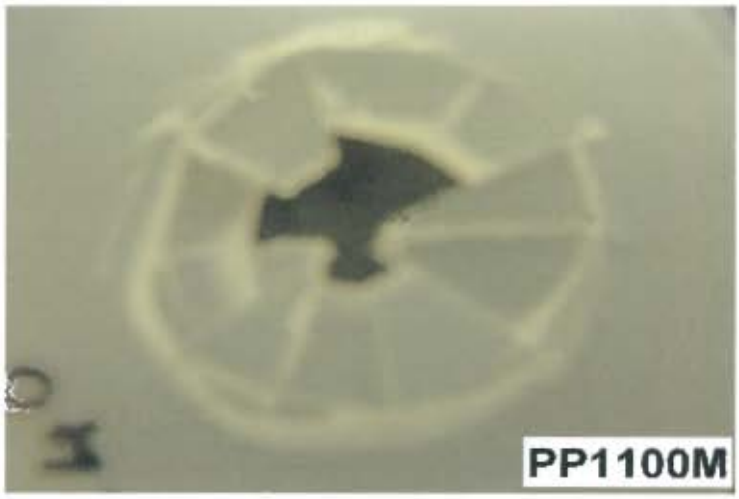

Figure 4.34: *Brittle fracture of PP1100M at –35 °C after drop-weight impact.*

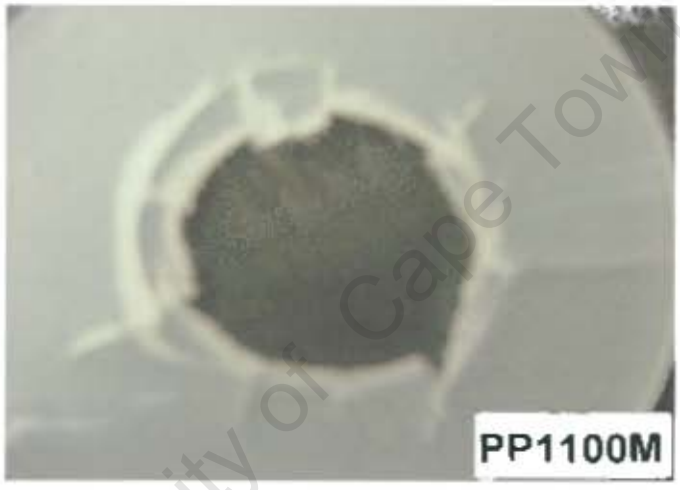

Figure 4.35: *Brittle fracture of PP1100M from a drop height of 1200 mm.*

Figure 4.36: *Cone fracture in short fibre reinforced polyamide 6-6 specimens.*

4.4 FILLER ORIENTATION

Short fibres rotate in the melt and assume different orientations as a result of non-uniform melt flow across an injection moulded bar specimen. Light microscopy (LM) and scanning electron microscopy (SEM) were used to determine the fibre orientation by observing a polished section across the specimen bar. The observations are shown in Figures 4.37 to 4.40. Figure 4.37 represents the section taken near the surface of the short glass fibre reinforced polypropylene bar specimen. The double arrows indicate the length of the specimen and the arrow point towards the centre of the bar specimen. It can be seen in Figure 4.37 that the fibres are aligned along the specimen length near the surface while the orientation tend to be random towards the core of the specimen. Fibres are orientated randomly at the middle of the specimen (see Figure 4.38).

The fibre orientation was also investigated using SEM. Micrographs of 30SGFRPP taken near the surface and in the core of the specimen are shown in Figure 4.39 (A) and (B), respectively. The double arrows indicate the specimen length. Micrograph (A) shows the fibres that are aligned along the length of the bar specimen. The change in the fibre orientation can be seen in the micrograph (B). Talc filled polypropylene specimens were also observed under the light microscope to determine the orientation of talc plates (see Figure 4.40). The double arrow indicates the width of the specimen. The talc plates are seen laying flat in the melt flow direction.

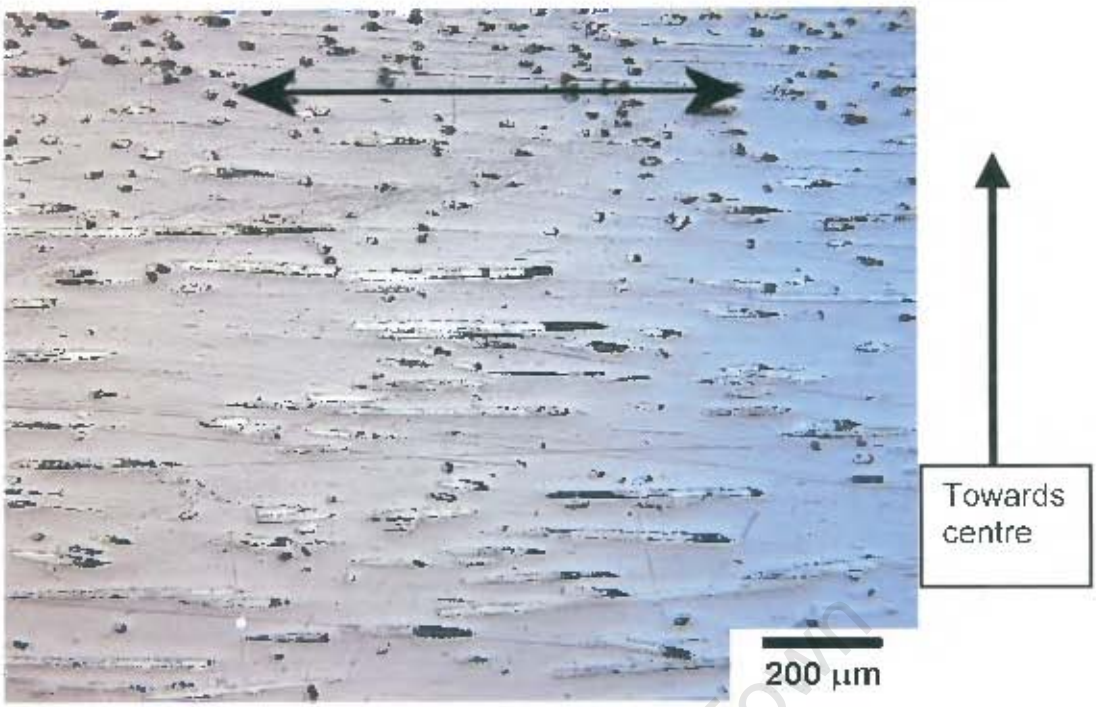

Figure 4.37: *Micrograph of a polished outer section of short glass fibre reinforced polypropylene (30SGFRPP) bar specimen.*

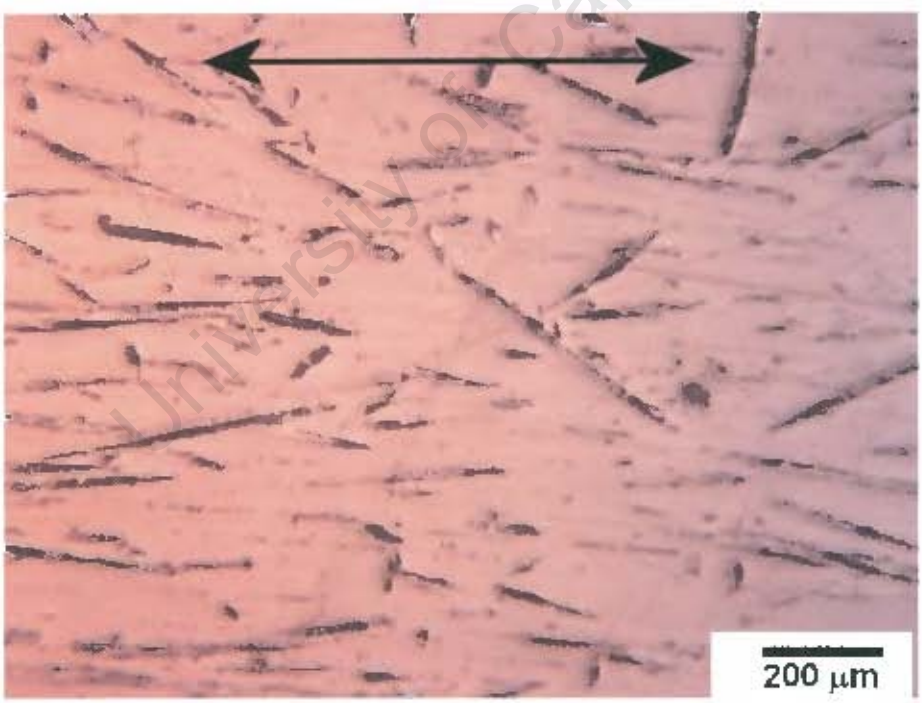

Figure 4.38: *Micrograph of a polished middle section of short glass fibre reinforced polypropylene (30SGFRPP) bar specimen.*

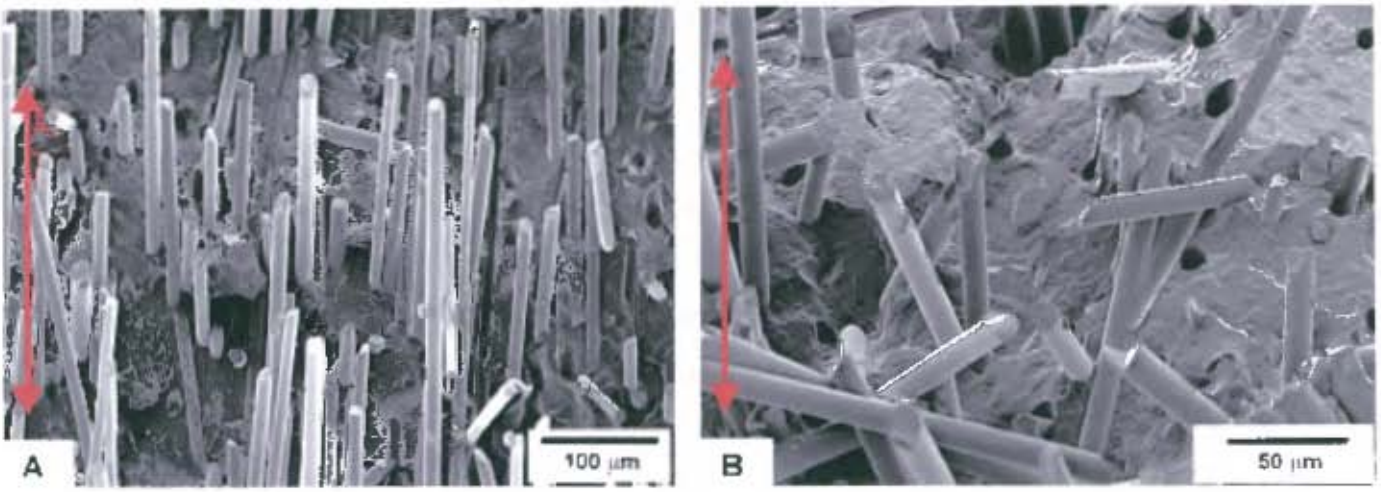

Figure 4.39: *SEM micrographs of the tensile fractured surface of 30SGFRPP specimens showing fibre orientation at (A) the surface and (B) in the core of the specimen.*

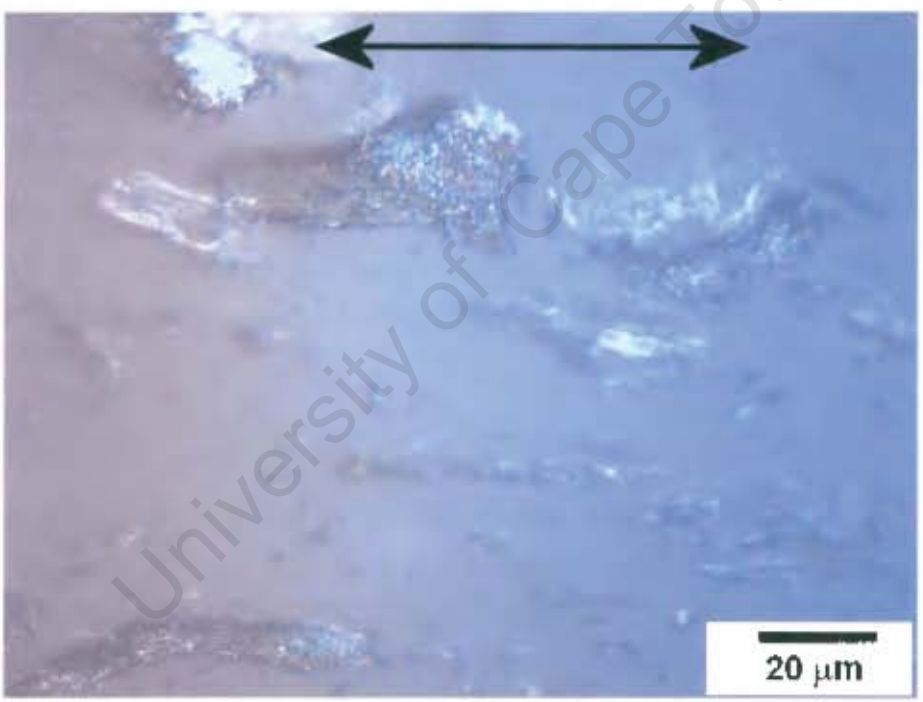

Figure 4.40: *A polished cross section of talc filled polypropylene (30Talc/PP) bar specimen.*

a cluster of fibres that are covered with the polymer matrix resin. This is a result of a strong interface bond in the polyamide 6-6 composite. The drop-weight fracture surfaces of polypropylene and polyamide 6-6 composites also show the relatively weak and strong interface bond, respectively (see Figure 4.42 (A) and (B)). The polypropylene fracture surface (A) shows clean fibres and the arrow shows a separation between the fibre and the matrix. Micrograph (B) shows glass fibres that are covered with the polyamide 6-6 resin.

Figure 4.42 (C) and (D) show the tensile and three-point bend fracture surfaces of talc filled polypropylene, respectively. The tensile fracture surfaces show signs of matrix plastic deformation between the talc plates (see the arrows). Talc plates can be observed clearly on the three-point bend fracture surface (D). No plastic deformation is observed on the three-point bend fracture surface. Figure 4.42 (E) and (F) represent the three-point bend fracture surfaces of the polypropylene composite (30SGFRPP) and unfilled polypropylene (PP1100M) specimens processed by the manually operated injection-moulding machine. The polypropylene composite fracture surface shows extensive matrix plastic deformation with clean fibres. These observations are different from those observed on the specimen prepared by the automated machine (Figure 4.41 (E)). The three-point bend specimen of polypropylene prepared by the manually operated machine fractured during testing and the fracture surface show a brittle fracture (Figure 4.42 F).

Temperature and strain rate effects can also be recognised on the fracture surfaces. Figure 4.43 (A) and (B) show the micrographs showing the changes in the matrix fracture when the temperature was altered to 20 ^{0}C and -35 ^{0}C, respectively. The fracture surface shows more brittle fracture morphology at –35 ^{0}C. The specimen tested at 20 ^{0}C shows fracture surfaces with fibres covered with the matrix while that of the specimen tested at –35 ^{0}C shows little matrix covering the fibres. Figure 4.43 C and D show the fracture surfaces of unfilled

polyamide 6-6 (EFE1147) specimens that were impacted from 600 mm and 1200 mm drop heights, respectively. The fracture surfaces show a brittle fracture with striation marks. Stepped features are observed in micrograph (C) which was tested at the lower impact speed. These features seem to be less visible when the specimens were tested at higher impact speeds.

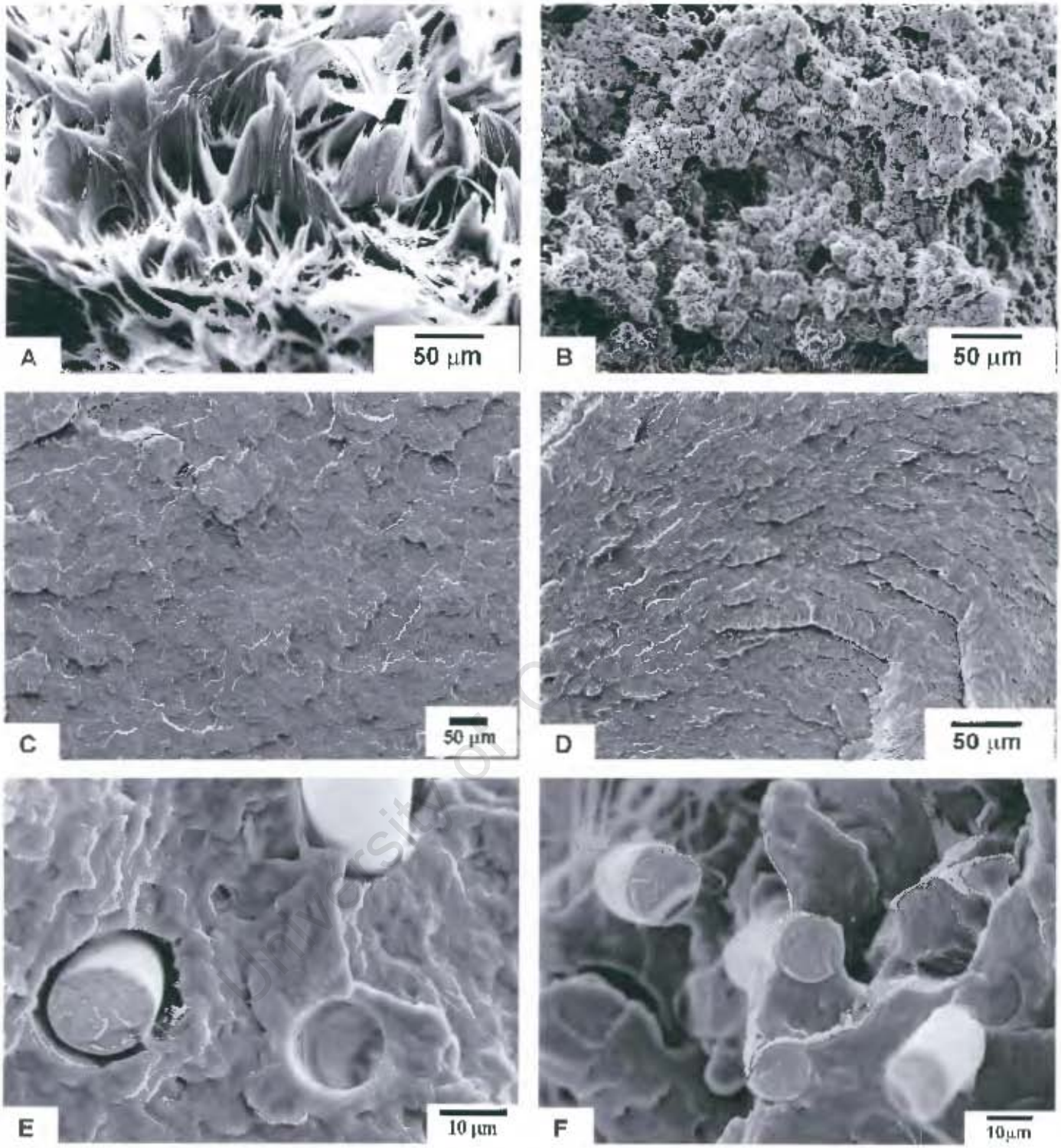

Figure 4.41: *SEM micrographs of the fractured surface of: (A) tensile PP1100M-Au, (B) tensile EFE1147-Au, (C) Charpy PP1100M-Au, (D) Izod EFE1147-Au, (E) 3-point bend 30SGFRPP-Au and (F) 3-point bend 30SGFRPA 6-6-Au.*

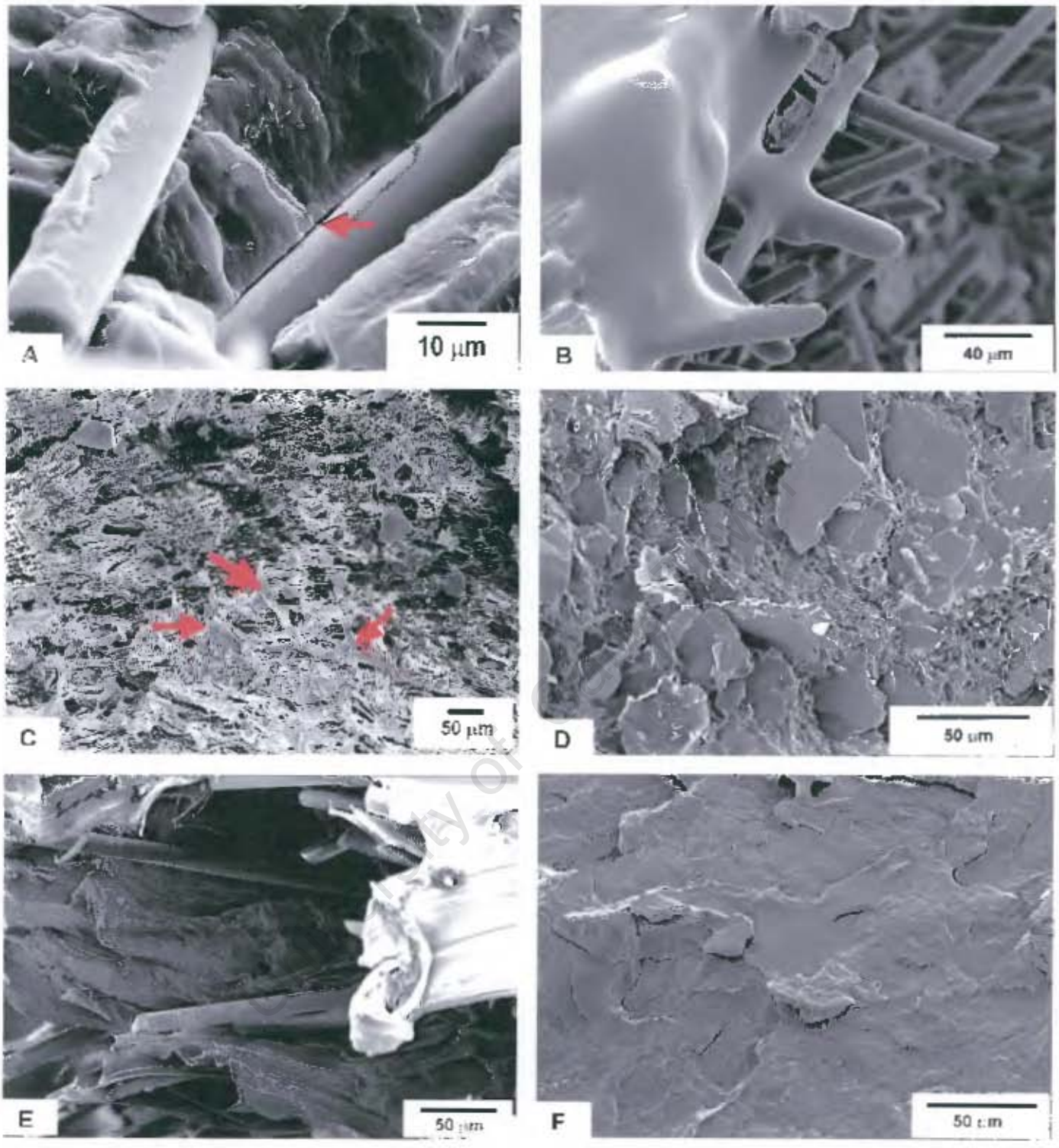

Figure 4.42: *SEM micrographs of the fractured surfaces of: Drop-weight (A) 30SGFRPP-Au and (B) 30SGFRPA 6-6-Au, (C) tensile 30Talc/PP-Au, (D) 3-point bend 30Talc/PP-Au and 3-point bend (E) 30SGFRPP and (F) PP1100M specimens.*

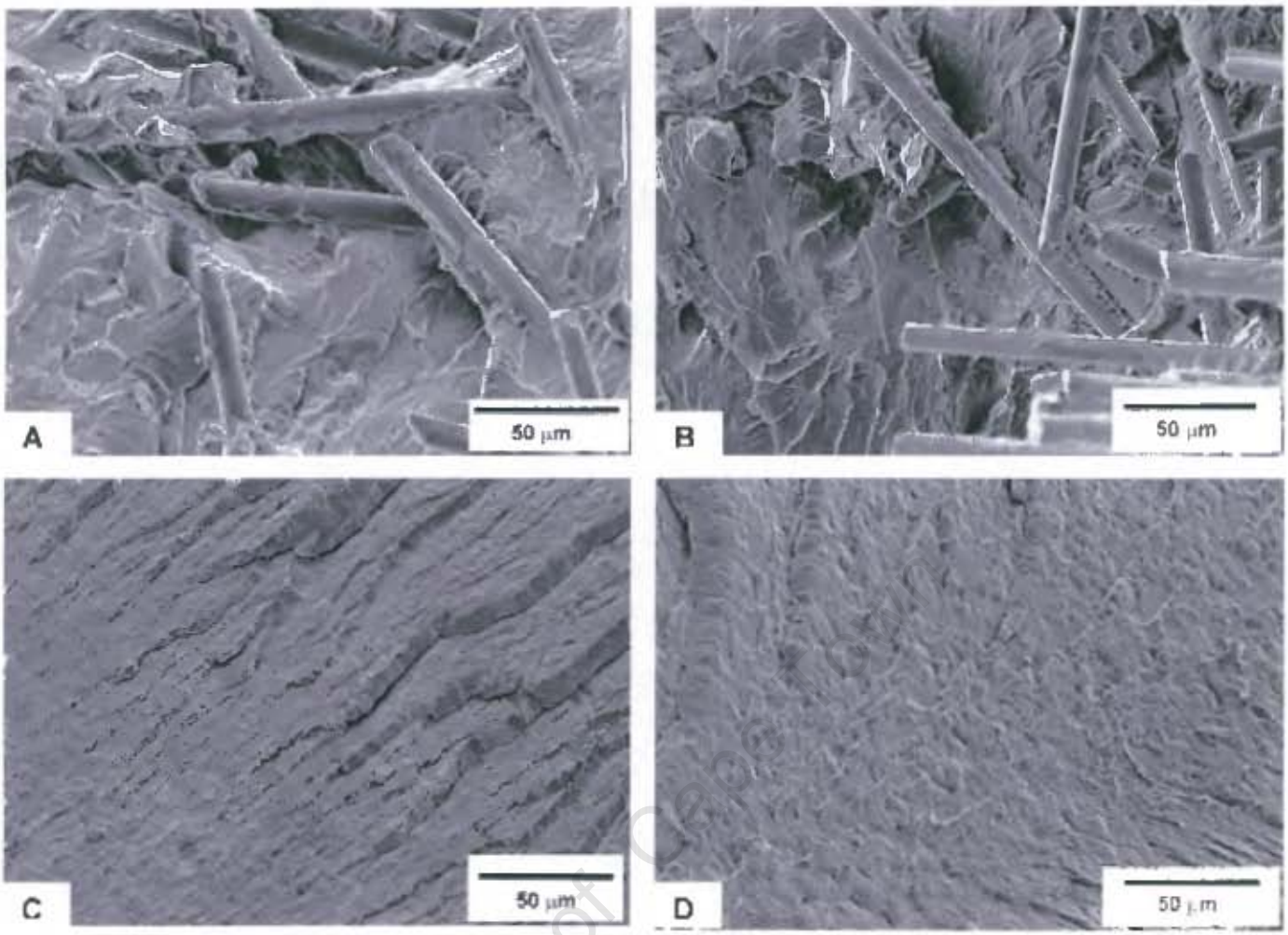

Figure 4.43: *Fracture surfaces of (A) 30SGFRPA 6-6 tested at 20 ^{0}C, (B) 30SGFRPA 6-6 tested at –35 ^{0}C, EFE1147 tested at (C) 600 mm and (D) 1200 mm drop heights.*

4.6 SURFACE MORPHOLOGY AND CRACK PROPAGATION

Polymer composites contain micro-voids, which can enhance damage when the material is stressed. Surface defects can be seen in Figure 4.44 (A) along the fibres. These are voids and micro cracks formed near the fibres during specimen preparation as a result air bubbles and insufficient wetting of the fibres by the matrix. Micrograph (B) in Figure 4.44 shows a magnified void, which can enhance the propagation of a crack by coalescing with other voids. The mechanism of crack propagation by coalition of voids can be seen in Figure 4.44 (C) on the surface of short glass fibre reinforced polyamide drop-weight specimen where the arrows show cracks propagating and joining leading to catastrophic failure. Crack propagation on the three-point bend specimen shows a sinusoidal movement representing different mechanisms of propagation and fibre breakage. The crack on the three-point bend specimen is on the tensile side.

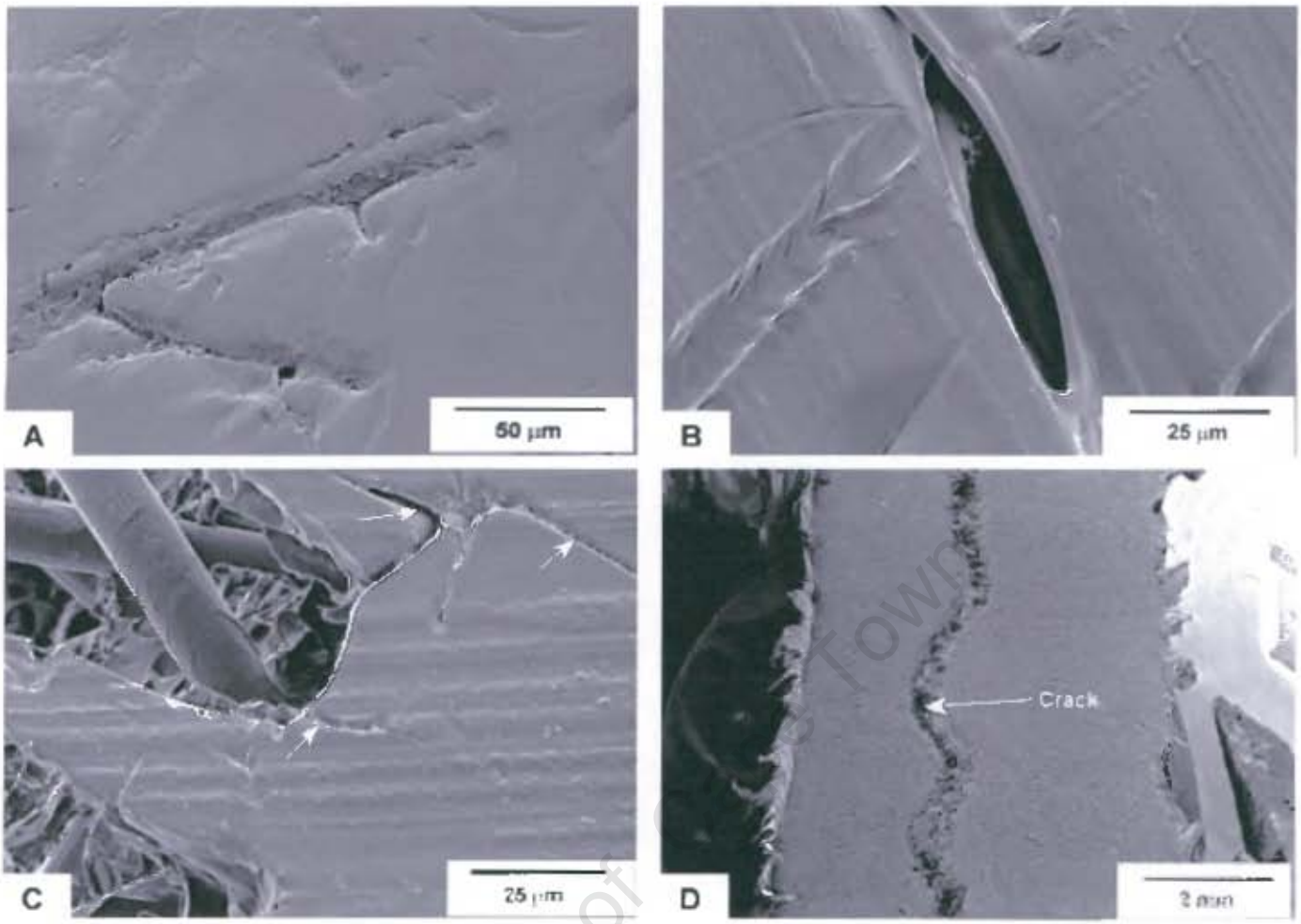

Figure 4.44: *SEM micrographs showing (A and B) surface defects on the surface of 30SGFRPP bar specimen and (C and D) crack propagation on the surface of 30SGFRPA 6-6 and 30SGFRPP specimens.*

CHAPTER 5

DISCUSSION

There are several factors that influence the mechanical properties and the mechanisms of failure for polymer composites. The use of different experimental techniques allow for the investigation of factors and microscopic features that are involved in the failure of thermoplastic matrix composites materials. Changes in the microstructural properties of polymeric materials occur as a result of filler additions, processing conditions and the variations in the mechanical testing conditions.

This chapter gives the details of the observations reported in chapter four about the variations in the mechanical properties of thermoplastic polymers and their composites when they were exposed to different test and processing conditions. Some of the mechanical properties obtained is this research are different from those provided by PLASTAMID Pty Ltd. This is due to different test conditions. The changes that are observed in the microstructural features are also discussed. All the results obtained in this research work are discussed in this chapter.

5.1 MOISTURE ABSORPTION OF POLYAMIDE 6-6

The higher sensitivity of polyamide 6-6 materials to moisture has been proven. The results of the experiment show that polyamide 6-6 and short glass fibre reinforced polyamide 6-6 have moisture contents that is close to zero after injection moulding. However, the moisture content increases to a saturation level over a period of time. This is indicated by the initial linear relationship between moisture uptake and time that is followed by the saturation. This behaviour was expected since moisture absorption follows Fick's law of diffusion. Both materials reach saturation in less than 24 hours. Moisture attacks the hydrogen bond of the amide group in polyamide 6-6. This results in the disruption in the structure and the decrease in a glass transition temperature. The movement of molecular chains is increased by moisture and this result in matrix plasticization.

In glass fibre reinforced polyamide 6-6, moisture, apart from the hydrogen bonds in the polymer structure, attacks the hydrogen bond between the matrix resin and the fibres. This is because water has polar molecules and it can therefore be said to compete with the hydroxyl group on the coupling agent of the glass fibre at the interface. This weakens the fibre-matrix interface bond strength. However, additions of short glass fibres in polyamide 6-6 have resulted in a decrease in the moisture uptake. Mohdishak et al deduced that this is a result of the decrease in the direct moisture absorption into the polymer matrix because of hindrance by the complex fibre orientation in the composite[13]. This reduction in moisture absorption with glass fibre additions is also due to the fact that glass fibres do not participate in moisture absorption and they have replaced 30% of the hygroscopic polyamide 6-6.

5.2 FACTORS THAT INFLUENCE THE FAILURE MECHANISMS

5.2.1 Influence of the Polymer Matrix Type

The chemical composition of different polymers is different and so is their expected mechanical response. It was found in this research that the tensile, flexural and the impact test response were different for polypropylene and polyamide 6-6. Polyamide 6-6 has a higher tensile and flexural stress and elastic modulus than polypropylene. These variations in strengths are due to the differences in the molecular composition and structure of polypropylene and polyamide 6-6. Dasari et al and Tai et al have shown that different material compositions and structure give different stress-strain behaviour[38,62]. They found the differences to be due to different polymer chain size, the percentage crystallinity and the combined effects of the blended polymers.

The molecular structure of polypropylene is less complex and undergoes long chain disentanglement during tensile and flexural testing. Because of its complex molecular structure with the amine group and strong hydrogen bonding between the molecules, polyamide 6-6 polymer chains are not as closely packed and are also not easy to untangle. This can also be explained by the little amount of plastic deformation in polyamide 6-6 as compared to the extensive plastic deformation in polypropylene specimens at low strain rates. The findings of Fu et al show polypropylene to have a ductile type of stress strain curve due to the extensive plastic deformation when the polymer is stressed[48]. The fibril structure observed on the SEM fracture surface of polypropylene in this research work is evidence of the higher plastic deformation. The SEM fracture surface of polyamide has a clustered fibril structure that is due to little plastic deformation during necking. When the two polymers are compared, polyamide is said to have failed in a relatively brittle manner. Figure 5.1 shows (A) necking and extensive

plastic deformation in polypropylene specimen and (B) necking and little plastic deformation in polyamide 6-6 specimen.

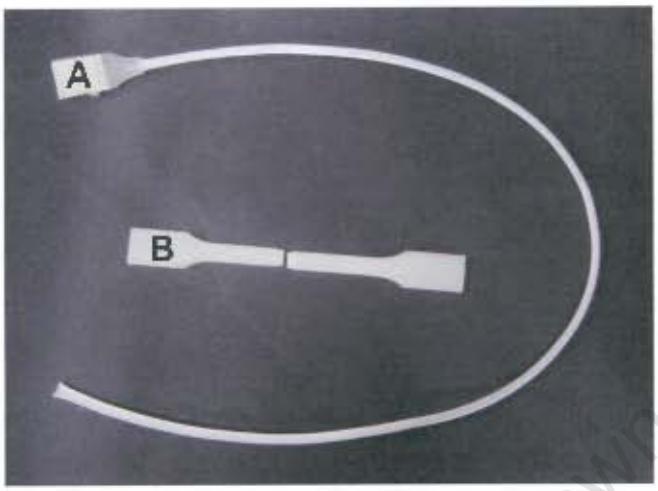

Figure 5.1: *Necking and plastic yielding in (A) polypropylene and (B) brittle fracture in polyamide 6-6.*

5.2.2 Influence of the Filler Additions

The addition of short glass fibres to polypropylene and polyamide 6-6 has increased their tensile and flexural stress and elastic modulus. The Izod and Charpy impact energies are also enhanced by glass fibres additions. The influence of glass fibres additions is due to the transfer of the applied stress from the low strength matrix to the high strength fibres. In fibre-reinforced composites, the fibres carry most of the stress. Talc fillers do not always enhance the strength and impact energy of polypropylene. This is due to the geometry of the talc filler particles. Addition of 30% short glass fibres to polypropylene did not affect the tensile strength of specimens prepared by the manually operated machine. The Izod and Charpy impact resistance of all specimens were also not affected. However, talc fillers are relatively cheap and they have a low density as compared to polypropylene. Talc fillers are therefore considered necessary for

reduction of the cost and density of the manufactured component. Nevertheless, the flexural stress of polypropylene is enhanced and the tensile stress of specimens prepared by the automated machine is reduced by the additions of talc fillers.

5.2.3 Influence of the Fibre-Matrix Interface Bond

Naturally many polymers do not sufficiently wet the surface of the reinforcing fillers. Coupling agents increase the wettability thereby increasing the filler-matrix interface bond strength. However, the strength of the polypropylene-glass fibre interface bond is not strongly enhanced by the coupling agent. This research has found that the dominant mechanism of failure in short fibre reinforced polypropylene is fibre-matrix debonding. This is a result of weak interfacial bond strength. When the fibre-matrix interface bond is weak, the applied stress is not sufficiently transferred from the matrix to the fibres. Fibre breakage is less dominant and the composite failure mechanism is matrix tearing and debonding. The SEM investigation revealed clean fibres and a clear separation of the polypropylene matrix from the glass fibres.

Polyamide 6-6 has greater wettability to the glass fibres than polypropylene. The SEM fracture surfaces of the polyamide 6-6 composite have shown fibres that are still covered with the matrix resin after failure. This indicates greater interface bond strength that allowed sufficient transfer of the applied stress from the matrix to the fibres. This resulted in fibre breakage and matrix tearing being the dominant failure mechanisms. The stronger interface bond has contributed to the higher tensile and flexural stress and impact resistance of the polyamide 6-6 composite.

5.2.4 Influence of the Stress Direction and the Type of Test

Stress direction is an important factor in the failure mechanisms of polypropylene and polyamide 6-6 composites. The stress in the tensile and the three-point bend test is applied in different directions. During tensile testing the stress is applied parallel to the reinforcing fibres the along specimen length while in the three-point bend testing the load is applied perpendicular to the specimen and fibre length. Three point bend specimens are stressed in tension and in compression while tensile specimens are not subjected to any compression stresses. More fibre breakage will occur in three-point bend specimens whereas fibre pullout will be dominant in tensile specimens. These are the reasons why the flexural strength and modulus are higher than the tensile strength and modulus. The high alignment of fibres along the length of the bar specimen near the surface of the specimen makes it difficult to compress and stretch the surfaces of the bar specimen during three-point bend testing hence higher stresses and moduli. Jeng and Chen found that fibres are aligned in the melt flow direction near the surface of the specimen and that the dominant mechanism of failure that absorbed most of the energy during flexure was crack initiation[54].

The influence of the change in the stress direction is also observed on the tensile, flexural and impact test fracture surfaces. Polypropylene undergoes plastic deformation during tensile testing forming fibril structures on the fracture surface while there is no plastic deformation observed on the fracture surfaces of the Charpy and Izod impact tests. However the major variation in the tensile and the impact test is the rate of strain. Varying the test type at constant stress direction does not significantly influence the material energy absorption. This research has found no significant changes in the Charpy and Izod impact energy and impact resistance.

5.2.5 Influence of the Processing Conditions

The mechanical properties and the failure mechanisms are affected by the processing conditions. The tensile and flexural stress and modulus of polypropylene and polyamide 6-6 composites for specimens prepared by the automated machine are different from those specimens prepared by the manually operated machine. The tensile and flexural stress and modulus of talc filled polypropylene were higher for specimens prepared by the manually operated machine as a result of the uncontrolled cooling time. These specimens have undergone fast cooling, which is influenced by talc fillers that encourage fast moulding cycles. Differential cooling occurs in the specimen resulting in the formation of the residual stresses and stiffening of the bar specimen hence higher stress and modulus.

For short glass fibre reinforced polypropylene, the stress and the modulus are lower for specimens prepared by the manually operated machine. The differences in the mechanical properties of the polypropylene composites prepared by the two machines are due to different machine settings. All the moulding conditions were known for the automated machine. With the manually operated machine, the injection speed and the holding pressure and time are not controlled. There was also no total control of the mould temperature between moulding cycles during manual moulding. Higher stiffness of the matrix is attained due to slower cooling of the specimens prepared by the manual machine. This may be due to higher crystallisation in the matrix that occurs during slow cooling. In glass filled polypropylene composites, the glass fibres are not significantly affected by processing conditions. However, the fibre-matrix interface is weakened resulting in insufficient transfer of stress from the matrix to the high strength fibres. This is the reason that short glass fibre reinforced polypropylene specimens prepared by the manual machine have lower strength and modulus than those prepared by the automated machine.

5.2.6 Influence of the Test Temperature

Temperature has a significant influence on the mechanical properties of polypropylene, polyamide 6-6 and their composites. The findings of this research compare the decrease in the maximum applied force of the polyamide 6-6 and short glass fibre reinforced polyamide 6-6 with a decrease in the test temperature. This is due to the stiffening of the matrix and weakening of the fibre-matrix interface strength that occurs when the test temperature is decreased. The ductile polyamide 6-6 matrix becomes brittle and the impact force and energy is reduced. The lower amplitudes of the sinusoidal curve of polyamide 6-6 composite indicate that temperature mainly affect the matrix. In the polyamide 6-6 composite the amount of stress transferred to the fibres is reduced hence the reduction in the impact force and energy. An increase in the applied force is seen in polypropylene, talc filled polypropylene and short glass fibre reinforced polypropylene composites when the test temperature is reduced.

The different behaviours observed in polypropylene and polyamide 6-6 composites when the temperature is reduced are due to the glass transition temperatures of their polymer matrices (Tg =-10 and 57 for polypropylene and polyamide 6-6, respectively). All the test temperatures are below the glass transition temperature of polyamide 6-6. This implies that polyamide is glassy at both testing temperatures. Therefore, reducing the test temperature from 20 ^{0}C to –35 ^{0}C makes it more glassy and brittle. Polypropylene, however, has a glass transition temperature that is between the two test temperatures. At 20 ^{0}C, polypropylene is rubbery with a lower impact force than at a temperature of –35 ^{0}C where the structure changes from rubbery to glassy thereby increasing the impact force. However, the impact energy is higher at 20 ^{0}C than at –35 ^{0}C.

The amount of plastic deformation is reduced in all materials tested in this research when the test temperature is reduced. This is also attributed to the

embrittlement of the matrix. The fracture surface of the polyamide 6-6 composite shows a large area of the fibres that are not covered by the matrix. This is a result of a weak fibre-matrix debonding failure mechanism that occurred after the interface bond strength was weakened by the decrease in the test temperature. At low temperature, the polymer matrix becomes stiff and brittle. The interface shear strength is reduced by this embrittlement of the matrix resulting to weak interface strength and extensive cracking of the matrix (Megusar)[64]. Gorbatkina and Sulyaeva investigated the effect of low temperature (below the glass transition temperature of the polymer composite) on the interface strength of thermoplastic composite and thermosetting composites. They found that the interface strength is reduced by the decrease in the test temperature. Gorbatkina and Sulyaeva said the decrease in the interface strength can be attributed to the increased thermal residual stresses, formed at the interface during fabrication, when the temperature is reduced[63]. The impact energy was found to be lower for specimens tested at lower temperatures. This is due to the decrease in the area under the force-deflection curve with a decrease deflection and the maximum impact force.

5.2.7 Influence of the Strain Rate

The impact behaviour of thermoplastics and thermoplastic composites is dependent on strain rate. The impact force and the deflection of polypropylene and polyamide 6-6 increase with an increase in the impact velocity. This is due to the increased energy for the unfolding of the molecular chains. Polymer resins dissipate a significant amount of energy through plastic deformation on impact. The increase in the impact velocity increases the amount of plastic deformation in the unfilled polypropylene and polyamide 6-6. The deflection of polypropylene- and polyamide 6-6 composites decrease with increase in the impact velocity. This is attributed to the reduced amount of polymer resin that is involved in the plastic deformation mechanism. Okoli determined the impact behaviour of woven

glass/epoxy laminates at increasing rates of strain and found that the absorbed impact energy increases as the strain rate is increased. Okoli said this is a result of the increased matrix yielding at higher test speeds[56].

The matrix yielding is indeed the most energy dissipating mechanism during drop-weight impact. This is proven by the decrease in the absorbed impact energy in polypropylene and polyamide 6-6 composites at the highest impact velocity. Polypropylene undergoes higher plastic deformation than polyamide 6-6 but polyamide absorbs more energy on impact than polypropylene. This is due to the stronger hydrogen bonds in the molecular structure of polyamide 6-6 and its complex chain structure.

5.3 TEMPERATURE AND STRAIN RATE SENSITIVITY

The sensitivity of thermoplastic composites to temperature and strain rate is dependent on the composition and the fibre-matrix bond strength. It was found in this research that the sensitivity is different for different materials tested. Figure 5.2 and 5.3 compares the sensitivity of the tested materials to temperature and strain rate, respectively. The temperature sensitivity was obtained by calculating the percentage decrease in the impact energy when the test temperature was reduced from 20 ^{0}C to –35 ^{0}C while the strain rate sensitivity was obtained by calculating the percentage change in the impact energy when the impact height was increased from 300 mm to 600 mm and from 600 mm to 1200 mm.

Polypropylene is more sensitive to temperature than Polyamide 6-6. This is due to the glass transition temperature where the decrease in temperature causes a transition from a rubbery state to a glassy state in polypropylene. The impact energy is reduced by these changes in the polypropylene matrix when the test

temperature is reduced. For polyamide 6-6, the decrease in temperature causes an increase in the glassy state but the percentage decrease in the impact energy absorbed on impact is less than that in polypropylene that was transformed from rubbery to glassy state. Polypropylene composites also have higher sensitivity than polyamide 6-6 composites. This could be attributed to the weakening of the fibre-matrix interface bond strength at lower temperature (–35 ^{0}C). Polyamide 6-6 is susceptible to moisture attack. The hydrogen bonds of the polymer-matrix interface are disrupted by moisture at –35 ^{0}C thereby reducing the interface bond. When the interface bond is weak, the applied stress is less transferred from the matrix to the fibres. This leads to failure by debonding and matrix plastic deformation. Since debonding will occur in both polypropylene and polyamide 6-6 composites and polypropylene undergoes higher plastic deformation, polypropylene absorbs less energy at low temperature though since no or little plastic deformation occurs at –35 ^{0}C. Amongst the polypropylene composites, short glass fibre polypropylene is less sensitive to temperature than talc filled polypropylene because talc does cause less embrittlement than glass.

Polypropylene is also highly sensitive to strain rate compared to polyamide 6-6. This can be seen in Figure 5.3 where the strain sensitivity is high for polypropylene when the drop height was increased from 300 mm to 600 mm and from 600 mm to 1200 mm. When the drop height is increased from 300 mm to 600 mm, the sensitivity is higher for polypropylene composites than for polyamide 6-6 composites. This is due to the fast fracture that occurs, which does not allow any high-energy absorption mechanism in the glassy and embrittled polyamide 6-6 composite when the test speed is increased. Polypropylene composites still undergo fibre-matrix debonding that dissipates more energy than brittle cracking. When the strain rate is increased further, the impact energy of the composite materials decreases and the percentage decrease of the polyamide 6-6 composite is higher than that of the polypropylene composites. Mohdishak et al found that the fracture properties of short fibre reinforced polyarylamide composites are influenced by the strain rate. The fracture toughness is reduced

when the test speed is increased. Mohdishak et al attributed this to the embrittlement of the matrix and the reduction in the matrix plastic deformation under high velocity conditions[13]. The percentage decrease in the impact energy is indicated by the negative sensitivity in Figure 5.3.

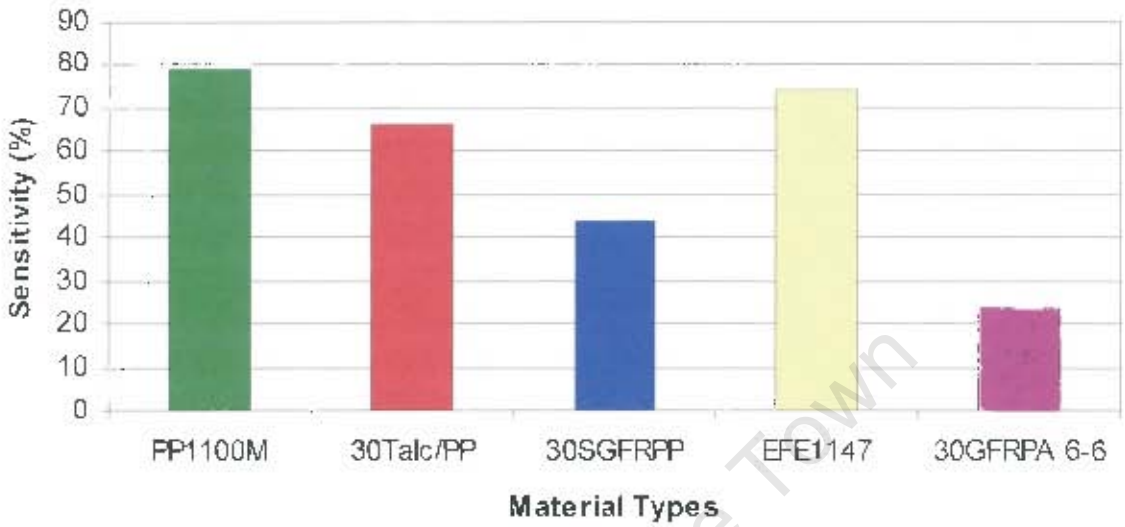

Figure 5.2: *Comparison of material's sensitivity to temperature.*

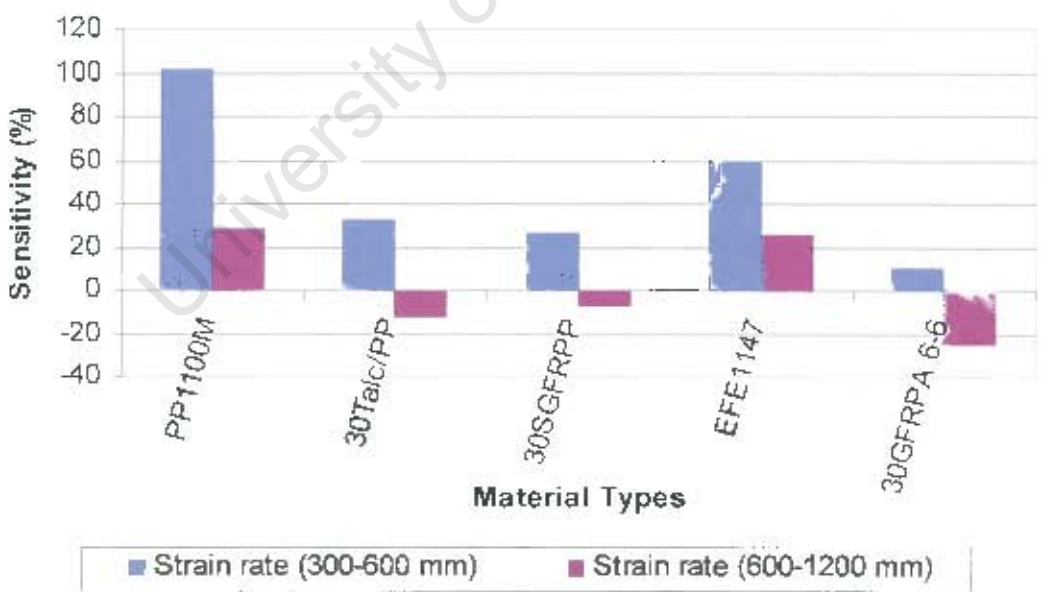

Figure 5.3: *Comparison of material's sensitivity to strain rate.*

5.4 FILLER DISTRIBUTION IN THE POLYMER MATRIX

The orientation of fillers has an influence on the mechanical properties of thermoplastic composites. Orientation in the moulded specimen is determined by the processing conditions and the geometry of the fillers. In short fibre composites, fibres orientate parallel to the injection moulded bar specimen near the surface while the orientation is random in the core of the specimen. This orientation is observed in short glass fibre reinforced polypropylene and polyamide 6-6. This orientation pattern can be attributed to the flow profile and the variation in the cooling that occurs across the bar specimen. During mould packing, cooling initiates from the mould walls towards the middle of the specimen. The solid layer is formed near the mould wall with fibres orientated in the melt flow direction. Different flow patterns are present in the core of the bar specimen. This causes the fibres to orientate in different directions in the core. These are the reasons for the three layers that are observed on the polished surface of the bar specimen. Jeng and Chen also found the three layers, two surface layers with fibres aligned in the melt flow direction and the middle layer with random orientation of fibres. They said the differences in the orientation are due to the flow profile in the bar specimen[54]. The orientation of talc plates is also influenced by the melt flow. Talc plates are laid flat in the melt flow direction.

5.5 DAMAGE GROWTH IN THERMOPLASTIC COMPOSITES

Damage occurs by crack initiation and propagation in thermoplastic composite specimens. Crack propagation involves mechanisms such as plastic deformation, matrix crazing and tearing, fibre fracture and fibre-matrix debonding. The deformation behaviour is different in different materials with the different types of mechanical testing. This was seen in the damaged drop-weight specimens and on the fracture surfaces in the SEM micrographs. Polypropylene

shows a brittle fracture at the middle of a circular disc specimen with radial cracks radiating towards the periphery. This behaviour is due to the stress that is applied at the centre of the specimen, which spreads out causing the plastic deformation resulting in crazing and crack initiation. This behaviour is seen at 20 ^{0}C and low strain rates. Tough materials show an indent in the specimen at 20 ^{0}C and low strain rates. This is ductile failure that is observed in polyamide 6-6. In polypropylene- and polyamide composites, the fibres arrest the radial cracks and the specimens show a brittle cone fracture.

A decrease in temperature or an increase in the strain rate results in the introduction of the circumferential crack and extension of the radial cracks. These cracks join and small pieces break off the specimen increasing the circular fracture. Temperature embrittles the polymer reducing the ductility hence fast cracking and brittle fracture. Higher test speeds do not allow time for plastic deformation, therefore a crack propagates fast causing a brittle fracture. Tai et al found similar observations on polypropylene specimens that were tested at 0 ^{0}C and 20 ^{0}C and it was said that the fracture pattern is due to matrix embrittlement at 0 ^{0}C[62].

Crack propagation can be explained in the drop-weight specimens using the force deflection curve. The initiation of the crack cannot be seen on the curves of polypropylene and polyamide 6-6. In polypropylene- and polyamide composites, the crack initiation point is the beginning of the sinusoidal shape. The sinusoidal shape represents the different energies absorbed on tearing the matrix and breaking the fibres. Akay et al have observed a sinusoidal behaviour for long fibre-reinforced polyamide 6-6 and a non-sinusoidal curve for unfilled polyamide 6-6 materials and they suggested that the initiation of the crack is marked by the beginning of the harmonic motion in the force deflection curve of long fibre-reinforced polyamide 6-6[43]. Cracks can initiate on the surface or inside the specimen. Crack initiation on the surface is due to the coalition of micro-voids on

the surface on impact. The surface crack that occurs on the tension side of the three-point bend specimen forms a zigzag pattern as a result of the crack tip deflection mechanisms. When a crack reaches a fibre, depending on the length of the fibre, it changes the direction of propagation and propagates by breaking the fibre-matrix interface bond. If the crack is at the middle of a long fibre, fibre breakage will occur. These mechanisms of crack propagation are observed on the three-point bend bar specimen and on the surface of the drop-weight specimens. The deformation mechanisms (matrix plastic deformation, fibre pullout, fibre breakage, matrix tearing and fibre-matrix debonding) mentioned above and in the previous sections can be seen in the SEM micrographs of the fracture surface.

CHAPTER 6

CONCLUSIONS

- Polyamide 6-6 was shown to absorb more than 2% moisture in less than 24 hours. The moisture absorption process in polyamide 6-6 and 30% short glass fibre reinforced polyamide 6-6 follow the prediction of Fick's law. Addition of short glass fibres to polyamide 6-6 causes a reduction in the moisture uptake.
- Short glass fibres enhance the strength and the impact energy of the polypropylene and polyamide 6-6 composites. The percentage elongation of the polypropylene and the polyamide 6-6 materials is, however, reduced by the addition of short glass fibres and talc fillers. Talc fillers reduce the tensile strength, Izod and Charpy impact strength of polypropylene. The flexural strength and the drop-weight impact in enhanced by the addition of talc fillers.
- The tensile, flexural and impact properties of short fibre reinforced polyamide 6-6 composite are higher than those of short glass fibre reinforced polypropylene composite. The maximum flexural strength was found to be higher than the maximum tensile strength for all the materials tested. 30% short glass fibre reinforced polypropylene has higher Charpy impact strength than polyamide 6-6 but polyamide 6-6 has higher Izod and drop-weight impact strength than 30% short glass fibre reinforced polypropylene at room temperature. This indicates that the type of impact test has an influence on the mechanical response of the composite materials.

- The reduction in the test temperature causes a reduction in the impact strength of polypropylene- and polyamide 6-6 composites. This is also because the plastic yielding is reduced at lower temperatures. The drop-weight impact energy increases with an increase in the drop height. However, the impact energy is reduced at high drop heights. Thermoplastic materials are therefore very sensitive to the strain rate.
- Processing conditions play a significant role in the mechanical response of thermoplastic composites materials. Processing conditions determine the fibre orientation, which in turn determine the mechanical properties.
- Polypropylene has higher plastic yielding than polyamide 6-6. However, polyamide 6-6 is tougher than polypropylene. The dominant mechanisms of failure observed in polypropylene and polyamide 6-6 composites are matrix plastic deformation, matrix tearing, fibre-matrix debonding, fibre pullout and fibre fracture. Plastic yielding is the most energy dissipating mechanisms and materials with higher plastic deformation will absorb more impact energy. It was found in this research project that polypropylene has higher plastic deformation than polyamide 6-6 but polyamide 6-6 has higher impact energy. Polyamide 6-6 is ductile and tough. Therefore, ductile and tough materials are the most energy dissipating.
- The specific design requirements can be reached by careful choice of the materials and control of the interface bond as well as the filler orientation.

CHAPTER 7

RECOMMENDATIONS FOR FUTURE WORK

Many researchers have investigated the behaviour of metal matrix composites at high strain rate and few researchers on polymer matrix composites using thermosetting matrices. More work has to be done on investigating the high strain rate response of short fibre reinforced polymer matrix composites based on thermoplastic matrices. This is because high strain rate loading occurs in many of the thermoset- and thermoplastic matrix composites, viz. bird strikes in aircraft structures, under water mine blasts on ship hulls, ballistic impact on civil structures and armoured vehicles and automobile accidents[65,66,67,68]. Knowledge of high strain rate response of thermoplastic matrix composites could also lead to new developments in applications that are subjected to dynamic loading. It is of great importance that researchers are able to predict failure of thermoplastic matrix composites structures under dynamic loading. The Split Hopkinson Pressure Bar (SHPB) can be used to characterize the dynamic response of thermoplastic matrix composites at the strain rate range from 100 s^{-1} to 5000 s^{-1}.

The SHPB was originally developed to generate high strain rate data of materials under compression. It was modified to extract dynamic material properties under tension and torsional loading[69]. This allows dynamic loading on thermoplastic matrix composites in different stress applications. The schematic representation of the Split Hopkinson Pressure Bar set-up is shown in Figure 7.1. During testing, the specimen is placed between the incident and the transmission bar with the strain gauges mounted in the middle of the bars. The incident and the transmission bar sandwich the specimen during testing. During testing, the striker bar is released, by releasing the nitrogen gas in the gas chamber, to

impact at the free end of the incident bar. The impact induces a longitudinal compressive stress wave in the incident bar called the incident wave or incident pulse. Once the wave reaches the incident bar specimen interface, a portion of it is reflected back into the incident bar as a tensile pulse and the other portion is transmitted into the specimen as a compressive pulse. The pulse propagates through the specimen and reaches the specimen transmission bar interface. A portion of the pulse is reflected back into the specimen and the remaining portion is transmitted into the transmission bar as a transmitted pulse. The reflection of the pulse back into the incident bar and the transmission of the pulse into the transmission bar can be attributed to the difference in mechanical impedance between the bars and the specimen. The incident, reflected and transmitted waves are recorded by the strain gauges mounted on the incident and the transmission bars (see Figure 7.2 for the signal out put). The results in Figure 7.2 are used to derive the stress-strain relationship.

The SHPB set up available at the University of Cape Town has the striker, incident and transmission bars made of high strength 1045-maraging steel. This material is suitable for testing of metallic materials but not for polymeric materials because of impedance mismatch. If the steel bars are used for testing of polymeric materials the transmitted pulse often have small amplitudes that sacrifices proper interpretation of the measured results (see Figure 7.3)[70]. However, the amplitude of the transmitted pulse can be increase by replacing the steel bars with the high strength aluminium alloy. Further increases in the transmitted pulse can be obtained by using a hollow aluminium bar. Results found by Chen, Zhang and Forrestal show an increase in the transmitted pulse with a modified split Hopkinson bar and even more increases when a hollow transmission bar was used (see Figure 7.4).

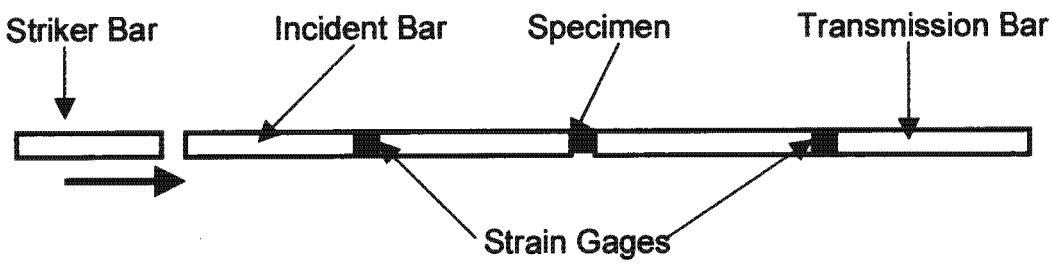

Figure 7.1: *Compression Split Hopkinson Pressure Bar set up.*

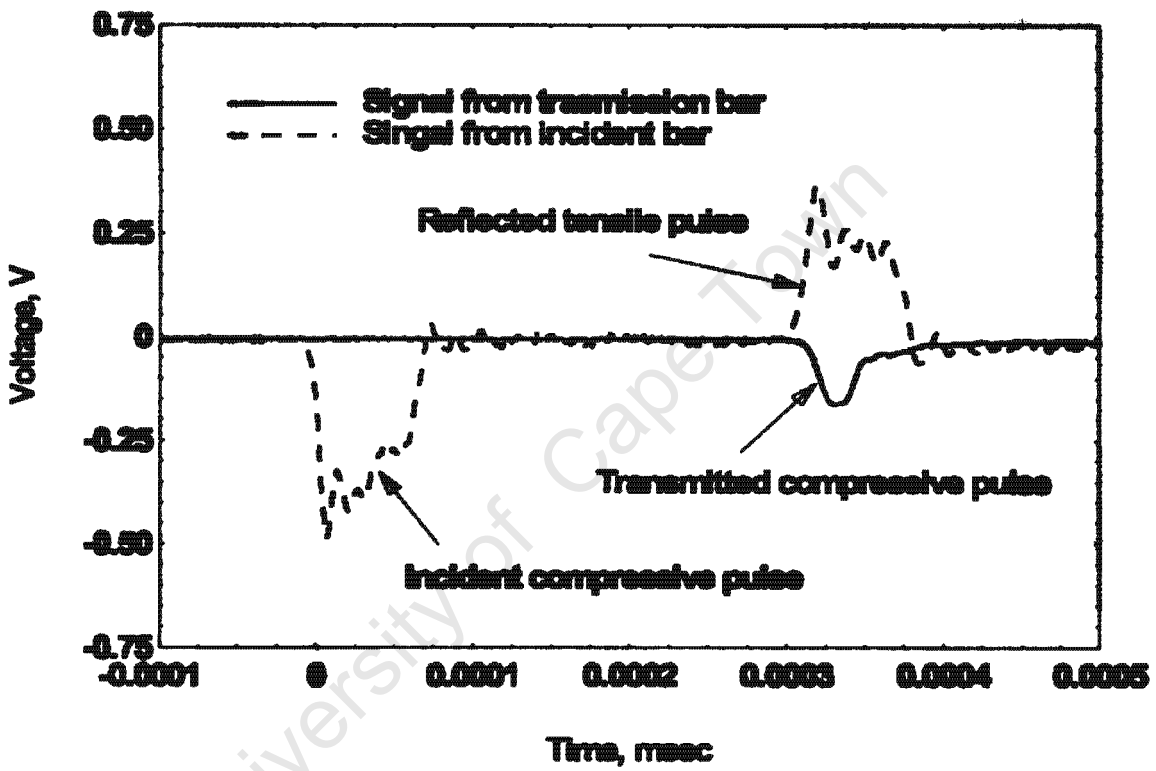

Figure 7.2: *Typical wave signals obtained using the SHPB*[65].

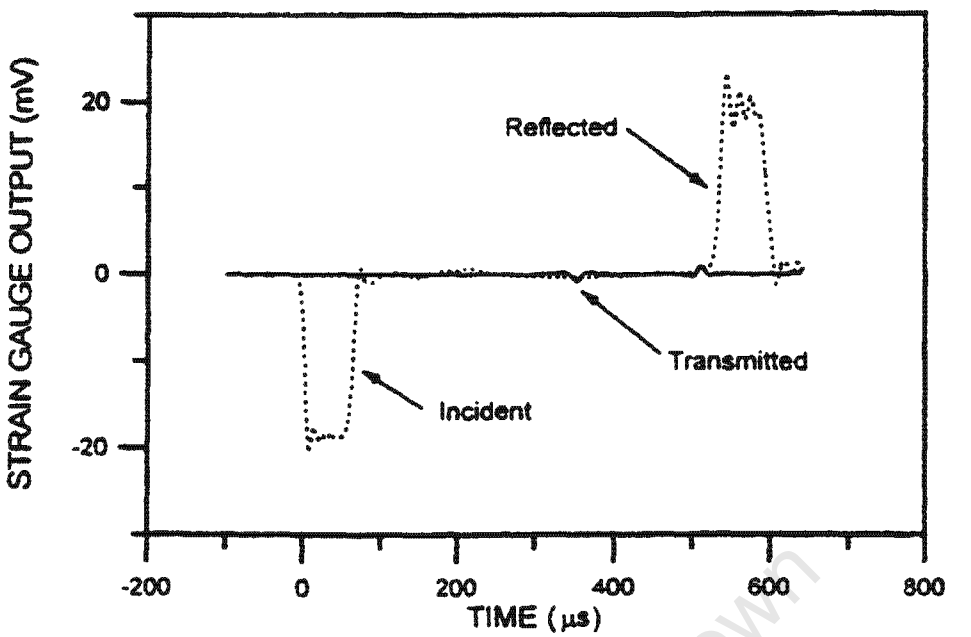

Figure 7.3: *Typical wave signals obtained for low impedance materials using steel bars[70].*

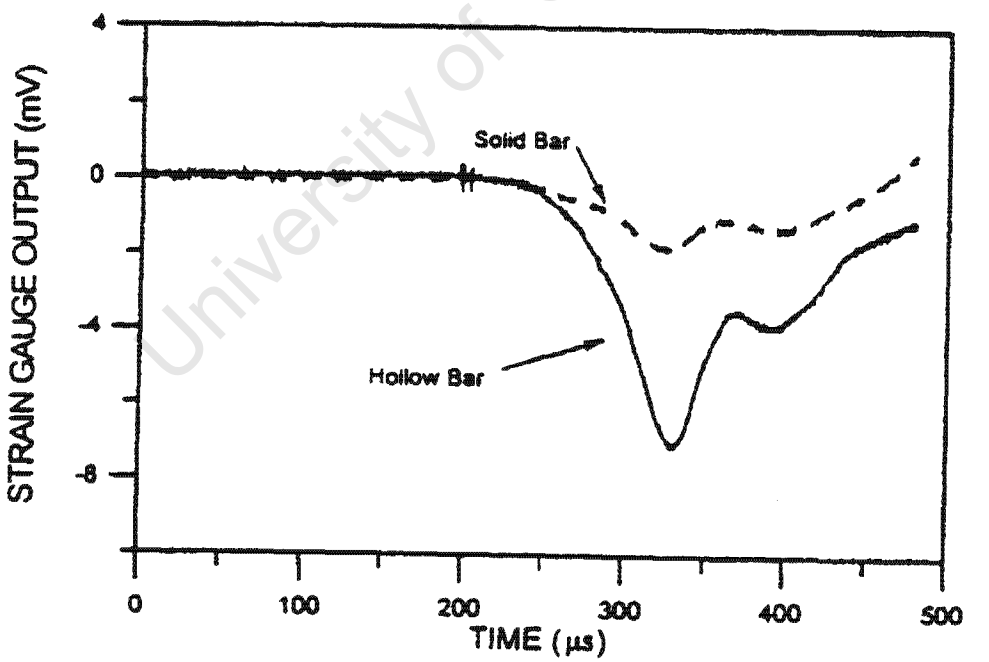

Figure 7.4: *Transmitted pulse obtained using the high strength aluminium alloy bars[70].*

CHAPTER 8

REFERENCES

1. WWW.industrie.gouv.fr/biblioth/docu.
2. (www.addcomp.com) C. DeArmitt and K.D. Breese, *Filled polypropylene: cost-performance comparison of common fillers,* Plastic Additives and Compounding, 2001, pages 28-33.
3. www.golcha.com/uses/htm (*Talc uses*).
4. D.D. Ebbing, *General Chemistry*, 4th Edition, Houghton Mifflin Company, 1993, pages 1045-1049.
5. P.A. Grandilli, *Technician's Handbook of Plastics*, Van Nostrand Reinhold Company, 1981.
6. W.E. Nelson, *Nylon Plastic Technology*, Newnes-Butterworth, 1976.
7. B.M. Sole, *The abrasive wear behaviour of mineral-filled polypropylene,* Ph.D Thesis, Centre for Materials Engineering, University of Cape Town, 1997.
8. T.A. Osswald and G. Menges, *Materials Science of Polymers for Engineers,* Hanser/Gardner Publications Inc, 1995
9. J. Karger-Kocsis, *Polypropylene (Structure, Blends and Composites), Vol. 1, Structure and Morphology*, Chapman and Hall, 1995.
10. W.D. Callister. Jr., *Materials Science and Engineering-An Introduction,* 4th Edition, John Wiley & Sons Inc., New York, 1996.
11. E.P. Moore. Jr., *Polypropylene Handbook,* Hanser/Gardner Publications Inc, New York, 1996.

12. www.chemheritage.org/HistoricalServices/sloan/sloan%20presentation/NYLON/chem/name.html ~ 5k ~ 8 Sep 2002.

13. Z.A. Mohdishak, U.S. Ishiaku and J. Karger-Kocsis, *Microstructure-related fracture behaviour of injection moulded short fibre reinforced polyarylamide in dry and wet states*, Journal of Material Science, Vol. 33, 1998, pages 3377-3389.

14. H. Salehi-Mobarakeh, J. Brisson and A. Ait-Kadi, *Interfacial polycondensation of nylon 6-6 at the glass fibre surface and its effect on fibre-matrix adhesion*, Journal of Materials Science, Vol. 32, 1997, pages 1297-1304.

15. J. Karger-Kocsis, *Microstructural aspects of fracture in polypropylene and in its filled, chopped fibre and fibre mat reinforced composites*, Polypropylene Structure, Blends and Composites, Vol. 3, Composites, Chapman and Hall, 1995, pages 142-191.

16. A.G. Gibson, *Processing and Properties of Reinforced Polypropylenes*, Polypropylene Structure, Blend and Composites, Vol. 3, Composites, Chapman and Hall, 1995, pages 71-110.

17. K.K. Chawla, *Composite Materials*, Springer-Verlag, 1987.

18. J.A. Catherall, *Fibre reinforcement*, Mills & Boom Ltd., 1973, pages 30-35.

19. D.W. Dwigdt, *Glass fibre reinforcements*, Comprehensive Composite Materials, Fibre reinforcements and general theory of composites, Vol. 1, pages 231-261.

20. F.R. Jones, *Glass fibres - type and form*, Handbook of Polymer-fibre Composites, Longman Group UK Ltd., 1994, pages 38-42.

21. K. Friedrich and J. Karger-Kocsis, *Fractography and failure mechanisms of unfilled and short fibre reinforced semi-crystalline thermoplastics. Fractography and Failure Mechanisms of Polymers and Composites*, Elsevier Science Publishers Ltd., 1989, pages 437-494.

22. R. Gachter and H. Muller, *Plastic additives handbook*, Carl Hanser Verlag Munchen Wien, 1987.

23. www.mineralstech.com/uses/htm

24. D.H. Solomon and D. G. Hawthorne, *Chemistry of pigments and fillers*, John Wiley & Sons, Inc., 1983.

25. K.H.G. Ashbee, *Fundamental principles of fibre reinforced composites*, Technomic Publishing Company, 1989.

26. H.F. Wu, D.W. Dwight and N.T. Huff, *Effects of silane coupling agents on the interphase and performance of glass-fibre-reinforced polymer composites*, Composites Science and Technology, Vol. 57, 1997, pages 975-983.

27. P. Mareri, S. Bastide, N. Binda and A. Crespy, *Mechanical behaviour of polypropylene composites containing fine mineral filler: effect of filler surface treatment*, Composite Science and Technology, Vol. 58, 1998, pages 747-752.

28. M. Wang and W. Bonfield, *Chemically coupled hydroxyapatite-polypropylene composites: structure and properties*, Biomaterials, Vol. 22, 2001, pages 1311-1320.

29. J.L. Thomason, *Interfacial strength in thermoplastic composites – at last an industry friendly measurement method?* Composites, Part A, Vol. 33, 2002, pages 1283-1288.

30. A.G. Gibson, *Bulk moulding compounds and dough moulding compounds*, Handbook of Polymer-fibre Composites, Longman Group UK Ltd.,1994, pages 150-153.

31. F. Johannaber, *Injection moulding machines-A User Guide*, 2nd ed., Carl Hanser Verlag Munchen Wien, 1983.

32. T. Matsuoka, *Fibre orientation prediction in injection moulding*, Polypropylene Structure, Blends and Composites, Vol. 3, Composites, Chapman and Hall, 1995, pages 113-141.

33. G. Menges, *How to make injection moulds*, Carl Hanser Verlag Munich Vienna New York, 1986.

34. F.R. Jones, *Laminates-crossply cracking, Handbook of polymer-fibre composites*, Longman Group UK Ltd., 1994, pages 249-253.

35. B.H. Min, *A study on quality monitoring of injection-molded parts*, Journal of Materials Processing Technology, Vol. 136, 2003, pages 1-6.

36. J.Z. Liang and J.N. Ness, *The calculation of cooling time in injection moulding*, Journal of Materials Processing Technology, Vol. 57, 1996, pages 62-64.

37. S. Turner, *Mechanical testing of plastics*, The Plastic Institute, 1973.

38. A. Dasari, J. Rohrmann and R.D.K. Misra, *Microstructural evolution during tensile deformation of polypropylenes*, Materials Science and Engineering, A351, 2003, pages 200-213.

39. G. Dorey, *Impact performance-CFRP laminates*, Handbook of polymer-fibre composites, Longman Group UK Ltd., 1994, pages 327-330.

40. W.J. Cantwell and J. Morton, *The impact resistance of composite materials – a review*, Composites, Vol. 22, number 5, 1991, pages 347-361.

41. J.M. Lifshitz, F. Gov and M. Gandelsman, *Instrumented low-velocity impact of CFRP beams*, International Journal of Impact Engineering, Vol. 16, No. 2, 1995, pages 201-215.

42. G. Zhou and G.A.O. Davies, *Impact response of thick glass fibre reinforced polyester laminates*, International Journal of Impact Engineering, Vol. 16, No. 3, 1995, pages 357-374.

43. M. Akay, D.F. O'Regan and R.S. Bailey, *Fracture toughness and impact behaviour of glass-fibre-reinforced polyamide 6,6 injection mouldings*, Composites Science and Technology, Vol. 55, 1995, pages 109-118.

44. L.C. Sawyer and D.T. Grubb, *Polymer microscopy*, Second edition, Chapman and Hall, 1996.

45. P.J.E. Forsyth, *Fibre-strengthened materials*, The Institute of Metallurgists, 1966.

46. J.O. Iroh and J.P. Berry, *Mechanical properties of nucleated polypropylene and short glass fibre-polypropylene composites*, European Polymer Journal, Vol. 32, No. 12, 1996, pages 1425-1429.

47. D. Hull, *An Introduction to Composite Materials*, Cambridge University Press, 1981.

48. S.-Y. Fu, B. Luake, E. Mader, C.-Y. Yue and X. Hu, *Tensile properties of short-glass-fibre-and short-carbon-fibre-reinforced polypropylene composites.* Composites, Part A, Vol. 31, 2000, pages 1117-1125.

49. J.L. Thomason and M.A. Vlug, *Influence of fibre length and concentration on the properties of glass fibre-reinforced polypropylene: 1. Tensile and flexural modulus*, Composites: Part A, Vol. 27A, 1996, pages 477-484.

50. J.L. Thomason and W.M. Groenewoud, *The influence of fibre length and concentration on the properties of glass fibre-reinforced polypropylene: 2. Thermal properties*, Composites, Part A, Vol. 27A, 1996, pages 555-565.

51. J.L. Thomason and M.A. Vlug, *The influence of fibre length and concentration on the properties of glass fibre-reinforced polypropylene: 4. Impact properties*, Composites, Part A. Vol. 28A, 1997, pages 277-288.

52. J.L. Thomason, *Micromechanical parameters from macromechanical measurements on glass reinforced polypropylene*, Composites Science and Technology, Vol. 62, 2002, pages 1455-1468.

53. K.J. Din and S. Hashemi, *Influence of short-fibre reinforcement on the mechanical and fracture behaviour of polycarbonate/acylonitrile butadiene styrene polymer blend*, Journal of Materials Science, Vol. 32, 1997, pages 375-387.

54. C. Jeng and M. Chen, *Flexural failure mechanisms in injection-moulded carbon fibre/PEEK composites,* Composites Science and Technology, Vol. 60, 2000, pages 1863-1872.

55. M.Z. Shah Khan, G. Simpson and E.P. Gellert, *Resistance of glass-fibre reinforced polymer composites to increasing compressive strain and loading rates*, Composites, Part A, Vol. 31, 2000, pages 57-67.

56. O.I. Okoli, *The effect of strain rate and failure modes on the failure energy of fibre reinforced composites*, Composites Structures, Vol. 54, 2001, pages 299-303.

57. F. Ramsteiner and R. Theysohn, *Tensile and impact strengths of unidirectional, short fibre-reinforced thermoplastics*, Composites, 1979, pages 111-119.

58. D.A. Hemsley, *Applied polymer light microscopy*, Elsevier Science Publishers Ltd., 1989.

59. C. Eberhardt and A. Clarke, *Fibre-orientation measurements in short-glass-fibre composites. Part 1: automated, high-angular-resolution measurement by confocal microscopy*, Composites Science and Technology, Vol. 61, 2001, pages 1389-1400.

60. W. Dziadur, *Fractographic features of modified polyamide and polyoxymethylene*, Materials Chemistry and Physics, 2003, pages 1-4.

61. N.S Choi and K. Takahashi, *Characterisation of the damage process in short-fibre/thermoplastic composites by acoustic emission*, Journal of Materials Science, Vol. 33, 1998, pages 2357-2363.

62. C.M. Tai, R.K.Y. Li and C.N. Ng, *Impact behaviour of polypropylene/polyethylene blends,* Polymer Testing, Vol. 19, 2000, pages 143-154.

63. Y.A. Gorbatkina and Z.P. Sulyaeva, *Strength of the fibre/thermoplastic-matrix interface under cyclic cooling to low temperatures,* Composite Science and Technology, Vol. 57, 1997, pages 995-1000.

64. J. Megusar, *Low temperature fast-neutron and gamma irradiation of glass/epoxy composite. Part 1: deformation and fracture,* Journal of Nuclear Materials, Vol. 228, 1996, pages 168-175.

65. M.V. Hosur, J. Alexander, U.K. Vaidya and S. Jeelani, *High stain rate compression response of carbon/epoxy laminate composites*, Composite Structures, Vol. 52, 2001, pages 405–417.

66. J.M. Lifshitz and H. Leber, *Response of fibre-reinforced polymers to high strain-rate loading in interlaminar tension and combine tension/shear*, Composites Science and Technology, Vol. 58, 1998, pages 987–996.

67. M. Guden and I.W. Hall, *High strain-rate compression testing of a short-fibre reinforced aluminium composites*, Materials Science and Engineering, A232, 1997, pages 1-10.

68. W. Chen, F. Lu and Cheng, *Tension and compression tests of two polymers under quasi-static and dynamic loading*, Polymer Testing, Vol. 21, 2002, pages 113-121.

69. H. Zhao and G. Gary, *On the use of SHPB techniques to determine the dynamic behaviour of materials in the range of small strains*, International Journal of Solids Structures, Vol. 33. No.23, 1996, pages 3363-3375.

70. W. Chen, B. Zhang and M.J. Forrestal, *A split Hopkinson bar technique for low-impedance materials*, Experimental Mechanics, Vol. 39, 1999, pages 81-85.

APPENDICES

APPENDIX A

Appendix A1: Tensile Specimen Mould Design

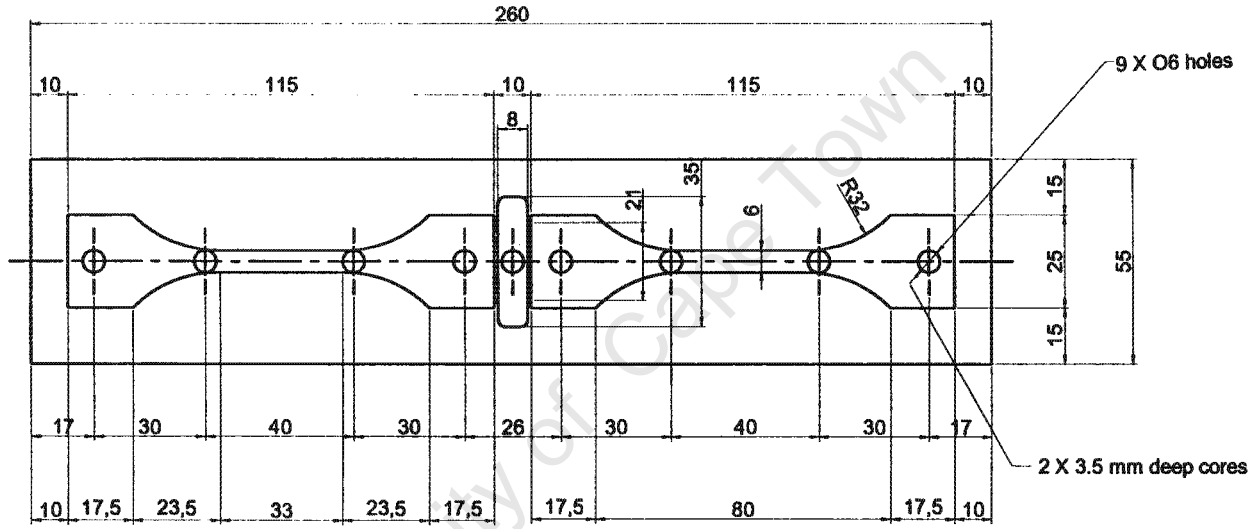

	University of Cape Town Department of Mechanical Engineering		
	MOULDS		
Dimensions in mm	Scale 1 : 1	Date 05-08-02	Sheet Of 1 2
Tolerances + 0.5	Drawn by PHUMUDZO NETANGAHENI		Drawing Number 1

Appendix A2: Impact Bar Mould Design

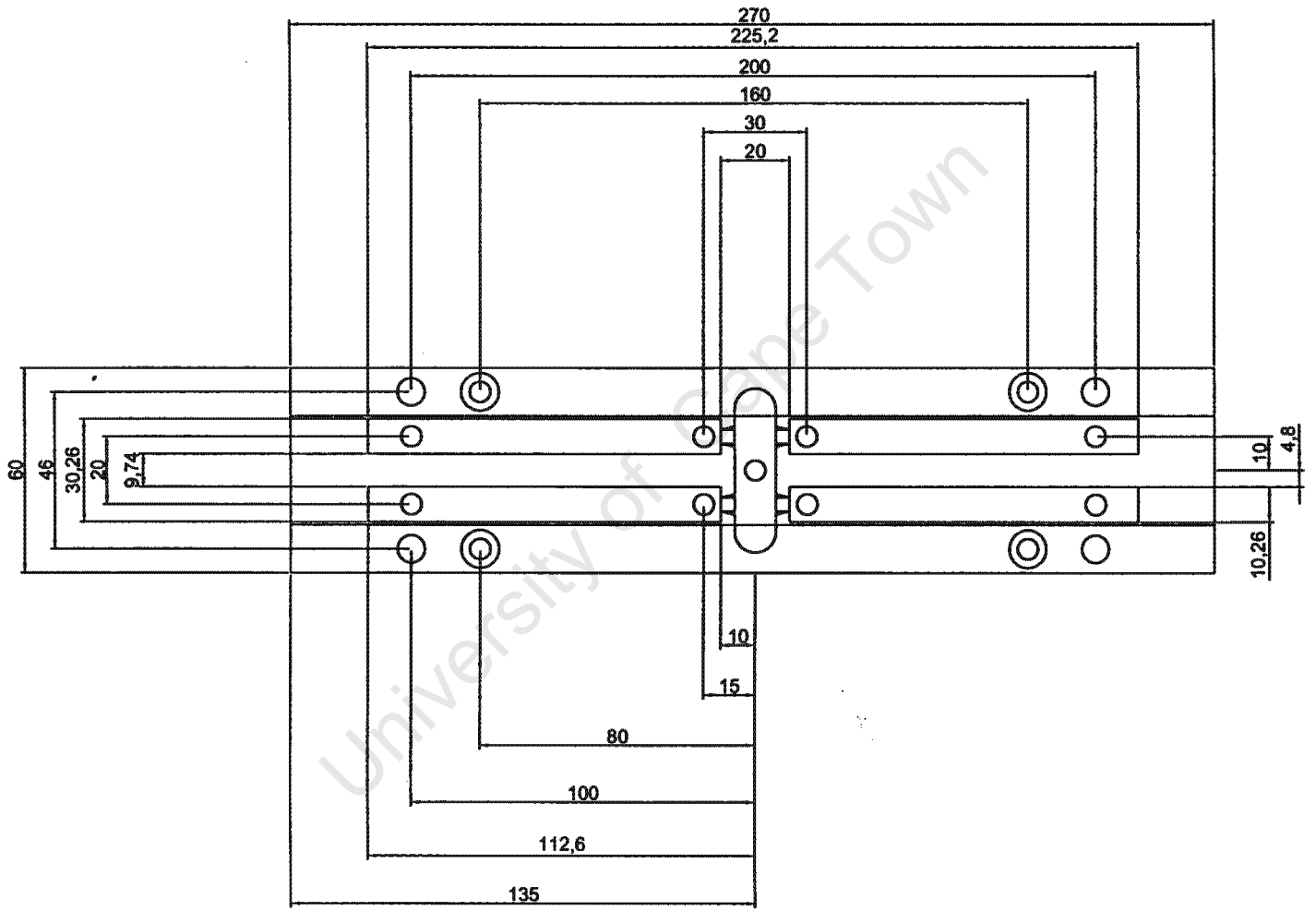

	University of Cape Town Department of Mechanical Engineering		
	MOULDS		
Dimensions in mm	Scale 1 : 1	Date 05-08-02	Sheet Of 2 2
Tolerances + 0.5	Drawn by PHUMUDZO NETANGAHENI	Drawing Number 1	

APPENDIX B

IMPACT RESULTS

CHARPY AND IZOD IMPACT RESULTS

Specimen Prepared by the Automated Machine

PP1100M:

Test Number	CHARPY		IZOD	
	Impact Energy (J)	Impact Resistance (kJ/m^2)	Impact Energy (J)	Impact Resistance (kJ/m^2)
1	0.14	4.24	0.14	4.30
2	0.14	4.36	0.14	4.30
3	0.13	4.15	0.13	4.11
4	0.14	4.36	0.11	3.52
5	0.13	4.03	0.11	3.52
6			0.14	4.50
7			0.14	4.30
8			0.13	3.92

Statistics:

Series N=5	CHARPY Impact Energy (J)	CHARPY Impact Resistance (kJ/m^2)	Series N=8	IZOD Impact Energy (J)	IZOD Impact Resistance (kJ/m^2)
$\bar{x}$	0.14	4.23	$\bar{x}$	0.13	4.06
s	0.00	0.14	s	0.01	0.37

30Talc/PP

Test Number	CHARPY Impact Energy (J)	CHARPY Impact Resistance (kJ/m^2)	IZOD Impact Energy (J)	IZOD Impact Resistance (kJ/m^2)
1	0.13	4.15	0.11	3.52
2	0.10	3.00	0.15	4.69
3	0.13	4.03	0.10	3.13
4	0.10	3.19	0.11	3.52
5	0.13	3.94	0.13	3.92
6	0.10	3.09	0.09	2.75
7	0.10	3.09		

Statistics:

Series N=7	CHARPY Impact Energy (J)	CHARPY Impact Resistance (kJ/m^2)	Series N=6	IZOD Impact Energy (J)	IZOD Impact Resistance (kJ/m^2)
$\bar{x}$	0.11	3.50	$\bar{x}$	0.12	3.59
s	0.02	0.51	s	0.02	0.67

EFE1147

Test Number	CHARPY		IZOD	
	Impact Energy (J)	Impact Resistance (kJ/m^2)	Impact Energy (J)	Impact Resistance (kJ/m^2)
1	0.3	9.45	0.49	15.21
2	0.19	5.81	0.26	8.06
3	0.27	8.44	0.30	9.47
4	0.20	6.38	0.48	15.00
5	0.20	6.26	0.23	7.06
6	0.32	9.96	0.28	8.87
7	0.20	6.26	0.49	15.21
8	0.22	6.73	0.25	7.67
9	0.17	5.46	0.24	7.46
10	0.18	5.70	0.32	10.09
11	0.31	9.70		
12	0.30	9.45		

Statistics

Series N=12	CHARPY Impact Energy (J)	CHARPY Impact Resistance (kJ/m^2)	Series N=10	IZOD Impact Energy (J)	IZOD Impact Resistance (kJ/m^2)
$\bar{x}$	0.24	7.46	$\bar{x}$	0.33	10.41
s	0.06	1.77	s	0.11	3.39

30SGFRPP

Test Number	CHARPY		IZOD	
	Impact Energy (J)	Impact Resistance (kJ/m^2)	Impact Energy (J)	Impact Resistance (kJ/m^2)
1	0.34	10.50	0.31	9.68
2	0.31	9.70	0.31	9.68
3	0.33	10.36	0.30	9.28
4	0.36	11.16	0.32	10.09
5	0.37	11.44	0.30	9.47
6	0.32	10.10	0.32	10.09
7	0.35	11.04	0.30	9.28
8	0.32	10.10	0.30	9.47

Statistics

Series N=8	CHARPY		IZOD	
	Impact Energy (J)	Impact Resistance (kJ/m^2)	Impact Energy (J)	Impact Resistance (kJ/m^2)
$\bar{x}$	0.34	10.55	0.31	9.63
s	0.02	0.60	0.01	0.32

30SGFRPA 6-6

Test Number	CHARPY		IZOD	
	Impact Energy (J)	Impact Resistance (kJ/m^2)	Impact Energy (J)	Impact Resistance (kJ/m^2)
1	0.48	14.95	0.47	14.80
2	0.46	14.51	0.53	16.47
3	0.42	13.08	0.49	15.21
4	0.46	14.23	0.59	18.36
5	0.44	13.66	0.55	17.31
6	0.43	13.36	0.55	17.31
7	0.41	12.68	0.54	16.90
8	0.42	13.08	0.52	16.26
9	0.51	15.98		
10	0.51	15.98		
11	0.42	13.08		
12	0.42	13.22		

Statistics

Series N=12	CHARPY		Series N=9	IZOD	
	Impact Energy (J)	Impact Resistance (kJ/m^2)		Impact Energy (J)	Impact Resistance (kJ/m^2)
$\bar{x}$	0.45	13.98	$\bar{x}$	0.53	15.58
s	0.04	1.15	s	0.04	1.16

Specimen Prepared by the Manual Machine

PP1100M:

Test Number	CHARPY		IZOD	
	Impact Energy (J)	Impact Resistance (kJ/m^2)	Impact Energy (J)	Impact Resistance (kJ/m^2)
1	0.08	2.48	0.09	2.94
2	0.09	2.70	0.08	2.56
3	0.08	2.58	0.08	2.56
4	0.09	2.70	0.08	2.35
5	0.08	2.58	0.08	2.56
6	0.12	3.82	0.09	2.94
7	0.09	2.70	0.09	2.75
8	0.09	2.70		
9	0.12	3.61		

Statistics:

Series N=9	CHARPY		Series N=8	IZOD	
	Impact Energy (J)	Impact Resistance (kJ/m^2)		Impact Energy (J)	Impact Resistance (kJ/m^2)
$\bar{x}$	0.09	2.87	$\bar{x}$	0.08	2.67
s	0.02	0.49	s	0.01	0.22

30Talc/PP

Test Number	CHARPY		IZOD	
	Impact Energy (J)	Impact Resistance (kJ/m^2)	Impact Energy (J)	Impact Resistance (kJ/m^2)
1	0.10	3.00	0.10	3.13
2	0.10	3.00	0.11	3.52
3	0.09	2.88	0.09	2.94
4	0.09	2.79	0.09	2.94
5	0.10	3.09	0.12	3.71
6	0.10	3.09	0.10	3.13
7	0.10	3.09	0.09	2.94
8	0.10	3.00	0.09	2.94
9			0.09	2.94

Statistics:

Series N=8	CHARPY		Series N=9	IZOD	
	Impact Energy (J)	Impact Resistance (kJ/m^2)		Impact Energy (J)	Impact Resistance (kJ/m^2)
$\bar{x}$	0.10	2.99	$\bar{x}$	0.10	3.13
s	0.00	0.11	s	0.01	0.29

30SGFRPP:

Test Number	CHARPY		IZOD	
	Impact Energy (J)	Impact Resistance (kJ/m^2)	Impact Energy (J)	Impact Resistance (kJ/m^2)
1	0.25	7.71	0.23	7.06
2	0.24	7.45	0.21	6.67
3	0.24	7.57	0.23	7.27
4	0.25	7.71	0.22	6.88
5	0.27	8.32	0.22	6.88
6	0.23	7.34	0.21	6.67
7	0.25	7.83	0.22	6.88
8	0.27	8.32	0.21	6.48
9	0.25	7.83	0.21	6.67
10	0.25	7.83	0.20	6.27

Statistics:

Series N=10	CHARPY		IZOD	
	Impact Energy (J)	Impact Resistance (kJ/m^2)	Impact Energy (J)	Impact Resistance (kJ/m^2)
$\bar{x}$	0.25	7.79	0.22	6.77
s	0.01	0.32	0.01	0.29

DROP-WEIGHT IMPACT RESULTS

Test Results at –35 ^{0}C

300 mm drop height

Material Type / Test Number	Impact Energy (J)				
	PP1100M	30Talc/PP	EFE1147	30SGFRPP	30SGFRPA 6-6
1	0.439	1.259	2.244	2.606	4.685
2	0.465	1.311	2.291	2.788	4.596
3	0.512	1.430	2.334	2.445	4.701
4	0.436	1.211	2.198	2.591	4.622
5	0.493	1.331	2.203	2.965	5.126

Statistics

Material Type / Series N=5	Impact Energy (J)				
	PP1100M	30Talc/PP	EFE1147	30SGFRPP	30SGFRPA 6-6
$\bar{x}$	0.46	1.31	2.25	2.8	4.7
s	0.03	0.08	0.06	0.2	0.2

Test Results at 20 ^{0}C

300 mm drop height

Material Type / Test Number	Impact Energy (J)				
	PP1100M	30Talc/PP	EFE1147	30SGFRPP	30SGFRPA 6-6
1	1.833	2.122	8.558	5.016	7.272
2	2.019	5.748	8.560	4.853	5.395
3	2.354	3.935	8.569	5.179	6.062

Statistics

Material Type / Series N=3	Impact Energy (J)				
	PP1100M	30Talc/PP	EFE1147	30SGFRPP	30SGFRPA 6-6
$\bar{x}$	2.1	3.9	8.56	5.0	6.2
s	0.3	1.8	0.01	0.2	1.0

600 mm drop height

Material Type / Test Number	Impact Energy (J)				
	PP1100M	30Talc/PP	EFE1147	30SGFRPP	30SGFRPA 6-6
1	4.516	5.189	14.191	6.296	6.184
2	4.144	4.425	13.095	6.384	7.592
3	3.772	5.956	13.643	6.316	6.888

Statistics

Material Type / Series N=3	Impact Energy (J)				
	PP1100M	30Talc/PP	EFE1147	30SGFRPP	30SGFRPA 6-6
$\bar{x}$	4.1	5.2	13.6	6.33	6.8
s	0.4	0.8	0.5	0.04	0.7

1200 mm drop height

Material Type / Test Number	Impact Energy (J)				
	PP1100M	30Talc/PP	EFE1147	30SGFRPP	30SGFRPA 6-6
1	5.209	4.598	17.118	5.744	5.346
2	5.334	5.010	18.214	5.910	4.391
3	5.459	4.189	16.016	6.156	5.662

Statistics

Material Type / Series N=3	Impact Energy (J)				
	PP1100M	30Talc/PP	EFE1147	30SGFRPP	30SGFRPA 6-6
$\bar{x}$	5.3	4.6	17.1	5.9	5.1
s	0.1	0.4	1.1	0.2	0.7

APPENDIX C

SEM MICROGRAPHS OF SPECIMENS PREPARED BY THE AUTOMATED MACHINE

TENSILE MICROGRAPHS

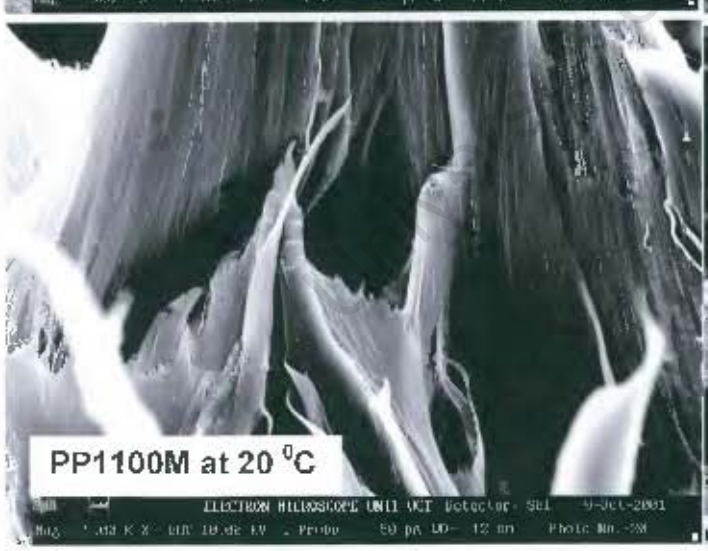

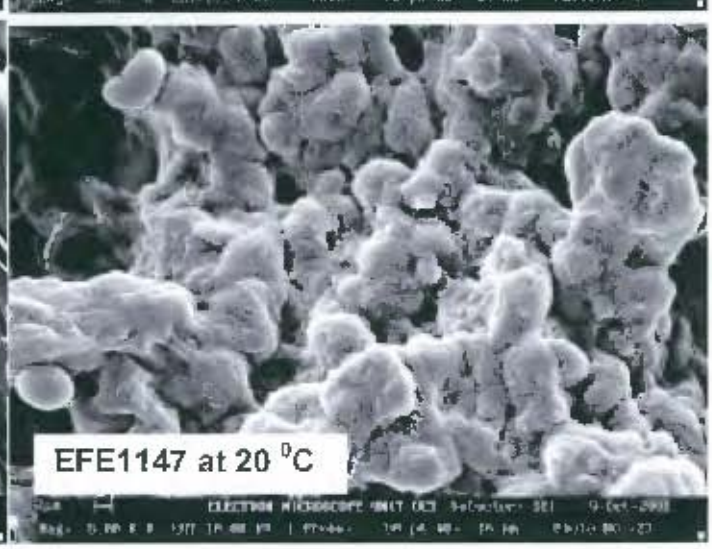

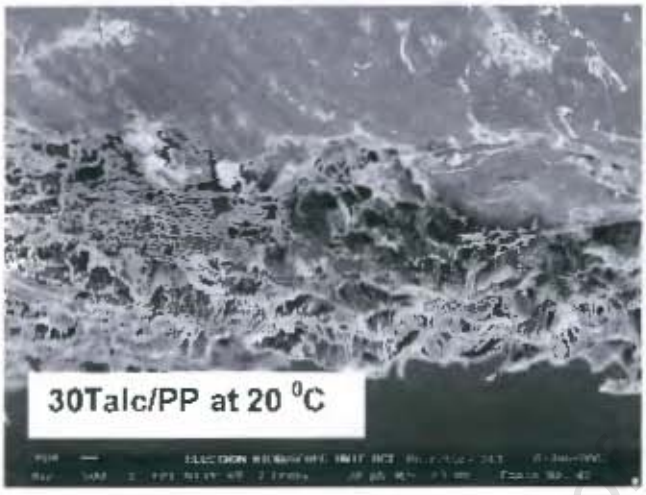

THREE-POINT BEND MICROGRAPHS

IZOD IMPACT MICROGRAPHS

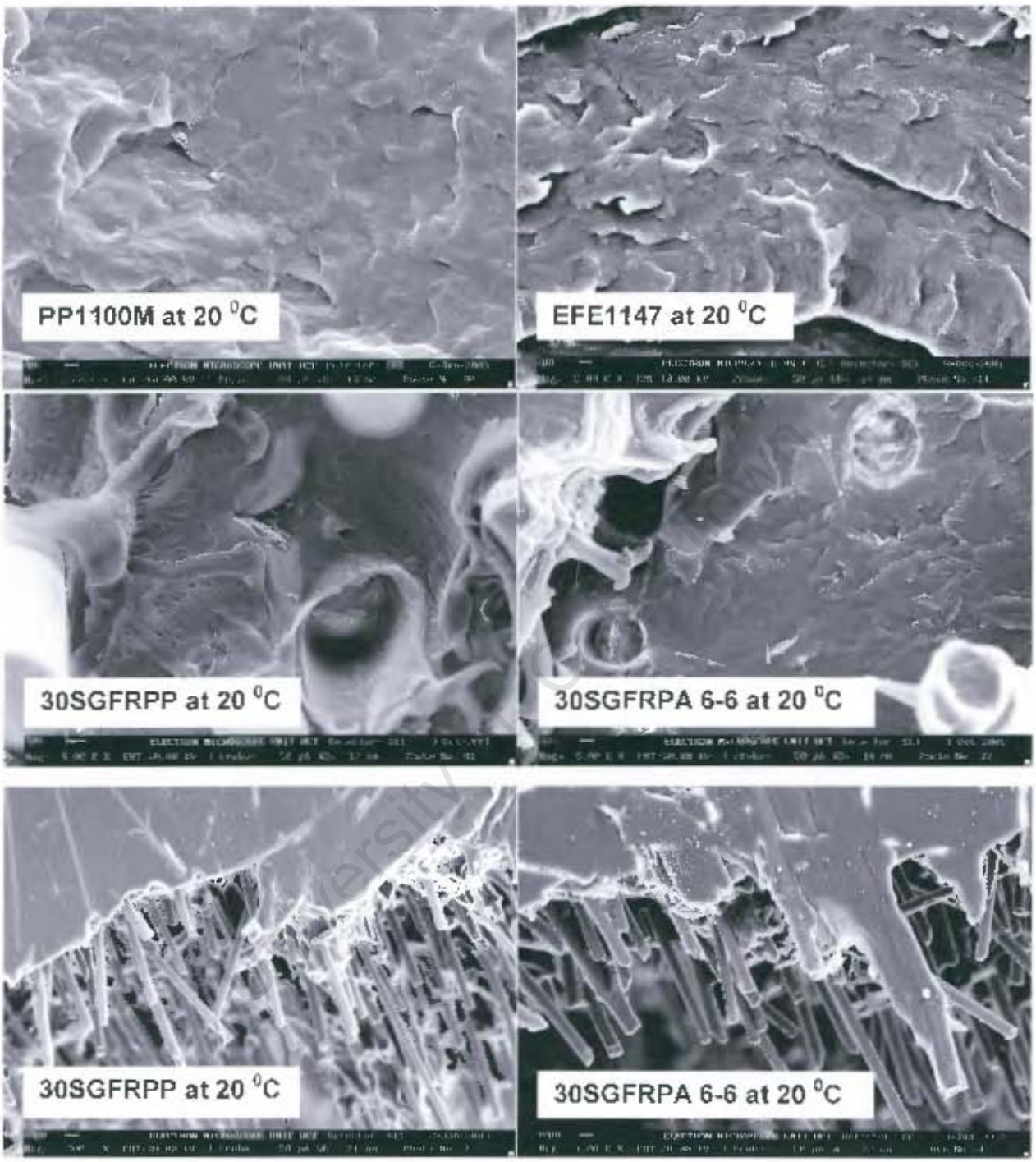

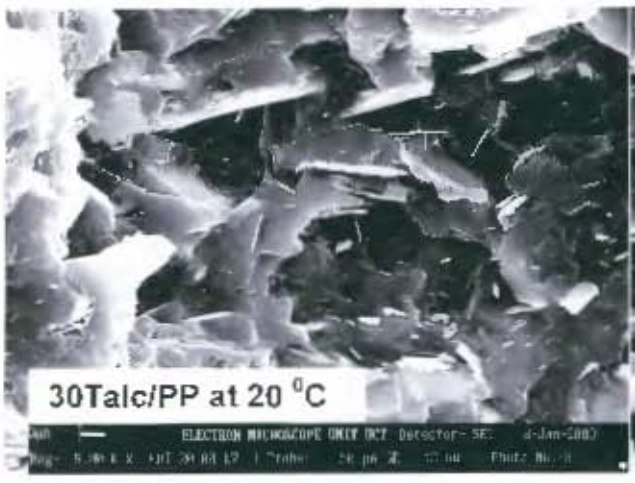

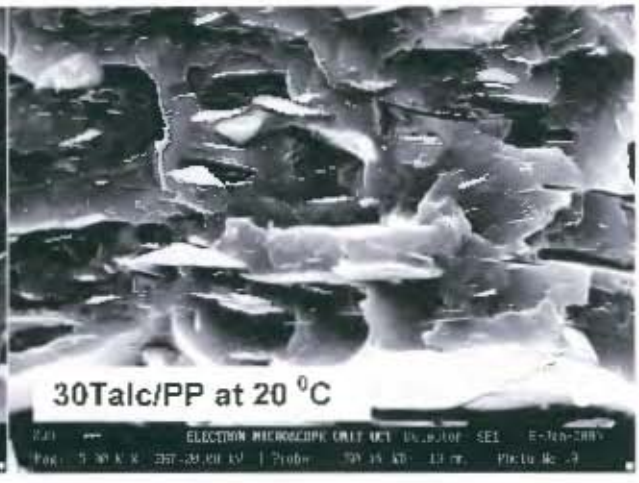

CHARPY IMPACT MICROGRAPHS

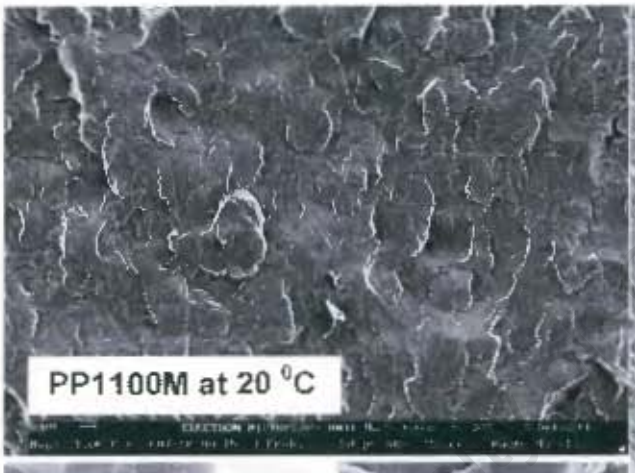

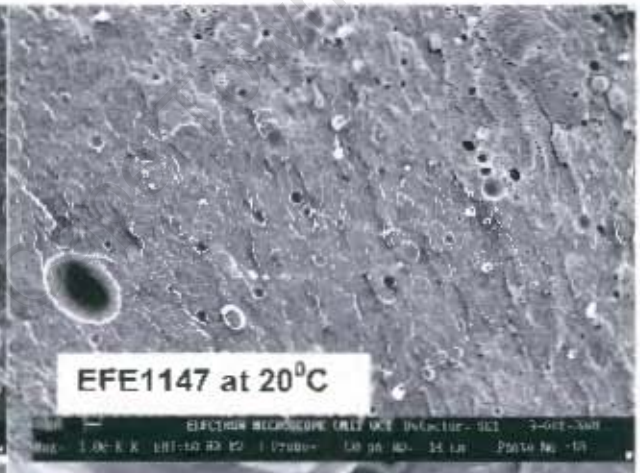

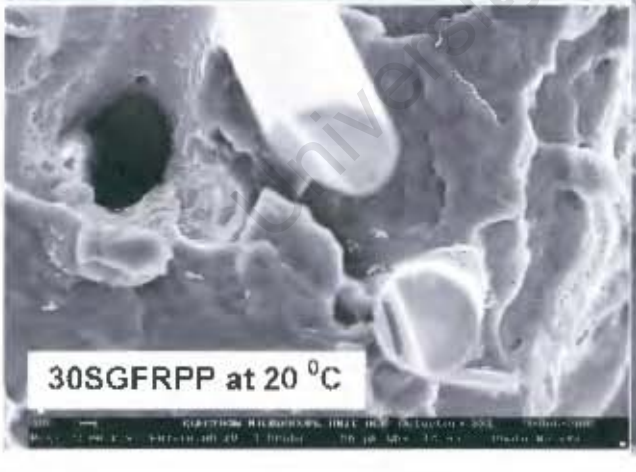

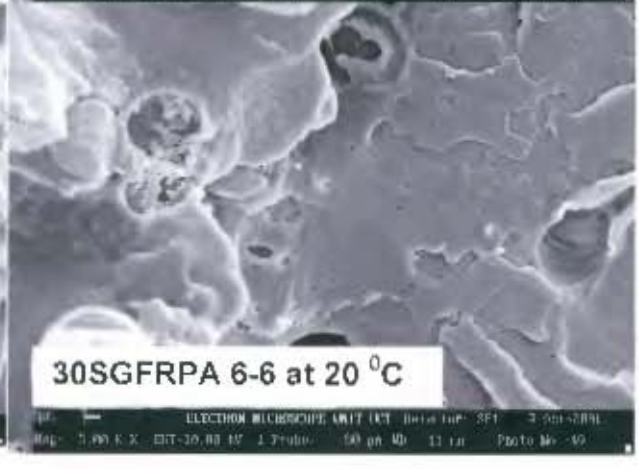

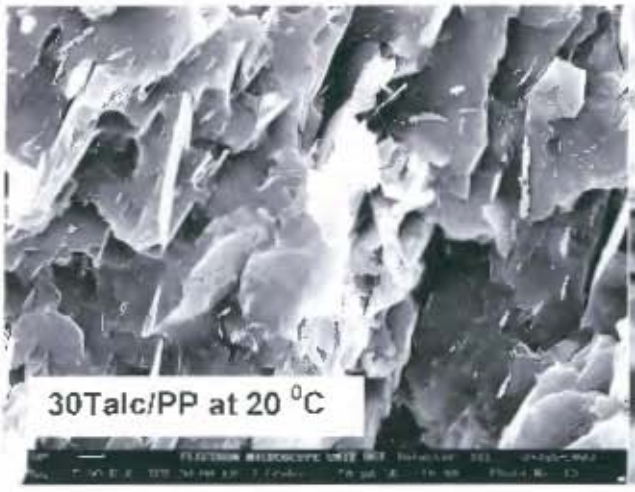

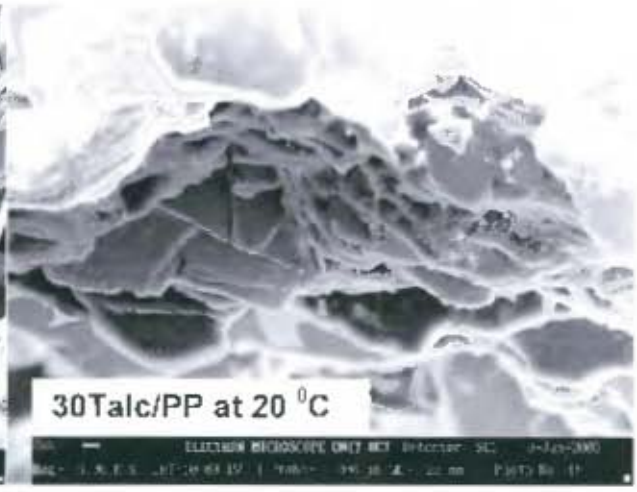

DROP-WEIGHT IMPACT MICROGRAPHS

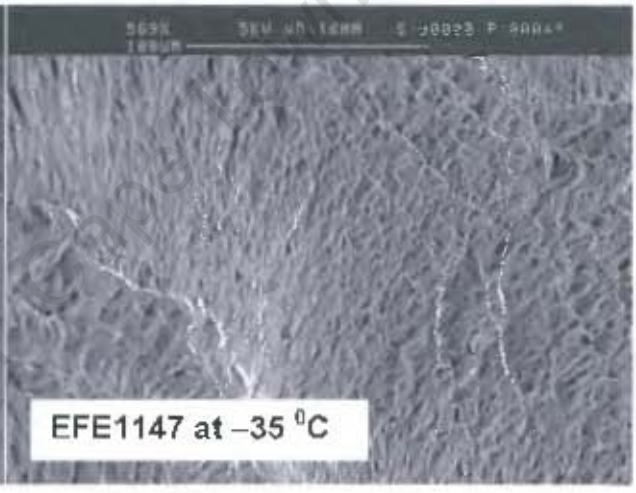

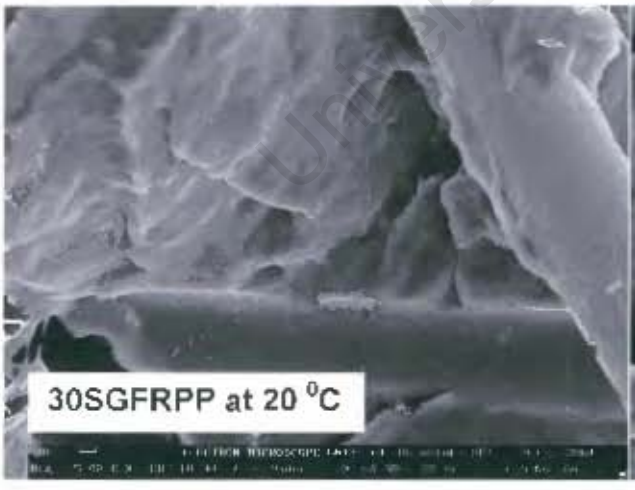

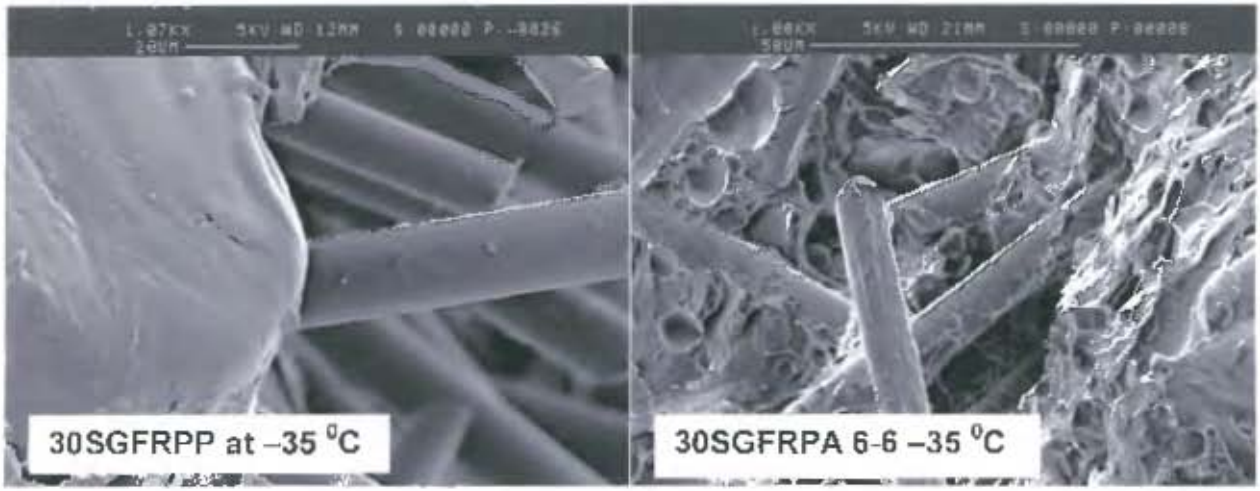

SEM MICROGRAPHS OF SPECIMENS PREPARED BY THE HAND OPERATED MACHINE

ALL THE SPECIMENS WERE TESTED AT 20 °C